Title
Characterizing the Mechanism of the INO80 family Chromatin Remodeling Machine

Permalink
https://escholarship.org/uc/item/3147r2gv

Author
Gourdet, Muryam

Publication Date
2022

Peer reviewed|Thesis/dissertation

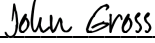Characterizing the Mechanism of the INO80 family Chromatin Remodeling Machine

by
Muryam Gourdet

DISSERTATION
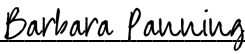Submitted in partial satisfaction of the requirements for degree of
DOCTOR OF PHILOSOPHY

in

Biochemistry and Molecular Biology

in the

GRADUATE DIVISION
of the
UNIVERSITY OF CALIFORNIA, SAN FRANCISCO

Approved:

DocuSigned by:

John Gross
533C6EEB4997487...
John Gross
Chair

DocuSigned by:

Geeta Narlikar
DocuSigned by:043B...
Geeta Narlikar

Barbara Panning
B18F20197C95417...
Barbara Panning

Committee Members

Acknowledgements

I dedicate this thesis to the following people. Their support made this body of work possible.

To the Narlikar Lab for providing me the space to thrive scientifically. The Narlikar lab became my lab family. We thought hard, worked hard, and played hard together.

To Yifan Cheng, Hao Wu, and Elise Muñoz for collaborating to solve the structure of INO80 bound the hexasome. This was a great learning experience to develop this story together.

To Nathan Gamarra, my rotation mentor. Nathan was the best rotation mentor I could have had. His joy and passion for science was infectious. It was through his mentorship, I was able to reignite my passion for discovery.

To Julia Smith and Laura Burrus, my previous advisors. Laura and Julia never gave up on me and provided so much support to me throughout the many years I have known them. I never would have completed my bachelor's degree, found my passion for science, or survived my first year at UCSF without them.

To the Holy Names University faculty. I specifically want to mention Ian Sammis, Dolores Grunbaum, and Vanessa Handley. These three faculty members positively impacted me during my time as an undergraduate student at Holy Names University. They had high expectations of me, and all their students, which I appreciated. They helped me discover my capabilities.

To the faculty and staff at San Francisco State University. I specifically want to mention Teaster Baird, Megumi Fuse, Blake Riggs, and Lisa Galli. All of these individuals provided a significant amount of support while I was a Master's student at San Francisco State University and/or when I transitioned to UCSF for my PhD.

To Toni Hurly, who was more than the Tetrad Program Coordinator. I struggled significantly during my first year as a graduate student at UCSF and she was so nurturing and made me feel seen.

To Carol Gross, my unofficial mentor and cheerleader. Carol Gross helped me feel like I wasn't alone. She ensured I received the support I needed in order to thrive at UCSF. I appreciate all that she has done to support me when I was struggling the most.

To Olivia Roberson for being you. Olivia provided me so much support while I was in the darkest place.

To D'anne Duncan for being a great support system in so many ways. There are not enough words to describe how grateful I am to receive all the support and care from you.

To Geeta Narlikar, my thesis advisor. Geeta showed me that you can be a brilliant, rigorous scientist and a great mother all at the same time. Thank you for being a person I can look up to and providing me the opportunity to thrive at UCSF.

To Laura Hsieh, my lab mentor and friend. She swindled me into this project and I will forever be grateful for all that she has done support my growth and development both as a scientist and

"normal person." Our friendship was unexpected, but one of the best things that came out of my experiences at UCSF.

To Malik Byers and the King Family. They are the family I needed to complete my goals. I am honored they made me a part of their village. A special thank you to Malik for putting us all together. Malik and his family did so much to ensure that I completed my goals, as if they were their own.

To my mother, Marie Gracia. Her high expectations of me, forced me to continuously reach for the stars. She taught me there are no challenges I cannot overcome.

To my sisters, Dominique Labossiere and Marie Gourdet. A special shout out to my big sister for providing with support and guidance. You are truly my best gym buddy and best friend.

To my daughter, Assata Byers. Her love and support drove me to complete all my goals. We earned this PhD together.

Contributions

Statement from the research adviser, Geeta J. Narlikar

Chapter 2 is based on the following publication: A hexasome is the preferred substrate for the INO80 chromatin remodeling complex, allowing versatility of function (2022) *Molecular Cell* 82, 2098–2112. The authors are: Laura J Hsieh, Muryam A Gourdet, Camille M Moore, Elise N Muñoz, Nathan Gamarra , Vijay Ramani , Geeta J Narlikar.

The student, Muryam A Gourdet is a co-first author on this manuscript having contributed equally as Laura J. Hsieh. In this work Muryam made the key observation that hexasomes are better substrates of INO80 than nucleosomes. She also made major contributions to the overall conceptualization of the project, along with L.J.H., and G.J.N.; to the methodology along with L.J.H., and G.J.N.; to the overall investigation of the results with L.J.H., M.A.G., E.N.M., and N.G.; and to the writing with L.J.H., and G.J.N. The work in this paper is of the the technical quality and scientific impact required for a thesis in the Tetrad graduate program.

Characterizing the Mechanism of the INO80 family Chromatin

Remodeling Machine

By Muryam Abiola Adoma Gourdet

Abstract

DNA encodes the genetic material to instruct all cellular processes and to establish cellular identity. Cellular identity is established by both genetic content and regulation of gene expression. In eukaryotes, gene expression is regulated by many factors including chromatin structure. Chromatin structure consists of nucleosomes, comprised of ~150 bp of DNA wrapped around a histone octamer. This structure regulates several DNA dependent processes including transcription and DNA damage repair. Understanding the mechanisms that regulate chromatin structure is key to understanding how biological systems are controlled in the cell.

DNA dependent cellular process are known to be regulated by chromatin remodelers. Chromatin remodelers couple the energy of ATP hydrolysis to slide nucleosomes, transfer histones, and/or distort the octamer— activities that are essential to regulate the chromatin state. A unique chromatin remodeler, INO80, requires both the RecA-like ATPase and accessory subunits to slide nucleosomes *in vitro*. *In vivo*, INO80 plays a role in both DNA damage repair and transcription. However, it is unclear how INO80 sliding activity contributes to its diverse biological roles. Recent work from our lab revealed the following about INO80 mechanism: (1) INO80 is regulated by two nucleosome cues: flanking DNA length and the H2A-

2B dimer acidic patch on the histone octamer; (2) INO80 remodeling reaction has at least one intermediate state and transition of this intermediate to a slid product is regulated by DNA length; (3) the Nhp10 accessory module regulates the transition between the intermediate state and the slid product. Others have shown that both Nhp10 and Arp8 modules recognize DNA. The Arp8 module alters how INO80 engages both the DNA and histones of the nucleosome, specifically altering how the Arp5 module engages the H2A-H2B dimer. Cryo-EM structures revealed that the Arp5 and Ies2 modules engage the H2A-H2B dimer acidic patch. It wasn't clear if the engagement of both Arp5 and Ies2 with the two respective H2A-H2B dimer acidic patches was required for INO80 remodeling. In this thesis, we investigated the requirement of the Arp5-H2A-H2B-acidic patch interaction versus the Ies2-H2A-H2B-acidic patch interaction in INO80 remodeling. We discovered that only the Arp5-H2A-H2B acidic patch interaction was required for INO80 remodeling and contributed to the generation of a nucleosome intermediate. Others have also shown that INO80 preferentially acts on nucleosome containing H2A.Z-H2B dimer, which has a more expansive acidic patch. H2A.Z-H2B containing nucleosomes are present during transcription. As INO80 acts during transcription, what alternative substrates generated during transcription could INO80 act on? Others have shown that hexasomes, nucleosomes missing one H2A-H2B dimer, are generated by polymerase during transcription. In this thesis, we further investigated the role INO80 plays in remodeling hexasomes. We identified that INO80 not only regulates hexasome positions in yeast, but INO80 is also preferentially stimulated by hexasomes. Surprisingly, the dimer missing in the hexasome is the dimer Arp5 contacts in the nucleosome. This led us to hypothesize that Arp5 must make alternative contacts on the hexasome, that allow INO80 to be more active. In this thesis, we additionally obtained the structure of INO80 bound to a hexasome. We showed that not only does Arp5 make alternative contacts with the H3-H4 tetramer, but the Ino80 ATPase engages the hexasome at SHL-2, which reflects a ~180° rotation compared to the nucleosome. Most remodelers bind at SHL2 of the nucleosome. This provides an explanation for why INO80 is

more active on a hexasome compared to a nucleosome. We hypothesize that INO80 generates a hexasome-like intermediate while remodeling a nucleosome. We speculate that Ino80 migrates from SHL-7/-6 towards SHL-2 on path to remodeling a nucleosome. Overall this thesis highlights the versatility with which remodelers like INO80 act on various substrates. Such versatility which may allow INO80 to act in diverse processes in vivo.

Table of Contents

List of Figures

List of Tables

Chapter 1: Introduction

1) Chromatin regulates cellular health

The development of multicellular organisms, such as humans, is a highly regulated process. The genetic information that dictates how an organism develops and functions is encoded in the form of DNA. Packaging of DNA in the form of chromatin allows regulation of all processes that require access to genetic information. The smallest unit of chromatin is the nucleosome in which ~150 bp of DNA is wrapped around a histone octamer consisting of two H2A/H2B dimers and one H3/H4 tetramer (Figure 1.1A). The wrapped DNA can be divided into waypoints at superhelical locations across the surface of the histone octamer, which are mirrored on opposing faces(1) (Figure 1.1A). The nucleosome acts as a barrier to transcription because the histone octamer interactions with the DNA make those regions inaccessible. Furthermore, inter-nucleosomal interactions in collaboration with other factors result in higher order chromatin compaction. Different degrees of compaction result in regions that are transcriptionally inactive and active, termed heterochromatin and euchromatin, respectively. Heterochromatic regions contain densely compacted nucleosomes, which limit access to DNA, and prevent recruitment of factors essential for transcription (Figure 1.1B). Contrarily, euchromatic regions contain less densely compacted nucleosomes, allowing the DNA to be more accessible for transcription (Figure 1.1B). During transcription, chromatin structure is continuously modified by covalent and non-covalent modifications. Non-covalent conformational changes of nucleosomes expose specific genetic regions and allow DNA-interacting proteins to access the DNA(2). This requires the hydrolysis of ATP by ATP-dependent chromatin remodeling enzymes to transform nucleosome structure(2).

ATP-dependent chromatin remodelers play a critical role in establishing the overall chromatin structure. These enzymes carry out different functions that are important in biological processes such as DNA damage repair and transcription. Mutations in these enzymes have been implicated in various cancers consistent with their important roles in DNA dependent processes(3). Although

2

many studies have demonstrated that chromatin remodelers are key regulators of chromatin, their mechanisms remain ill-defined.

2) Chromatin remodelers are highly conserved regulatory machines.

ATP-dependent chromatin remodelers are highly conserved regulators of chromatin structure. ATP-dependent chromatin remodelers are members of the Superfamily II nucleic acid translocases, and all share an evolutionary related ATPase subunit composed of two RecA fold lobes(2). Differences in the sequence of this ATPase subunit divide chromatin remodelers into four different families: CHD (chromodomain, helicase, DNA binding), SWI/SNF (switching defective/sucrose nonfermenting), ISWI (imitation switch), and INO80 (inositol requiring 80)(2). However, distinct non-catalytic accessory domains confer specific properties on different remodelers. These complexes transform the nucleosome in various ways including sliding an intact histone octamer, disassembling an intact histone octamer, exchanging histone variants, and altering the nucleosome conformation (Figure 1.1C). The majority of remodelers are involved in sliding an intact histone octamer on DNA in vitro(2). However, in vivo, these remodelers contribute to different biological processes to regulate genome architecture through distinct mechanisms.

Differences in the accessory subunits of each chromatin remodeler may regulate substrate recognition and activity. Biochemical studies have begun to interrogate the role of the accessory subunits in contributing to the unique core functions of chromatin remodelers. Thus, it is essential to further understand the biochemical basis for chromatin remodeler mechanisms to suggest models for how their activities could be regulated during transcription and other DNA dependent processes.

3

3) INO80: Unlike the rest?

Recent work suggests that the subunit differences between chromatin remodelers include sequence motifs with autoregulatory functions essential for substrate recognition and the remodeling outcome. The INO80 family of chromatin remodelers is unique compared to other classes of remodelers, because the RecA-like lobes in the ATPase are interrupted with a large insertion domain (~ 300 amino acids)(2). Contrary to other remodeling families, the INO80 family requires their accessory subunits for their core activity. The INO80 class contains two members, the INO80 complex (INO80) and the SWR complex (SWR) (Figure 1.2). Interestingly, despite belonging to the same family and playing overlapping in vivo roles in DNA damage and transcription, INO80 and SWR execute different functions in vitro. INO80 primarily slides nucleosomes while SWR unidirectionally exchanges canonical H2A/H2B dimers with variant H2A.Z/H2B dimers(4–6) (Figure 1.2B). Although SWR and INO80 have such distinct biochemical functions, they share core architectural features including homologous non-catalytic subunits. The insertion domain, unique to the INO80 family, recruits the Rvb1/2 AAA+ ATPases and the core non-catalytic subunits. Cryo-electron microscopy (cryo-EM) structures of INO80 and SWR bound to nucleosomes, revealed that despite structural similarities they engage the substrate through distinct interactions(7–9) (Figure 1.2C). SWR, like most other ATP-dependent chromatin remodelers, interacts with nucleosome at superhelical location SHL2 (9) (Figure 1.2C). Surprisingly, INO80 binds to nucleosomes at SHL-6/7, which suggests that INO80 employs a distinct mechanism for moving DNA across the octamer surface(7, 8) (Figure 1.2C). This raises the question of what makes INO80 so unique compared to other remodelers, including its own family member SWR?

4) Previous biochemical and structural studies of INO80

INO80 is a large, ~1MDa, multisubunit complex, composed of several non-catalytic subunits that form the following functional modules: Nhp10, Arp8, Arp5 and, Ies2 modules(7, 8, 10) (Figure 1.2A). Cryo-EM studies on nucleosomes with flanking DNA on only one side revealed that the INO80 complex asymmetrically engulfs the nucleosome with the support of the non-catalytic subunits(7, 8). INO80 makes extensive contacts with the flanking DNA, core DNA, and histone octamer(7, 8, 11, 12). The Arp5 module contacts the SHL-3 region of the core nucleosomal DNA(7). Furthermore, the Ino80 ATPase contacts SHL-6/7 near the flanking DNA, where the DNA is peeled away from the histone octamer core(7, 8, 12). Flanking DNA length regulates INO80's activity by promoting binding to nucleosomes(13) and regulating its sliding activity(14) (Figure 1.3A). Previously our lab showed that INO80 does not efficiently slide nucleosomes with 40bp of flanking DNA or less(14). However, by increasing the flanking DNA length to 80 bp, a 300-fold increase is observed in INO80's sliding activity (Figure 1.3A). Interestingly, altering the flanking DNA length from 40 to 80 bp only had a minor effect on its ATPase activity. This data led to a model where INO80 generates a nucleosome intermediate prior to nucleosome sliding. Surprisingly, reducing flanking DNA length only modestly decreased INO80's ability to form the nucleosome intermediate. As a result, we hypothesized that INO80's remodeling activity consists of at least two steps: (1) forming at least one nucleosome intermediate and (2) sliding the nucleosome. In addition, we hypothesized that the flanking DNA length dependence occurs in step 2 (Figure 1.3A).

The Ino80 ATPase, Arp8 and Nhp10 modules, all make contacts with the flanking DNA(10, 12). The Arp8 and Nhp10 modules, when purified in isolation from the INO80 complex can interact with DNA(10). Previous work from our lab revealed that the Nhp10 module negatively regulates INO80's sliding activity(14). Deletion of Nhp10, abolishes length sensing by INO80, and rescues

sliding of nucleosomes with 40bp of flanking DNA by ~100 fold(14). This result highlights that the Nhp10 module has a role in inhibiting INO80's sliding activity on nucleosomes with short flanking DNA. The Arp8 module, coordinates INO80's nucleosome contacts, as it directly interacts with the helicase SANT-associated (HSA) domain of the ATPase(10, 15). The HSA domain is a known DNA binding domain(15, 16). Therefore, the Arp8 module was proposed to contribute to flanking DNA binding by Ino80(12, 15, 16). Deleting the N-terminal domain of Arp8 to break Arp8's contacts with DNA alters how the Nhp10 module and Ino80 ATPase engage flanking DNA(12). Interestingly, altering these contacts also affects how the INO80 complex contacts the histone octamer(12). This highlights how the modules coordinate their contacts with all components of the nucleosome, the DNA and the histones (Figure 1.3).

In addition to flanking DNA, INO80 makes extensive contacts with the histone octamer, specifically with the H2A-H2B acidic patch(7, 8). The acidic patch is a highly negatively charged region between H2A and H2B and plays an essential role in many chromatin remodelers activity(7, 17–20). A major role for the acidic patch is maintained for INO80 as mutating the H2A/B acidic patches reduces its sliding activity by 100-fold(19). Cryo-EM studies reveal that the two nucleosomal acidic patches make contacts with the Arp5 and Ies2 modules(7, 8). How these two interactions contribute to INO80's remodeling activity remains elusive (Figure 3C).

The Ies2 module wraps around the nucleosome and contacts the acidic patch distal to the flanking DNA(7). Structural studies show that Ies2 also makes contacts with multiple components of INO80(7, 10). The Ies2 module plays a key role in maintaining the INO80 complex. Upon deletion of Ies2, the INO80 complex loses Ies2 and the Arp5 module(21). The Arp5 module engages the dimer acidic patch proximal to the flanking DNA and contacts the nucleosomal DNA between SHL-2 and SHL-3(7). The Arp5 subunit of the Arp5 module contains a domain called the grappler. The Arp5 grappler bridges the Arp5 module contacts between the nucleosomal DNA and the

6

dimer(7). The Arp5 grappler adopts two conformations, the open and closed state. In the closed state, the Arp5 module binds to nucleosomal DNA near the dyad, flanking DNA at SHL-7.5 and the acidic patch(7). In the open state, the Arp5 grappler contacts the DNA at SHL-1 and the exit DNA (7). In this conformation, the Arp5 module may block movement of the exit DNA. Based on biochemical and structural insights into the Arp5 module, it is hypothesized that the Arp5 module couples ATPase activity to sliding by gripping onto the octamer and DNA. Maintaining this hold allows for a ratcheting translocation step that is on path to generate a slid nucleosome. The Arp5 module's engagement of the nucleosome is hypothesized to be critical in allowing nucleosome sliding (7, 10). Furthermore, mutations in Arp8 affect how other subunits of INO80 engage the histones (12). Specifically, deletion of the N-terminal extension of Arp8 alters how Arp5 engages the H2A-H2B dimer (12). This provides evidence the Arp8 module may coordinate how other non-catalytic subunits engage the nucleosome. Since Arp8 makes contacts with the flanking DNA, does the Arp8 module contribute to flanking DNA length sensing by INO80 (Figure 1.3B)? Does the Arp8 module couple DNA length sensitivity to activation of the Ino80 ATPase? Further work needs to be done to understand how the Arp8 module contributes to INO80's sliding activity.

5) Open questions in INO80 mechanism.

A huge conundrum in the field is how INO80's biochemical activity relates to it's in vivo function. Previous data has shown that INO80 is involved in nucleosome positioning at the +1 position and into the gene body (22–25). The DNA flanking the +1 nucleosome exceeds 40 bp, however the spacing between nucleosomes in the gene body is approximately 20 bps (26) (Figure 1.4A). This raises the question of how INO80 remodels nucleosomes in the gene body when biochemically it does not efficiently remodel nucleosomes with 40bp or less of flanking DNA. Removal of some non-catalytic subunits (i.e., Nhp10), relieves this inhibition on nucleosomes with shorter flanking DNA lengths. Therefore, one possibility is that INO80 can exist in subcomplexes in vivo, thereby

modulating its activity based on nucleosome density. Another possibility is that the features of the nucleosomes vary in vivo which relieves INO80's autoinhibitory action. How can these substrates vary in vivo? Various factors change histone composition by exchanging canonical histones for non-canonical histones that alter the surface features and dynamics of the nucleosome. One prevalent non-canonical histone is H2A.Z. H2A.Z is found at promoters and can be deposited by SWR and histone chaperones (6, 27)(Figure 1.4B). This variant contains an extended dimer acidic patch, which has been shown to promote INO80's sliding activity(7). In addition to having an extended dimer acidic patch, others have suggested that nucleosomes containing H2A.Z are less stable(28). Structural analysis suggests H2A.Z dimers have fewer stabilizing interactions with the DNA allowing the dimer to more readily dissociate from the nucleosome (28, 29). Does INO80 act better on H2A.Z nucleosomes it because the histone acidic patch of H2A.Z-H2B dimers is more extended, or is it because this dimer is less stably bound (Figure 1.4C)? What alternative substrates can INO80 act on? Are other noncanonical substrates preferred by INO80 (Figure 1.4E)? There has been increasing evidence that subnucleosomal particles exist in vivo(30, 31). These subnucleosomal particles typically are missing one H2A/H2B dimer(30). These can be generated by factors such as histone chaperones. Additionally, during transcription, RNA polymerase generates hexasomes in gene bodies and repositions these products(30) (Figure 1.4D). Could INO80 act on these hexasome particles (Figure 1.4E)? If so, is this how INO80 regulates nucleosomal positions within the gene body?

Chapters 2-4 address various aspects of these open questions.

Figures
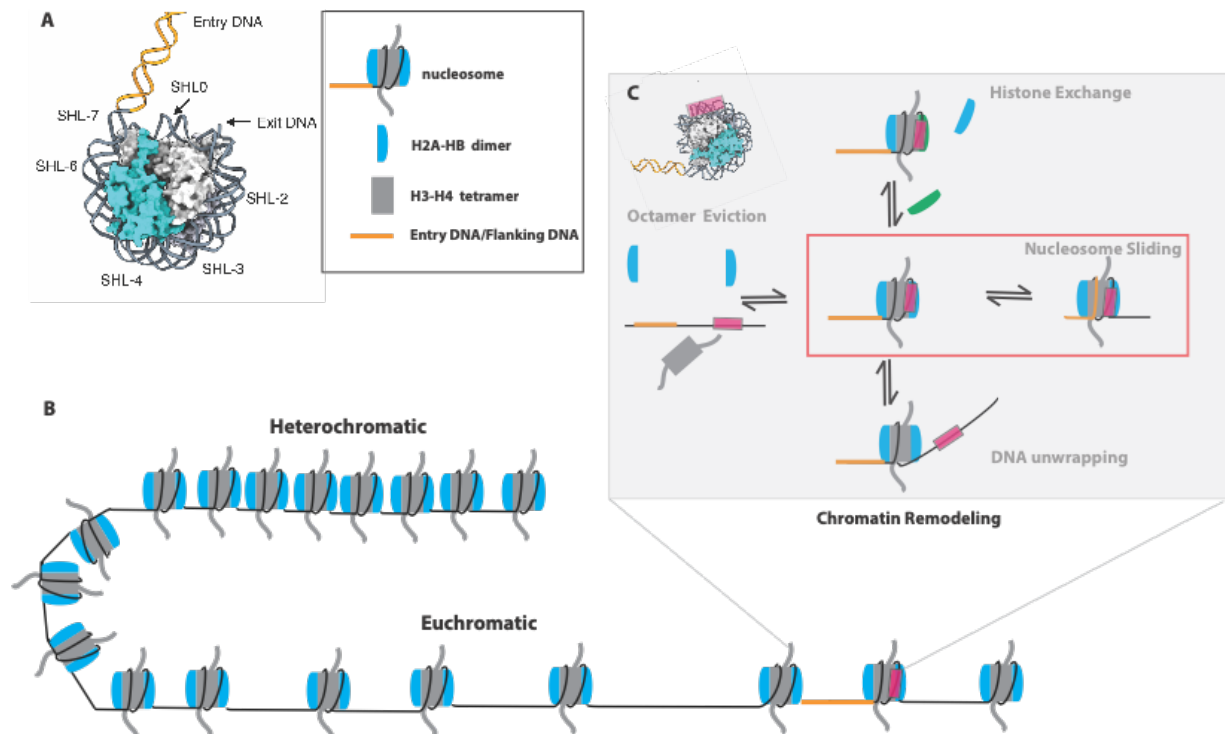
Figure 1.1. Chromatin organization.
A) Nucleosomes are composed of two H2A-H2B dimers (in blue) and one H3-H4 tetramer (grey). Approximately ~150bp of DNA wraps around the histone octamer core. This DNA is divided into "waypoints" called Super Helical Locations (SHL). Entry/flanking DNA (in orange) extends beyond SHL-7. B) This cartoon shows the organization of the chromatin structure. Regions in which nucleosome packaging is condensed or relaxed, are referred to as heterochromatic and euchromatic regions, respectively. C) A cartoon showing the different ways chromatin remodelers noncovalently modify nucleosomes (octamer eviction, histone exchange, DNA unwrapping, and nucleosome sliding).
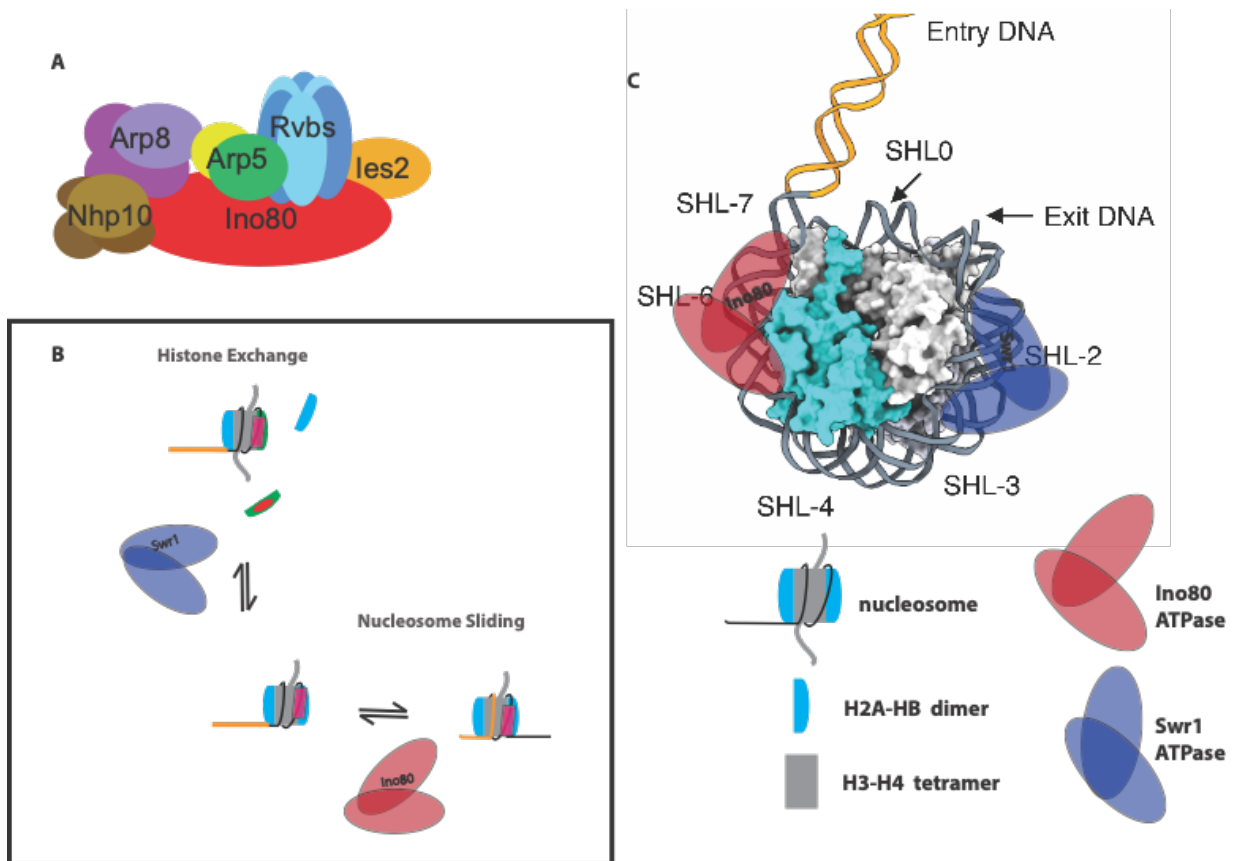
Figure 1.2. INO80 Family: INO80 and SWR
The INO80 family is composed of the multi-subunit complexes INO80 and SWR. A) This cartoon of INO80, demonstrates how multiple non-catalytic subunits interact with the Ino80 ATPase. B) INO80 and SWR function differently biochemically. INO80 primally slides nucleosomes, while SWR exchanges the canonical H2A-H2B dimer for the H2A.Z-H2B variant (in green and red). C) The Ino80 ATPase (red) engages the nucleosome at SHL-7/-6, while theSwr1 ATPase (dark-blue) engages at SHL2.
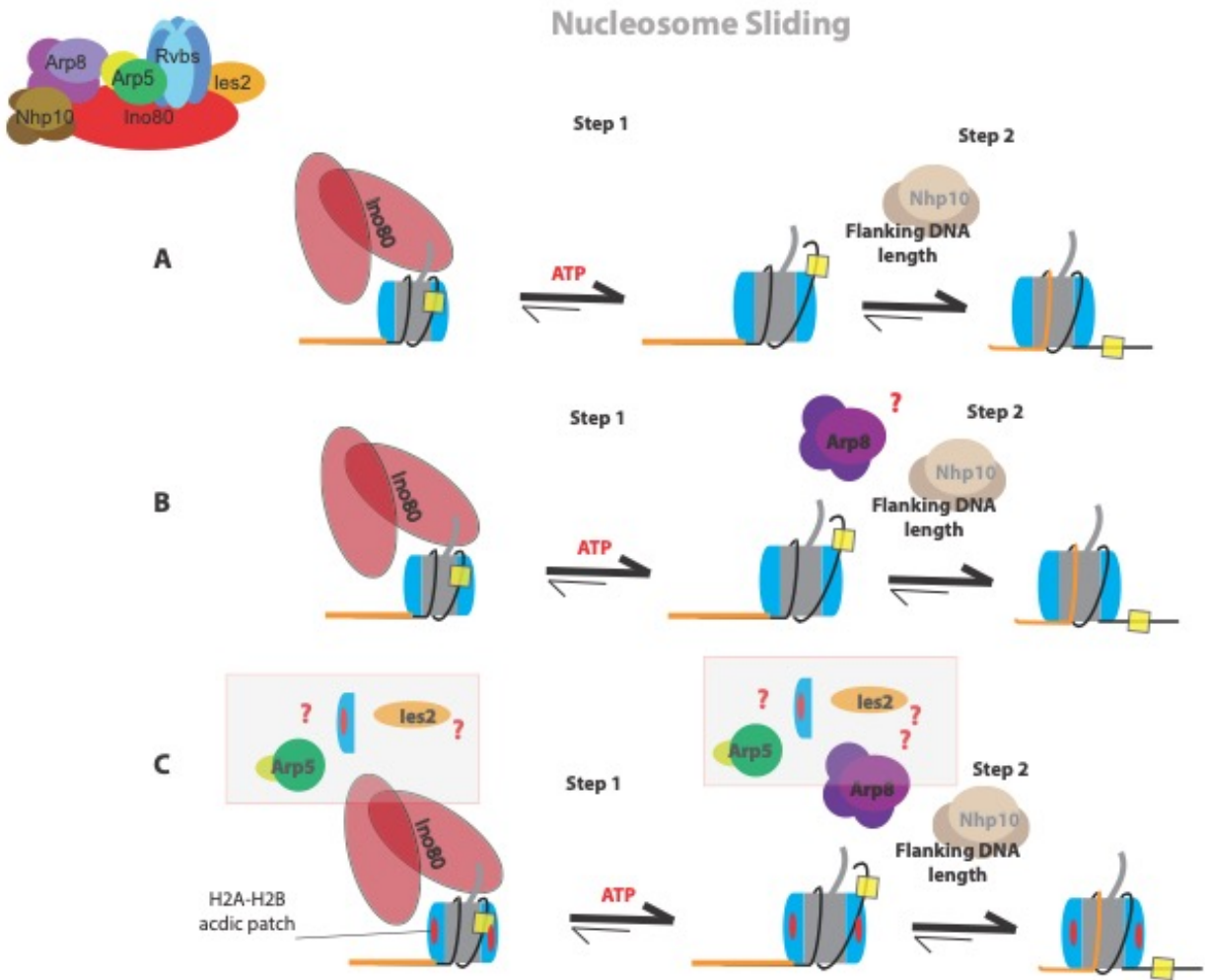
Figure 1.3. Mechanisms that regulate INO80 nucleosome sliding activity
INO80 nucleosome sliding contains at least two steps, (1) generation of nucleosome intermediate and (2) nucleosome sliding. These steps are uniquely regulated. A) Step 2, nucleosome sliding, is regulated by flanking DNA length. Nucleosome sliding is inhibited on nucleosomes with <40bp flanking DNA. Removing Nhp10 module rescues this inhibition, so Nhp10 may contribute to Step2 of INO80 nucleosome remodeling. B). The Arp8 module recognizes DNA. The Arp8 module coordinates how the Nhp10 module and Ino80 ATPase contacts the nucleosome flanking DNA. The Arp8 module may contribute to Step2. C) INO80 nucleosome sliding is stimulated by the H2A-H2B acidic patch. It is not clear which step requires the H2A-H2B acidic patch. The Arp5 and Ies2 modules makes contacts with this acidic patch. It is not clear if both contacts are required to stimulate INO80 sliding activity.
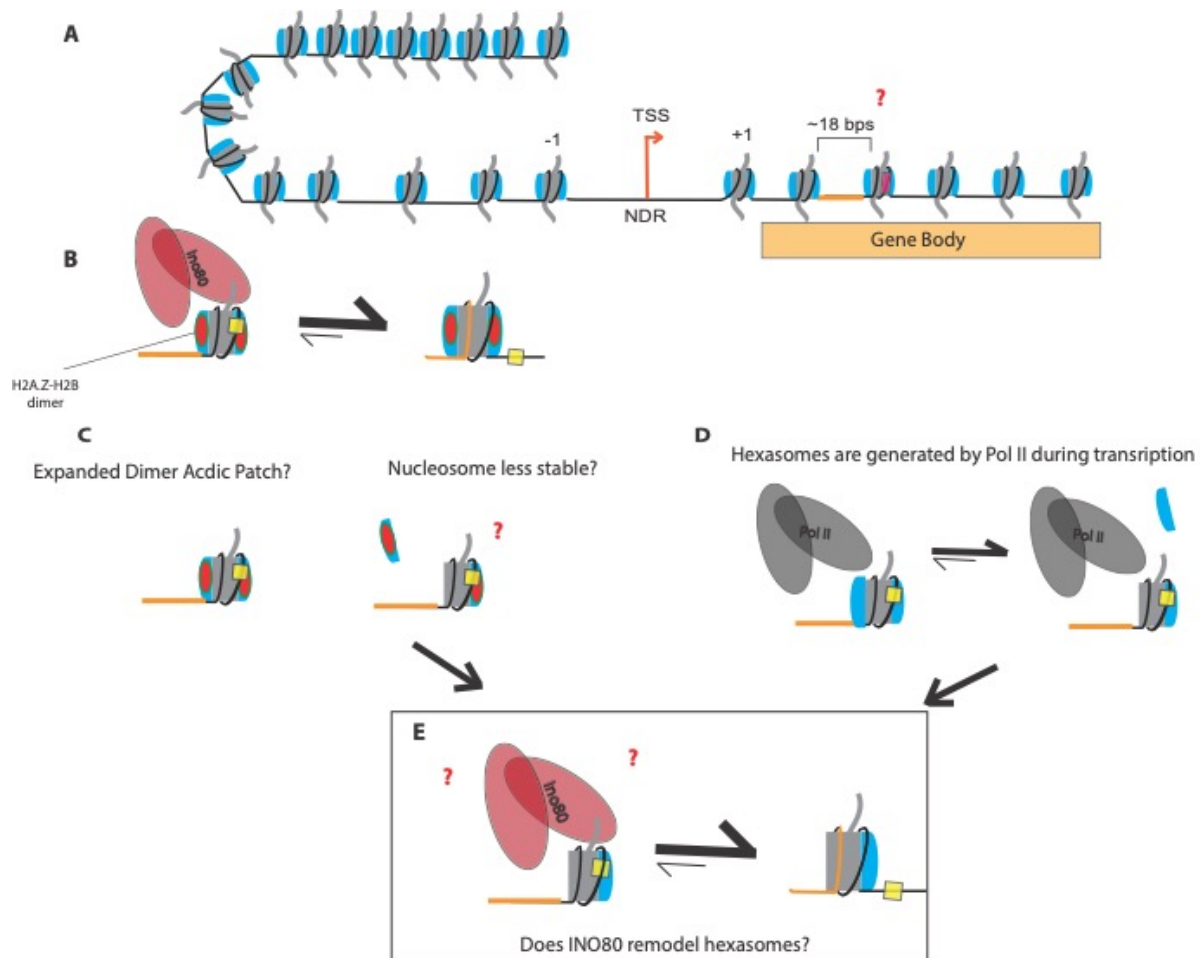
Figure 1.4. Open questions about INO80 action
A) INO80 regulates nucleosome positions in gene bodies, despite only ~18bp of DNA between the nucleosomes. It is not clear how INO80 can act on these nucleosomes, while biochemically INO80 cannot effeciently remodel nucleosomes with <40bp flanking DNA. INO80 is localized at genes during active transcription. During active transcription, H2A.Z-H2B dimers are deposited. B) INO80 sliding activity is increased with nucleosomes with H2A.Z-H2B dimers. C) H2A.Z-H2B dimers have an expanded acidic patch and are proposed make less stable contacts with the H3-H4 tetramer. Is INO80 more active on H2A.Z-H2B containing nucleosomes because (i) the expanded acidic patch or (ii) the instablilty between H2A.Z-H2B and H3-H4? C) During active transcription, RNA polymerase generates hexasomes. E) If hexasomes are generated either by destabilized H2A.Z-H2B nucleosomes or by RNA Polymerase, could the hexasome be a substrate for INO80?

References

1. K. Luger, A. W. Mäder, R. K. Richmond, D. F. Sargent, T. J. Richmond, Crystal structure of the nucleosome core particle at 2.8 Å resolution. Nature. 389, 251–260 (1997).

2. C. Y. Zhou, S. L. Johnson, N. I. Gamarra, G. J. Narlikar, Mechanisms of ATP-Dependent Chromatin Remodeling Motors. Annu Rev Biophys. 45, 153–181 (2016).

3. S. S. Nair, R. Kumar, Chromatin remodeling in Cancer: A Gateway to regulate gene Transcription. Mol Oncol. 6, 611–619 (2012).

4. X. Shen, G. Mizuguchi, A. Hamiche, C. Wu, A chromatin remodelling complex involved in transcription and DNA processing. Nature. 406, 541–544 (2000).

5. X. Shen, R. Ranallo, E. Choi, C. Wu, Involvement of Actin-Related Proteins in ATP-Dependent Chromatin Remodeling. Mol Cell. 12, 147–155 (2003).

6. G. Mizuguchi, X. Shen, J. Landry, W.-H. Wu, S. Sen, C. Wu, ATP-Driven Exchange of Histone H2AZ Variant Catalyzed by SWR1 Chromatin Remodeling Complex. Science. 303, 343–348 (2004).

7. S. Eustermann, K. Schall, D. Kostrewa, K. Lakomek, M. Strauss, M. Moldt, K.-P. Hopfner, Structural basis for nucleosome remodeling by the INO80 complex. Nature. 556, 386–390 (2018).

8. R. Ayala, O. Willhoft, R. J. Aramayo, M. Wilkinson, E. A. McCormack, L. Ocloo, D. B. Wigley, X. Zhang, Structure and regulation of the human INO80–nucleosome complex. Nature. 556, 391–395 (2018).

9. O. Willhoft, M. Ghoneim, C.-L. Lin, E. Y. D. Chua, M. Wilkinson, Y. Chaban, R. Ayala, E. A. McCormack, L. Ocloo, D. S. Rueda, D. B. Wigley, Structure and dynamics of the yeast SWR1-nucleosome complex. Science. 362 (2018), doi:10.1126/science.aat7716.

10. A. Tosi, C. Haas, F. Herzog, A. Gilmozzi, O. Berninghausen, C. Ungewickell, C. B. Gerhold, K. Lakomek, R. Aebersold, R. Beckmann, K.-P. Hopfner, Structure and Subunit

Topology of the INO80 Chromatin Remodeler and Its Nucleosome Complex. Cell. 154, 1207–1219 (2013).

11. S. Brahma, M. I. Udugama, J. Kim, A. Hada, S. K. Bhardwaj, S. G. Hailu, T.-H. Lee, B. Bartholomew, INO80 exchanges H2A.Z for H2A by translocating on DNA proximal to histone dimers. Nat Commun. 8, 15616 (2017).

12. S. Brahma, M. Ngubo, S. Paul, M. Udugama, B. Bartholomew, The Arp8 and Arp4 module acts as a DNA sensor controlling INO80 chromatin remodeling. Nat Commun. 9, 3309 (2018).

13. M. Udugama, A. Sabri, B. Bartholomew, The INO80 ATP-Dependent Chromatin Remodeling Complex Is a Nucleosome Spacing Factor. Mol Cell Biol. 31, 662–673 (2011).

14. C. Y. Zhou, S. L. Johnson, L. J. Lee, A. D. Longhurst, S. L. Beckwith, M. J. Johnson, A. J. Morrison, G. J. Narlikar, The Yeast INO80 Complex Operates as a Tunable DNA Length-Sensitive Switch to Regulate Nucleosome Sliding. Mol Cell. 69, 677-688.e9 (2018).

15. K. R. Knoll, S. Eustermann, V. Niebauer, E. Oberbeckmann, G. Stoehr, K. Schall, A. Tosi, M. Schwarz, A. Buchfellner, P. Korber, K.-P. Hopfner, The nuclear actin-containing Arp8 module is a linker DNA sensor driving INO80 chromatin remodeling. Nat Struct Mol Biol. 25, 823–832 (2018).

16. R. Bakshi, T. Prakash, D. Dash, V. Brahmachari, In silico characterization of the INO80 subfamily of SWI2/SNF2 chromatin remodeling proteins. Biochem Bioph Res Co. 320, 197–204 (2004).

17. H. T. Dao, B. E. Dul, G. P. Dann, G. P. Liszczak, T. W. Muir, A basic motif anchoring ISWI to nucleosome acidic patch regulates nucleosome spacing. Nat Chem Biol. 16, 134–142 (2020).

18. A. M. Valencia, C. K. Collings, H. T. Dao, R. St. Pierre, Y.-C. Cheng, J. Huang, Z.-Y. Sun, H.-S. Seo, N. Mashtalir, D. E. Comstock, O. Bolonduro, N. E. Vangos, Z. C. Yeoh, M. K.

Dornon, C. Hermawan, L. Barrett, S. Dhe-Paganon, C. J. Woolf, T. W. Muir, C. Kadoch, Recurrent SMARCB1 Mutations Reveal a Nucleosome Acidic Patch Interaction Site That Potentiates mSWI/SNF Complex Chromatin Remodeling. Cell. 179, 1342-1356.e23 (2019).

19. N. Gamarra, S. L. Johnson, M. J. Trnka, A. L. Burlingame, G. J. Narlikar, The nucleosomal acidic patch relieves auto-inhibition by the ISWI remodeler SNF2h. Elife. 7, e35322 (2018).

20. R. F. Levendosky, G. D. Bowman, Asymmetry between the two acidic patches dictates the direction of nucleosome sliding by the ISWI chromatin remodeler. Elife. 8, e45472 (2019).

21. W. Yao, S. L. Beckwith, T. Zheng, T. Young, V. T. Dinh, A. Ranjan, A. J. Morrison, Assembly of the Arp5 (Actin-related Protein) Subunit Involved in Distinct INO80 Chromatin Remodeling Activities*. J Biol Chem. 290, 25700–25709 (2015).

22. A. Klein-Brill, D. Joseph-Strauss, A. Appleboim, N. Friedman, Dynamics of Chromatin and Transcription during Transient Depletion of the RSC Chromatin Remodeling Complex. Cell Reports. 26, 279-292.e5 (2019).

23. N. Krietenstein, M. Wal, S. Watanabe, B. Park, C. L. Peterson, B. F. Pugh, P. Korber, Genomic Nucleosome Organization Reconstituted with Pure Proteins. Cell. 167, 709-721.e12 (2016).

24. W. Yao, D. A. King, S. L. Beckwith, G. J. Gowans, K. Yen, C. Zhou, A. J. Morrison, The INO80 Complex Requires the Arp5-Ies6 Subcomplex for Chromatin Remodeling and Metabolic Regulation. Mol Cell Biol. 36, 979–991 (2016).

25. K. Yen, V. Vinayachandran, B. F. Pugh, SWR-C and INO80 Chromatin Remodelers Recognize Nucleosome-free Regions Near +1 Nucleosomes. Cell. 154, 1246–1256 (2013).

26. T. N. Mavrich, I. P. Ioshikhes, B. J. Venters, C. Jiang, L. P. Tomsho, J. Qi, S. C. Schuster, I. Albert, B. F. Pugh, A barrier nucleosome model for statistical positioning of nucleosomes throughout the yeast genome. Genome Res. 18, 1073–1083 (2008).

27. D. N. Bagchi, A. M. Battenhouse, D. Park, V. R. Iyer, The histone variant H2A.Z in yeast is almost exclusively incorporated into the +1 nucleosome in the direction of transcription. Nucleic Acids Res. 48, 157–170 (2020).

28. R. K. Suto, M. J. Clarkson, D. J. Tremethick, K. Luger, Crystal structure of a nucleosome core particle containing the variant histone H2A.Z. Nat Struct Biol. 7, 1121–1124 (2000).

29. C. Jin, G. Felsenfeld, Nucleosome stability mediated by histone variants H3.3 and H2A.Z. Gene Dev. 21, 1519–1529 (2007).

30. S. Ramachandran, K. Ahmad, S. Henikoff, Transcription and Remodeling Produce Asymmetrically Unwrapped Nucleosomal Intermediates. Mol Cell. 68, 1038-1053.e4 (2017).

31. H. S. Rhee, A. R. Bataille, L. Zhang, B. F. Pugh, Subnucleosomal Structures and Nucleosome Asymmetry across a Genome. Cell. 159, 1377–1388 (2014).

Chapter 2: A hexasome is the preferred substrate for the INO80 chromatin remodeling complex, allowing versatility of function.

Abstract

The critical role of the INO80 chromatin-remodeling complex in transcription is commonly attributed to its nucleosome sliding activity. Here we've found that INO80 prefers to mobilize hexasomes over nucleosomes. INO80's preference for hexasomes reaches up to ~60-fold when flanking DNA overhangs approach the ~18 bp linkers in yeast gene bodies. Correspondingly, deletion of INO80 significantly affects the positions of hexasome-sized particles within yeast genes in vivo. Our results raise the possibility that INO80 promotes nucleosome sliding by dislodging an H2A/H2B dimer, thereby making a nucleosome transiently resemble a hexasome. We propose that this mechanism allows INO80 to rapidly mobilize nucleosomes at promoters and hexasomes within gene bodies. Rapid repositioning of hexasomes that are generated in the wake of transcription may mitigate spurious transcription. More generally, such versatility may explain how INO80 regulates chromatin architecture during the diverse processes of transcription, replication, and repair.

Introduction

In eukaryotes, most DNA dependent processes have to contend with chromatin. The most prevalent building block of chromatin is a nucleosome, which is composed of ~147 bp of DNA wrapped around a histone octamer containing two H2A/H2B dimers and an H3/H4 tetramer. Several studies indicate that the octameric histone composition changes during processes such as transcription and replication, which require transient disruption of histone-DNA contacts(*1*). In particular, transcription results in accumulation of subnucleosomal particles, many of which are hexasomes that are missing a single H2A/H2B dimer (*2*). Extensive work has addressed how nucleosome positions are regulated during transcription (*3–6*). In comparison, whether and how hexasome positions are regulated is poorly understood.

18

Nucleosome positions during transcription are regulated by ATP-dependent chromatin remodeling enzymes, which can evict octamers, exchange histones, and distort and slide the histone octamer(7). These highly conserved enzymes often fall into four main classes, ISWI, SWI/SNF, CHD and INO80. Together these enzymes collaborate to maintain a nucleosome depleted region (NDR) at promoters and specific nucleosome positions in the gene body (Figure 2.1A) (8, 9). In vitro, enzymes from these different classes such as *S. cerevisiae* Chd1, INO80 and ISW2 superficially show a similar ability to slide nucleosomes (10). Yet in vivo, these enzymes play non-overlapping roles. In such comparisons, it is commonly assumed that nucleosomes are the preferred substrates. Indeed, specific features of nucleosomes are recognized by these enzymes, such as the length of the DNA overhang flanking a nucleosome, an acidic patch found on the H2A/H2B dimer and histone post-translational modifications (10, 11). Amongst these features, interactions with the acidic patch play a significant role in nucleosome remodeling by the ISWI, SWI/SNF, CHD and INO80 classes of enzymes (12–16). At the same time however, the prevalence of subnucleosomal particles in vivo (2, 17) provokes the question of whether the action of these remodeling enzymes differs on hexasomes, thereby contributing to some of their unique functions in vivo.

Recent studies with *S. cerevisiae* Chd1 provide some insight. Chd1 can bi-directionally slide nucleosomes (18). However, removal of one H2A/H2B dimer inhibits sliding in one direction, resulting in unidirectional sliding (19). Whether other remodeling enzymes are similarly regulated is unclear. Here we addressed this question in the context of the multi-subunit *S. cerevisiae* INO80 complex, which plays central roles in DNA repair, replication and transcription. Unlike CHD and ISWI enzymes, where the ATPase subunit is sufficient for remodeling, INO80 sliding is highly regulated by its additional subunits. *S. cerevisiae* INO80 has 14 subunits in addition to the Ino80 ATPase subunit (20, 21). These additional subunits are organized in separable modules (Figure 2.1B). In particular, the Arp5/Ies6 module plays an activating role for sliding nucleosomes (13, 20,

22, 23). Further, unlike the CHD and ISWI ATPases, which bind at the internal location of Super Helical Location (SHL) +2 on a nucleosome, the Ino80 ATPase, binds near the entry-exit site of the nucleosome at SHL-5/-6 (*13, 24*) (Figure 2.2A). These significant biochemical and structural differences between INO80 versus CHD and ISWI enzymes led us to examine more carefully INO80's substrate specificity in vivo and in vitro.

Here, using a combination of in vivo and biochemical studies we have uncovered a new biological activity of INO80. We find that in addition to regulating nucleosome positioning, INO80 contributes to the steady-state positioning of subnucleosomal particles in gene bodies. Surprisingly, in vitro, INO80 is not just capable of sliding hexasomes, but prefers hexasomes over nucleosomes. The preference for hexasomes was unexpected given INO80's reliance on the acidic patch of H2A/H2B for nucleosome sliding. However, our results raise the possibility that during nucleosome sliding, the Arp5/Ies6 module of INO80 enables transient detachment of an H2A/H2B dimer through interactions with the acidic patch, allowing a hexasome-like intermediate. Overall, our work shows that INO80's specific biochemical mechanism uniquely gives it the versatility to act on both nucleosomal and hexasome substrates based on genomic context.

Results

INO80 regulates both nucleosome and subnucleosomal spacing in vivo

Most genes in *S. cerevisiae* have a stereotypical chromatin architecture near promoters, which includes an NDR at the transcription start site (TSS). The NDR is flanked by two well-positioned nucleosomes, a +1 nucleosome, the first nucleosome in the gene body and a -1 nucleosome, the first upstream nucleosome (*4*) (Figure 2.1A). Nucleosomes further in the gene body (+2 to +9) show some degree of defined positioning with an average inter-nucleosomal linker DNA spacing of ~18 bp (*4*) (Figure 2.1A).

20

INO80 has been shown to position the +1 nucleosome at TSSs, specifically at metabolic genes in budding yeast (*8, 9, 23, 25*). However, while there is increasing evidence for subnucleosomal particles at promoters and gene bodies of active genes arising from the high rates of nucleosome turnover during transcription, little is known on how remodelers affect these particles (*2, 17*). To identify potential roles of INO80 in regulating subnucleosomal particles, we performed MNase-seq in the context of WT *S. cerevisiae* cells and cells deleted for the ATPase subunit of INO80, Ino80 (*Δino80* cells), and mapped nucleosomal and subnucleosomal particles as previously described (*2*) .

A prior study demonstrated that a prevalent set of subnucleosomal particles found near TSSs correspond to MNase protected fragments of ~100bp, which were identified as hexasomes, (i.e. nucleosomes missing one H2A/H2B) (*2*). We therefore first mapped all fragments >90 bps to TSSs of the yeast genome using chemical cleavage mapping data (see Materials and Methods(*26*)) in WT and *Δino80* cells (Figure 2.1A). We then filtered the fragments by size to differentiate potential hexasomes from nucleosomes (Figure 2.1C). Consistent with prior data, we observed that in the *Δino80* strain, nucleosomes at the +1 position are not as well positioned compared to WT cells(*9, 23*) (Figure 2.1C, top right panel). Previous studies have focused on the role of INO80 on positioning the +1 nucleosome (*9, 23*). Here, in addition to the changes in positioning of the +1 nucleosome, we observe that nucleosomes further into the gene body (up to +6) also show altered positions in *Δino80* cells (Figure 2.1C, top right panel). Thus, our data suggest that INO80 is also important for maintaining spacing of nucleosomes within the gene body.

Intriguingly, we found that particles suggestive of hexasomes at the +1 position also show disrupted positioning in *Δino80* cells compared to WT cells, similar to the effects seen on +1

nucleosomes. Furthermore, there is a clear directional change in the positioning of potential hexasomes within the gene bodies in Δ*ino80* beyond the +1 position, analogous to results observed with nucleosomes (Figure 2.1C, top left panel, bottom right and bottom left panels). The mispositioning of nucleosomes and hexasomes is also obvious in a heat map representation showing all genes, where the +1 to +6 nucleosomes show fuzzier profiles in Δ*ino80* cells compared to WT cells (Figure 2.1D and 2.1E). Overall, these results show that INO80 is important for both nucleosome and hexasome positioning at the TSS and in the gene body.

Next, we analyzed the genes that were most affected by deletion of Ino80 by calculating the Spearman Rho correlation coefficient for WT and Δ*ino80* nucleosome signals (see Materials and Methods). The genes with the lowest Spearman Rho value represent the genes that had most differences in nucleosome positioning between WT and Δ*ino80* cells (Figure 2.1F). In other words, the nucleosome positions within these genes in the Δ*ino80* cells are most disrupted relative to WT cells (Figure 2.1F). These same genes also have substantially mispositioned hexasomes (Figure 2.1G), suggesting that INO80 contributes to positioning both nucleosomes and hexasomes at the same class of genes. An iPAGE heat map of genes (*27*) sorted by least to most correlated between WT and Δ*ino80* shows the gene ontology (GO) enrichment terms of the different classes (Figure 2.1H). The GO enrichment terms are consistent with previously reported roles for INO80 at metabolism related genes(*23*). Our data show that genes involved in metabolism not only have changes in nucleosome positions, but also have changes in hexasome positions upon loss of INO80. Together, these results for the first time demonstrate that the locations of subnucleosomal particles at TSSs and within genes are regulated by INO80.

INO80 shows a large preference for remodeling hexasomes over nucleosomes

The effects of INO80 on hexasome positions in vivo described above could arise directly from the action of INO80 on hexasomes, or indirectly through INO80's action on nucleosomes, which are then partially disassembled by other factors. To distinguish between these possibilities, we asked if INO80 can act on a hexasome substrate in vitro.

Prior biochemical work has shown that RNA polymerase elongation through nucleosomes results in asymmetric loss of the H2A-H2B dimer in the direction of Pol II transcription (Figure 2.1I) (*28*). Consistent with these biochemical findings, in vivo MNase footprinting in *Drosophila* cells suggests that elongating RNA polymerase results in hexasome formation within the gene body with a bias for losing the promoter-distal H2A-H2B dimer (*2*). Our data above suggests that INO80 is important for sliding hexasomes within the gene body away from the promoter (+2 onwards, Figure 2.1C). Based on the prior biochemical and *Drosophila* studies we interpret this to mean that INO80 plays a role in sliding hexasomes towards the direction that the dimer is lost from. Therefore, we focused on testing INO80's activity on a hexasome lacking the dimer proximal to the flanking DNA, which would mimic a nucleosome with the dimer lost in the direction of Pol II transcription in vivo (Figures 2.1I, 2.2A and 2.2B). We define this dimer as the proximal (or entry side) dimer to reflect its proximity to the side of the DNA that enters into the nucleosome during nucleosome sliding. The other dimer is referred to as the distal or exit side dimer.

Previously, we have found that INO80 displays maximal remodeling activity on an end positioned nucleosome assembled on the 601 Widom sequence followed by at least 80 bps of flanking DNA (*7*). We therefore assembled hexasomes on the same 601 DNA template using recently described methods to obtain specifically oriented hexasomes(*19*) (Figure 2.2B). INO80 remodeled the hexasome, which we refer to as 601 +80 hexasome (H), ~2 fold faster than the 601 +80 nucleosome (N) (Figures 2.2C and 2.2D, Figure S2.3, and Table 2.2). The products of hexasome

remodeling are consistent with sliding of the hexamer towards the center of the DNA based on comparisons to 40-601-40 hexasome standards (Figure S2.7). The products of nucleosome remodeling also migrate at locations consistent with centered nucleosomes as seen previously (Figure S2.7). Additionally, INO80 remodeled 601+100 nucleosomes with comparable rates as 601+80 nucleosomes (Figure 2.2D and Table 2.2).

While 80 bps of flanking DNA is required for maximal remodeling of nucleosomes by INO80 in vitro, within gene bodies in yeast, the average linker DNA length is ~18 bp. In vitro, the flanking DNA on a nucleosome provides a context to mimic the linker DNA found in vivo. Interestingly, in vitro, reducing nucleosomal flanking DNA to 40 bp or less reduces rates of remodeling by INO80 by 300-fold, such that remodeling occurs on the order of hours(7). This observation raised the question of how INO80 acts on nucleosomes and subnucleosomal particles in gene bodies. Given that hexasomes are substrates for INO80, we asked if these substrates are more readily mobilized on shorter flanking DNAs resembling the linker DNAs found in gene bodies.

We found that a 601+40 hexasome is remodeled ~60-fold faster than a 601+40 nucleosome (Figure 2.2E, 2.2F and Table 2.2). A missing H2A-H2B dimer proximal to the linker DNA will release ~ 20 bp of DNA effectively increasing the length of the flanking DNA. To test if the faster hexasome sliding arises from the additional flanking DNA that is released, we measured remodeling on 601+20 hexasomes. The use of 601+20 hexasomes results in effectively a similar length of flanking DNA as the 601+40 nucleosomes (Table 2.2). We found that 601+20 hexasomes are also remodeled ~60-fold faster than 601+40 nucleosomes ruling out any effects from increased flanking DNA length.

Further, the 601+20 hexasome and the 601+40 hexasome are remodeled only 5-fold slower than a 601+80 hexasome (Figure 2.2F). These results indicate that while hexasome remodeling by

24

INO80 shows a flanking DNA length dependence, this dependence is less steep than for nucleosomes. As a result, the time scales for sliding 601+20 and 601+40 hexasomes ($t_{1/2} \sim 2$ minutes) are now more compatible with time scales of transcription elongation within yeast (*29, 30*).

Given that hexasomes are better substrates we next asked if this preference is also reflected in their ability to stimulate the ATPase activity of INO80. We found that 601+80 hexasomes stimulate the ATPase activity of INO80 6.3-fold more than 601+80 nucleosomes (Figure 2.2G and Table 2.1). In the course of these studies, we noticed another major difference in how nucleosomes and hexasomes stimulate INO80's ATPase activity. The hexasome stimulated ATPase activity shows a much bigger dependence on flanking DNA length than the nucleosome stimulated ATPase activity. Previously we showed that the ATPase activity of INO80 on nucleosomes is not strongly dependent on flanking DNA length (*7*). Consistent with these prior studies we find that a 601+80 nucleosome stimulates the ATPase activity of INO80 only ~1.5 -fold more than a 601+40 nucleosome (Figure S2.1B and Table 2.1). Additionally, a 601+100 nucleosome shows comparable ATPase stimulation as a 601+80 nucleosome (Figure S2.1 and Table 2.1). In contrast, a 601+80 hexasome stimulates the ATPase activity of INO80 7.6-fold more than a 601+20 hexasome (Figure 2.2H). Finally, a larger population of hexasomes are remodeled in comparison to the corresponding nucleosomes (Figure 2.2E), suggesting more productive DNA translocation with hexasomes compared to nucleosomes.

In principle, the faster observed remodeling of hexasomes could also be explained if INO80 irreversibly slides the hexasome in one direction but slides the nucleosome in both directions, thereby seeming to be less effective at sliding the nucleosome (*7*). Comparisons of rate constants from the gel-based sliding assay, bulk FRET and prior single-molecule FRET indicate that we are mainly capturing unidirectional sliding towards the longer flanking DNA for nucleosomes (Figure

S2.4). Importantly, the higher ATPase activation by hexasomes further indicates that reversibility is not an issue.

These results establish that a hexasome is the preferred substrate for INO80 in terms of remodeling rates, remodeling extent, and ATPase stimulation. These findings further raised the possibility that the slower remodeling of nucleosomes arises from a nucleosome-specific rate-limiting step. To uncover this step, we studied the functional significance of the interactions made by INO80 with the proximal H2A/H2B dimer that is missing in the hexasomes tested above.

INO80 largely uses only one acidic patch within the nucleosome

The acidic patch on the H2A/H2B dimer of the nucleosome has been shown to be crucial for the activities of many remodelers including INO80 (*13*, *14*). It's been shown through structural studies that within an INO80-nucleosome complex, the Arp5/Ies6 module binds the entry site (proximal) dimer, and the Ies2 subunit binds the exit site (distal) dimer (*13*, *24*). Both binding interactions involve contacts with the acidic patch on the respective H2A/H2B dimer (*13*, *24*) (Figures 2.3A and 2.3B). Importantly, the hexasome that we used above is missing the dimer that is normally contacted by the Arp5 module. We therefore sought to determine the role of the interactions made by INO80 with the acidic patch on the proximal dimer. Previous studies have shown that mutating the acidic patches on both H2A/H2B dimers causes a large decrease in nucleosome sliding by INO80 (*13*, *14*) . To determine the functional role of interactions with the proximal dimer's acidic patch, we generated asymmetric nucleosomes, which had a mutated acidic patch on either the proximal or the distal dimer (Figure 2.3C) (*15*).

Asymmetric nucleosomes are made by isolating hexasomes and adding in H2A/H2B dimers that are either WT or acidic patch mutant (APM) to reconstitute nucleosomes (Figure 2.3C). To confirm

26

that this method of nucleosome assembly generates a nucleosome that can be remodeled, we mixed WT hexasomes with WT dimer and subjected the nucleosome to remodeling by INO80. While this method of reconstitution led to more hexasomes in the starting substrate, the remodeling rate of the nucleosome substrate was comparable to canonically assembled nucleosomes (Figure S2.2A, S2.2C and Table 2.2). Further, to ensure that excess dimer was not contributing to the effects seen in remodeling, we added comparable amounts of excess dimer to canonically assembled nucleosomes and did not see significant effects on remodeling kinetics (Figure S2.2B).

Unexpectedly, introducing a single APM dimer at the proximal location slowed nucleosome sliding by 200-fold, an effect that was comparable to the 150-fold defect of mutating both acidic patches (Figure 2.3D, 2.3E, and Table 2.2). In contrast, introducing a single APM dimer at the distal location caused only a modest (<1.5 fold) remodeling defect (Figures 2.3D and 2.3E). Thus, despite recent EM structures showing contacts by INO80 with both acidic patches of the nucleosome, contacts with the acidic patch on the proximal dimer contribute significantly more to nucleosome remodeling. Further, mutating the distal acidic patch in the context of hexasomes did not significantly change the remodeling rates (Figure S2.2E-G and Table 2.2). Together, these results indicate that the interactions made by the Arp5 module with the acidic patch of the proximal dimer play a major role in INO80 remodeling, while the interactions made between Ies2 and the acidic patch of the distal dimer do not make a large contribution to remodeling. We propose that, the Ies2-acidic patch contacts may be important for binding the nucleosome rather than for catalysis (*31*). Thus, the interaction between the H2A/H2B acidic patch and the Arp5 module may regulate a key step in nucleosome remodeling.

A differential role for the Arp/Ies6 module in nucleosome vs hexasome remodeling

The results above suggested that the Arp5 module may play a bigger role in nucleosome sliding than hexasome sliding because its contacts with the proximal acidic patch promote nucleosome remodeling. To test this possibility, we purified a mutant INO80 complex from yeast lacking Arp5, which we denote as INO80($\Delta arp5$) (Figure S2.9). INO80($\Delta arp5$) did not display large defects in binding of hexasomes and nucleosomes (Figure S2.5). Previous studies have implied that deletion of the Arp5 module abrogates sliding by INO80 (*20*, *23*, *32*). However, upon assaying for longer times, we found that saturating concentrations of INO80($\Delta arp5$) display detectable nucleosome sliding activity (Figure 2.4A). Under excess and saturating enzyme conditions, we found that removing the Arp5 module still permits sliding on 601 +80 nucleosomes, albeit 200-fold more slowly that WT INO80 (Figure 2.4A, B and Table 2.2). The products generated by INO80($\Delta arp5$) align with the intermediate nucleosome positions generated by INO80(WT), indicating that these are INO80($\Delta arp5$) sliding products and not supershifted bound bands (Figure 2.4A and 2.4C and Figure S2.7). In contrast, remodeling of a hexasome by INO80($\Delta arp5$) is undetectable and is at least 800-fold slower than with WT INO80 (Figure 2.4A and 2.4C). These results indicate that the Arp5 module plays a larger activating role in the context of a hexasome than a nucleosome.

Superficially, this was a counterintuitive result as the hexasomes used here lack the dimer that the Arp5 module contacts in a nucleosome. However, in addition to contacting the acidic patch, the Arp5 module also contacts nucleosomal DNA at the internal location of SHL-2/-3 through the DNA binding domain of the Arp5 subunit and through parts of the Ies6 subunit (Figure 2.4D) (*13*). A consequence of removing the proximal H2A/H2B dimer is that nucleosomal DNA at this location is released, increasing the length and changing the flexibility of the flanking DNA (Figure 2.4E). Importantly, such a change would make the internal DNA location of SHL-2/-3 more accessible to binding the Arp5 module. We therefore hypothesized that the hexasome is a better substrate

in part because it allows INO80 to more productively engage the DNA at SHL-2/-3 resulting in unimpeded translocation of DNA. We further found that under saturating enzyme concentrations, the ATPase activity of INO80(*Δarp5*) on hexasomes is ~ 30-fold slower than that of INO80(WT) (Figure S2.1 and Table 2.1). These results are consistent with the possibility that the Arp5 module contributes to the proper positioning of the Ino80 ATPase on hexasomal DNA thereby explaining Arp5's bigger activating role in hexasome remodeling.

Based on these results, we propose that the Arp5 module uses the acidic patch interactions to loosen the contacts between the H2A/H2B dimer and the H3/H4 tetramer at SHL-4/-5, making the substrate transiently resemble a hexasome. To further test this model, we next investigated which additional steps in nucleosome remodeling rely on the Arp5-acidic patch interaction.

Interactions between Arp5 and acidic patch prime the nucleosome for DNA translocation

Our previous work has suggested that the INO80-nucleosome complex forms an intermediate upon addition of ATP, prior to sliding (*7*).[7](*7*). This experiment was done with 601 +40 nucleosomes to assess formation of the intermediate in the context of very slow or no sliding. To assess the role of the proximal dimer's acidic patch, we used nucleosomes containing acidic patch mutations in both dimers because these nucleosomes show comparable rates of sliding as nucleosomes with only the proximal dimer mutated (Figure 2.3D and 2.3E). These double APM nucleosomes were 10.8-fold slower at generating the REA accessible intermediate compared to a WT nucleosome (Figure 2.5B). These results suggest that the acidic patch is used in the formation of the intermediate. We next tested the effects of deleting the Arp5 module. With WT nucleosomes, INO80(Δ*arp5*) was ~5-fold slower in generating the REA accessible intermediate compared to INO80(WT) (Figure 2.5B). On APM nucleosomes, INO80(Δ*arp5*) showed only a modest (~1.5-fold, within error) further decrease in the generation of the REA accessible

29

intermediate (Figure 2.5B). These results suggest that the direct interaction between the Arp5 module and the acidic patch is essential to form the intermediate.

To test if the Arp5 module-acidic patch interactions are important for other remodeling steps, we used gel-based assays to measure sliding rates for APM nucleosomes with INO80($\Delta arp5$). INO80($\Delta arp5$) slid APM nucleosomes with similar rates as WT nucleosomes (Figure 2.5C and 2.5D), suggesting that the acidic patch does not contribute to INO80 remodeling in the absence of the Arp5 module. This result is consistent with the effects observed in the context of the REA assay (Figure 2.5B). Notably, mutating the acidic patch of 601+80 nucleosomes slows nucleosome sliding by 200-fold, but does not affect WT INO80's ability to center nucleosomes (Figure 2.5C and 2.5D). In comparison, as noted in figures 2.4A and 2.4C, deleting the Arp5 module alone results in off-centered products (Figures 2.5C). This comparison suggests that in the context of a nucleosome, the Arp5 module has an additional role in regulating the extent of nucleosome sliding, which is independent of the acidic patch interaction.

The results above most simply suggest that the Arp5-acidic patch interaction promotes intermediate formation, which then allows nucleosome sliding to proceed efficiently. Given the large stimulatory effects of the Arp5-acidic patch interaction for the overall reaction, we tested if this interaction is coupled to ATP hydrolysis. Surprisingly, we found that mutating the acidic patch residues has small effects on ATPase activity (Figure 2.5E). In contrast, consistent with previous work we find that that deleting the Arp5 module decreases nucleosome-stimulated ATP hydrolysis by at least 10-fold (*20*, *32*) (Figure 2.5F). Similar to the conclusions from figures 2.4A, 2.4C, and 2.5B, these results suggest that the Arp5 module plays additional roles during nucleosome remodeling that are independent of the acidic patch interaction.

30

Discussion

How INO80 achieves its many biological functions is poorly understood (*33*). We have found here that INO80 preferentially slides hexasomes over nucleosomes. Our findings explain how subnucleosomal particles are repositioned in cells and point to a sophisticated remodeling mechanism that regulates the extent of INO80's preference for hexasomes in a genomic context. Below we discuss the mechanistic and biological implications of these findings.

Mechanistic explanation for how INO80 acts on hexasomes and nucleosomes

The faster remodeling of hexasomes raises the possibility that nucleosomes may be remodeled via a hexasome like intermediate, which is mediated by the Arp5 module. This intermediate could involve transient loss of either the proximal or distal dimer. For the reasons discussed below we suggest that transient loss of the proximal dimer through interaction with the Arp5 module is the more parsimonious model. However, we cannot rule out alternative models that involve transient loss of the distal dimer and different roles for the Arp5 module.

We propose that the proximal H2A/H2B dimer inhibits movement of DNA that is translocated from the entry site by the INO80 ATPase. In this model the inhibition is relieved through transient dislodging of the H2A/H2B dimer by the Arp5 module though interactions with the acidic patch. Such dislodging may then allow unimpeded movement of the DNA translocated by the Ino80 motor (Figure 2.6A). This model is consistent with previous evidence for a nucleosomal intermediate that displays increased DNA accessibility and previous crosslinking studies, showing disruption of the H2A/H2B-DNA contacts by INO80 (*7, 22*). Such a model is also consistent with prior single-molecule findings showing an ATP-dependent pause preceding a rapid DNA translocation step (*7*) . We suggest that the ATP-dependent pause represents the time taken to dislodge the proximal dimer.

31

The absence of the proximal dimer will also increase the accessibility of DNA at SHL-2/-3, the region contacted by the DNA binding domain of Arp5 and by Ies6 (Figure 2.4E). We therefore speculate that Arp5 is able to better engage the DNA at SHL-2/-3 in hexasomes, thereby enabling more efficient passage of the translocated DNA. In a nucleosome, such productive engagement of the DNA at SHL-2/-3 would occur after the proximal dimer is transiently dislodged, adding an unfavorable step to the overall reaction. Prior cryo-EM studies showed that the Arp5 module can adopt two different conformations on a nucleosome, one that appears inhibitory for DNA translocation and one that appears permissive for DNA translocation (*13*). Additionally, action of the Ino80 ATPase has been proposed to introduce torsional strain at the proximal H2A/H2B dimer in a nucleosome (*22*). We therefore propose that in response to such strain the Arp5 module switches between the inhibitory and permissive conformations thereby transiently dislodging the proximal dimer to more effectively engage the DNA at SHL-2/-3.

To date the H2A/H2B acidic patch has been shown to be serve largely a binding purpose (*11*) and in the context of the human ISWI enzyme, SNF2h also has an allosteric activating role (*14*). Our studies suggest a third type of role wherein the interactions made with the acidic patch transiently displace an H2A/H2B dimer to promote nucleosome remodeling.

It has been debated whether INO80 exchanges an H2AZ/H2B dimer with an H2A/H2B dimer (*22, 34*, *35*). Our results suggest the exchange may be a side reaction. As INO80 transiently dislodges the dimer, it may fall off in certain reaction conditions and be replaced by free dimers in solution. If H2AZ destabilizes nucleosomes, this may preferentially dissociate H2AZ/H2B. Consistent with this possibility, the fraction of exchanged H2A/H2B dimers is less than slid nucleosomes (*36*).

Different flanking DNA length dependencies for hexasome versus nucleosome remodeling

Previous work has shown that the Arp8 module binds flanking DNA (*37*). Using our model, we propose that productive engagement of the DNA at SHL-2/-3 by the Arp5 module is necessary to allow appropriate engagement of flanking DNA by the Arp8 module. Such engagement of flanking DNA by the Arp8 module could then be coupled to activation of the Ino80 ATPase in a manner that depends on the length of flanking DNA bound by Arp8. This proposal is consistent with prior work showing that deletion of the Arp8 module changes the nucleosome contacts made by the Arp5 module (*37*). In a nucleosome, the DNA at SHL-2/-3 is partially occluded through interactions with the H2A/H2B dimer potentially inhibiting the productive engagement of the DNA by Arp5's DNA binding domain. In turn, such inhibition would reduce positive cooperation between the Arp5 and Arp8 module, resulting in a basal nucleosome stimulated ATPase rate that is not strongly dependent on the flanking DNA length. With a hexasome, given the greater accessibility of DNA at SHL-2/-3, the Arp5 and Arp8 modules would more effectively cooperate, resulting in higher ATPase activity that is also more strongly dependent on flanking DNA length.

Interestingly, unlike ATPase activity, remodeling of nucleosomes by INO80 is strongly dependent on flanking DNA length. Within the framework described here, the flanking DNA length dependence of nucleosome sliding may arise from two steps: (i) the DNA translocation steps carried out by the Ino80 subunit in the intermediate state, and (ii) ATP-independent collapse of the intermediate to the starting conformation (Figure 2.6A). The DNA translocation steps would get faster with longer flanking DNA reflecting productive engagement by Arp8 and Arp5. In contrast, the collapse step would get faster with shorter flanking DNAs, reflecting the increased instability of the intermediate due to weaker cooperation between Arp5 and Arp8. We note that the flanking DNA length dependence of the collapse step proposed here draws from a model we had proposed previously (*7*). In a hexasome, the flanking DNA length dependence would then

primarily arise from the DNA translocation step, as the starting state for a hexasome resembles the intermediate for a nucleosome.

Roles for the Arp5 module in nucleosome and hexasome sliding

Our results uncovered two unexpected effects of deleting the Arp5 module. First, deleting the Arp5 module causes greater than an ~800-fold defect in hexasome sliding compared to a ~200-fold defect in nucleosome sliding, indicating that this module makes a larger energetic contribution to hexasome sliding. We propose that in a hexasome, the interaction made by the Arp5 module with the DNA at SHL-2/-3 is substantially stronger than the corresponding interaction made in the nucleosomal intermediate due to the complete absence of the proximal dimer. Second, with 601+80 nucleosomes, where sliding was detectable upon deleting the Arp5 module, the nucleosome was moved substantially less far compared to the ~40 bp movement observed with WT INO80. We propose that without the Arp5 module, the intermediate would have a reduced lifetime, resulting in movement of less DNA.

INO80 regulates positions of nucleosomes and subnucleosome particles at genes

Most previous work has focused on INO80's role in establishing the +1 nucleosome at TSSs (*8, 9, 23, 25*). However prior work has also implicated INO80 in regulating elongation by RNA Polymerase II as well as nucleosome spacing in gene bodies independent of RNA Pol II (*38–41*). Our new findings that INO80 regulates the locations of both hexasomes and nucleosomes within the gene body provides some mechanistic basis for these latter set of studies.

Our findings also synergize with emerging evidence indicating an elevated prevalence of subnucleosomal particles at highly transcribed genes (*2, 17*). Many of these subnucleosomal particles have DNA footprints consistent with hexasomes. In these studies, it has been suggested

that hexasomes may arise during transcription as RNA polymerase navigates through a nucleosome. Indeed, careful biochemical studies have shown that RNA polymerases can dislodge an H2A/H2B dimer during transcription through a nucleosome (*42*). In this context our findings provide one mechanistic explanation for how hexasome positions are regulated in vivo.

INO80's role in regulating the position of the +1 nucleosome, where the average length of the NDR is ~140 bps(*4*) is compatible with INO80's in vitro activity of rapidly (order of minutes) sliding nucleosomes with flanking DNA greater than ~60 bps. However, within gene bodies in yeast, the average linker DNA length is ~18 bps(*4*), and INO80 slides nucleosomes very poorly in vitro (order of hours) when the flanking DNA is less than 40 bp. Interestingly we find that INO80 slides hexasomes with 20 bp of flanking DNA on the order of minutes. We therefore propose that INO80's effect on nucleosome positions within gene bodies is through its mobilization of hexasomes, some of which are then converted to nucleosomes with the aid of histone chaperones such as Nap1 and FACT (*43*, *44*). Consistent with this possibility, genes showing the most changes in nucleosome positioning upon Ino80 deletion also show mispositioning of both nucleosomes and hexasomes.

Restoration of hexasome positions by INO80 could regulate cryptic transcription. Indeed, INO80 is a key repressor of anti-sense transcription of long non-coding RNAs (*45*). Because inter-nucleosomal spacing is largely regular in yeast gene bodies, losing a dimer would promote directional sliding of hexasomes by INO80. Indeed our in vivo results suggest that INO80 moves subnucleosomal particles away from the promoter. However, we cannot exclude that misregulation of the +1 nucleosome impairs RNAPII elongation, also contributing to defects in hexasome positions. Interestingly genes showing large changes in nucleosome and hexasome positions in Δ*ino80* cells are enriched for metabolic functions (Figure 2.1H). Metabolism regulating

genes can show rapid changes in expression (*46*). Restoring nucleosomes and hexasome positions at such genes during transcription could be a critical function of INO80.

The *S. cerevisiae* Chd1 remodeler, was also shown to remodel hexasomes (*19*). However, unlike with INO80 where the loss of an H2A/H2B dimer stimulates sliding, with Chd1, the loss of an H2A/H2B dimer inhibits sliding in one direction, resulting in unidirectional sliding (*19*). These results demonstrate that while other remodelers such as Chd1 can recognize both hexasomes and nucleosomes, their specific mechanisms differ. In the future, determining how other remodelers such as those from the ISWI and SWI/SNF families act on subnucleosomal particles will provide more insights into how these particles are regulated *in vivo*.

Broader Implications

The model proposed here provides a means to imagine how histone variants or PTMs could regulate INO80 activity. For example, histone variants or PTMs that destabilize the H2A/H2B dimer-H3/H4 interface could specifically promote remodeling of nucleosomes. Altering interactions with the H2A/H2B acidic patch could also regulate INO80 activity. Indeed, replacing H2A with H2AZ or mutating H2A to possess an acidic patch more similar to H2A.Z results in faster remodeling (*13*, *22*). Additionally, the ability of INO80 to tune its preference for hexasomes versus nucleosomes based on linker DNA length provides INO80 the versatility to act in different genomic contexts that vary in nucleosome density. Such versatility could explain INO80's global role in DNA repair where rapid movement of nucleosomes as well as subnucleosomal particles may be needed for the repair machinery to access the damaged DNA. Finally, our results showing that deletion of the Arp/Ies6 module changes the outcome and speed of nucleosome remodeling raises the possibility that in cells INO80 activity can be tuned to carry out defined tasks through loss, or modification of specific modules. Indeed, prior work has suggested the presence of INO80

subcomplexes in yeast (*23*). INO80 has also been shown to be post-translationally modified by other enzymes(*47*). Overall, the ability to precisely tune its activities through both its subunits and substrates could allow INO80 to adopt multiple roles and explain INO80's involvement in diverse chromatin processes. Moving forward, it will be important to understand the different types of chromatin or "chromatin-like" structures INO80 encounters in cells and how INO80 uniquely acts at these sites to facilitate and regulate essential DNA based transactions.

Limitations of study

While our work provides an initial model for how INO80 acts on hexasomes, additional biochemical and structural work is needed to understand exactly how the different subunits of INO80 act together to slide hexasomes. In particular, the proposed role of the Arp5 module is a speculation based on its engagement of the acidic patch of the proximal dimer and the large defects from mutating this acidic patch. This role needs to be more directly tested with further mutagenesis and cryo-EM structural analysis of reaction intermediates.

37

Author Contributions

Conceptualization, L.J.H., M.A.G., and G.J.N.; Methodology, L.J.H., M.A.G., and G.J.N.; Software, C.M., and V.R.; Formal Analysis, C.M., and V.R.; Investigation, L.J.H., M.A.G., and E.N.M., N.G.; Data Curation, C.M., and V.R.; Writing – Original Draft, L.J.H., M.A.G., and G.J.N.; Writing – Review & Editing, L.J.H., M.A.G., C.M., E.N.M., N.G., V.R., and G.J.N.; Visualization, L.J.H., M.A.G, C.G., and E.N.M.; Supervision, G.J.N.

Declaration of Interest

Geeta Narlikar is on the Molecular Cell advisory board.

Diversity and Inclusion Statement

One or more of the authors of this paper self-identifies as an underrepresented ethnic minority in science. One or more of the authors of this paper received support from a program designed to increase minority representation in science.

Methods

Resource Availability:

Lead Contact

All inquiries for further information and requests for resources and reagents should be directed to and will be fulfilled by the lead contact, Geeta J. Narlikar (narlikar@ucsf.edu).

38

Materials Availability

All plasmids and cell-lines generated in this study are found in the key resources table including those uniquely made for this study. Additional information about the materials used can provided upon requests made to lead contact.

Data Code and Availability Resources

- The data reported in this paper is available on NCBI's Gene Expression Omnibus database with the accession number GSE168700, as listed in the key resources table.

- The code used in this study originated from Ramani et al (PMID30811994).

- Any additional information required to reanalyze the data in this paper is available from the lead contact upon request.

Experimental Model and Subject Details

Yeast strains

All yeast strains are MATa and in the s288c background. The Δino80 strain was a gift from the Ashby lab (*23*). The Δarp5 strain was generated by PCR knock-in of the KanMX cassette at the Arp5 locus. The yeast strains used in this study are listed in the key resources table. For protein purification, all yeast strains were grown at 30 degrees. Yeast were first inoculated in YPD from frozen glycerol stock then transferred to 18-20L of YPD. Yeast was grown until saturation, 50 g/L of YPD was added and cells were harvested after 1-2 overnight incubations at 30 degrees.

Method Details:

MNase-seq

Yeast chromatin was digested with MNase as previously described (*48*). A MNase titration was performed on the chromatin samples, and run on a 1% agarose gel (Figure S2.8). Similarly

digested chromatin among the different strains were chosen, and one replicate was size selected for mononucleosomes via gel extraction, while the other replicate was not size selected. Libraries were prepped using the Ovation Ultralow System V2 for DNA-Seq Kit (Nugen). Libraries were sequenced on a NextSeq.

MNase-seq data analysis & acquisition

Read Processing and Alignment: MNase-seq libraries were sequenced with paired end 80 bp reads on a NextSeq 500 instrument. Raw reads were clipped using SeqPrep and aligned to SacCer3 using bwa mem with default parameters. Aligned BAM files were sorted, deduplicated, and indexed using samtools and the PySAM API. The scripts and pipelines for mapping have been previously described (*49*).

Normalized Enrichment Heatmaps: The nucleosome and subnucleosomal particle dyads were derived from chemical cleavage mapping data. A custom Python script calling the PySAM API was used to create arrays mapping midpoints of all reads +/- 1000 bp from an established +1 dyad position in the yeast genome (*49*). An annotated list of 4,116 yeast +1 dyads mapped by chemical cleavage was used (*26*). Fragment midpoint enrichment was calculated as a simple z-score for each +1 nucleosome.

Line Plots: Normalized enrichment was averaged across all genes and plotted using ggplot2 in R.

Expression Sorting: Normalized enrichment arrays were sorted based on gene TPM count determined from RNA-Seq reads in wild type yeast (*50*).The arrays for the top 20% and bottom 20% of genes were averaged and visualized as described above.

Heatmaps: Normalized enrichment arrays were visualized as heatmaps using matplotlib. Maximum and minimum color intensity values were set to the 90th and 10th percentiles of data, respectively. Data above and below these values were also displayed.

40

Correlation Heatmaps: Normalized mutant data of fragment size 130-300 bp (nucleosome sized fragments) were correlated with normalized wild type arrays of the same fragment size on a gene-by-gene basis using Spearman's r. Arrays were sorted based on correlation and genes with r < 0.33 were visualized using the same parameters as other heatmaps. Arrays of fragment size 90-109 were also sorted based on the correlation of the nucleosome sized fragments and visualized using the same parameters.

iPAGE Analysis: Correlations were calculated for each gene as described above. iPAGE (*27*) was used to sort genes based on correlation (binned into 11 categories) and calculate significantly enriched GO groups using mutual information content.

Purification of INO80 complexes

FLAG-tagged Ino80 strains were grown at 30°C in YPD to saturation and harvested for purification. INO80 was purified using FLAG immunoprecipitation, as described previously (*7*), with a minor modification. A secondary elution for 15 minutes at 4°C was performed to increase yield.

Assembly of nucleosomes, asymmetric nucleosomes, and hexasomes

Recombinant *Xenopus laevis* histones were purified from bacteria as previously described. DNA constructs were generated using a plasmid containing 601 DNA. Large scale PCR was performed and the resulting DNA was separated on an 8% polyacrylamide gel, cut out, crushed and soaked into 1X TE. The gel particles were filtered through a 0.45 um filter, and the DNA was ethanol precipitated and resuspended in 1X TE. To label the DNA, primers with a Cy3 fluorophore modification were used (IDT). Nucleosomes and hexasomes were assembled using salt gradient dialysis. Nucleosomes were purified by ultracentrifugation with a 10-30% glycerol gradient. Hexasomes were purified using the Mini PrepCell (BioRad) with a 7% acrylamide gel as described

41

previously (*15*). Briefly, this method by Levendosky and Bowman takes advantage of the asymmetry of the 601 nucleosomes positioning sequence. The asymmetry results in weaker affinity of one side of the DNA sequence for H2A/H2B dimers compared to the other side. Placing the flanking DNA adjacent to the side of the 601 sequence that binds dimers more weakly then allows assembly of hexasomes missing the dimer that is proximal (i.e. adjacent) to the longer flanking DNA. The hexasomes are further purified over a prep-cell as described by Levendosky and Bowman, to separate out hexasomes from small amounts of nucleosomes. Purified hexasomes were mixed with 2.5-4X excess dimer to assemble the asymmetric nucleosomes.

Native Gel remodeling assay

Remodeling reactions were done under single turnover, saturating INO80 and saturating ATP conditions. The reaction conditions contained 10 nM nucleosomes, 30 or 60 nM INO80, 40 mM Tris pH7.5, 50 mM KCl, 1.1mM $MgCl_2$, 0.02% NP-40, 1 mM ATP•$MgCl_2$, and 3% glycerol, and reactions were carried out at 30˚C. INO80 was pre-bound to nucleosomes for 10 minutes at 30˚C before starting the reaction with the addition of ATP•Mg. The no ATP control was taken at the last time point of the reaction. Time points taken from the reaction were quenched with 0.6 mg/ml non-601 plasmid DNA, 4nM ADP, and 18% glycerol. Samples were loaded on a 6% polyacrylamide gel and resolved for 4 hours at 125V. Gels were scanned on a Typhoon Imager (GE Life Sciences). The fraction unremodeled was quantified over time using ImageJ. Undetectable remodeling was defined as reactions that displayed no change in the fraction unremodeled compared to the no ATP control after 6 hours. A limit for remodeling was determined by fitting the data to a 6 hour end point where ~5% of substrate was remodeled. The data were fit to a single exponential decay as indicated by Equation 1, using GraphPad:

$$\text{One-phase decay: } y = (y_0 - p)e^{-k_{obs}t} + p$$

42

EMSA assay

The reactions contained 2, 5 or 75 nM 601+80 nucleosomes (or hexasomes), varying concentrations of INO80(WT) and INO80(Arp5Δ) as noted on each figure, 40 mM Tris pH7.5, 50 mM KCl, 1.1mM MgCl$_2$, 0.02% NP-40, and 3% glycerol. Binding reactions were carried out for 30 minutes at 30˚C. The bound and unbound fractions were separated by electrophoresis on a 4% acrylamide, 0.5X TBE native gel.

ATPase assay

ATPase assays performed under conditions that closely mimicked remodeling assays. All ATPase assays were performed under multiple turnover conditions (ATP in excess of INO80). Experimentally we determined that 320 μM ATP•MgCl$_2$ was saturating for both 60 nM WT INO80 and 90 nM INO80(Δ arp5). Reactions were performed with 15 nM nucleosomes (or hexasomes), 60 nM WT INO80 (or 90 nM INO80(Δ arp5)), 40 mM Tris pH 7.5, 50 mM KCl, 320 μM ATP•MgCl$_2$, 0.5 mM MgCl$_2$, and trace amounts of g-^{32}P-ATP, at 30˚C. Each reaction was started with the addition of ATP•MgCl$_2$ after a 10-minute preincubation at 30˚C. The no ATP control was taken at the last time point of the reaction. Samples of the reactions were quenched at various timepoints with equal volumes of 50 mM Trips pH 7.5, 3% SDS, and 100 mM EDTA. Inorganic phosphate was separated from ATP•MgCl$_2$ on PEI-cellulose TLC plates with 0.5 M LiCl, 1 M formic acid. These plates were exposed overnight on a phosphoscreen and scanned on a Typhoon Imager (GE Life Sciences). To determine the rate constant, we measured the fraction of inorganic phosphate using ImageJ, and fit the initial 10% hydrolyzed.

Restriction enzyme accessibility (REA) assay

REA assays were performed under single turnover conditions (INO80 in excess of nucleosome). Experimentally, we determined that 60 nM WT and 90 nM INO80(Δ*arp5*) was saturating under

43

the following reaction conditions: INO80, 15 nM nucleosome, 40 mM Tris pH 7.5, 60 mM KCl, 1 mM ATP•MgCl$_2$, 5 mM MgCl$_2$, 0.01% NP40, 0.5 mg/mL FLAG peptide, and 3 U/μL Pst1 at 30˚C. Each reaction was started with the addition of ATP•MgCl$_2$ after a 10-minute preincubation at 30˚C. The no ATP control was taken at the last time point of the reaction. Samples of the reactions were quenched at various timepoints with equal volumes of 20 mM Tris pH 7.5, 2% SDS, and 70 mM EDTA, 20% glycerol, 0.2 mg/mL xylene cyanole, and 0.2 mg/mL bromophenol blue. All quenched timepoints were incubated with 4 mg/mL of Proteinase K for 20 minutes at 50˚C to digest all proteins. The DNA (cut and uncut fragments) were resolved for each timepoint with a native PAGE (10% acrylamide, 1X TBE) and scanned on a Typhoon Imager (GE Life Sciences). To determine the rate constant, we measured the fraction of DNA cut using ImageJ and fit the data to a single exponential decay using Prism 7 (GraphPad) (Equation 1).

Quantification and Statistical Analysis:

Error estimation for ensemble measurements

All ensemble measurements of rate constants are reported as the mean of three or more experimental replicates and standard error of the mean (SEM). These values are reported in the figure legends. Graphing and statistical analyses were done using GraphPad Prism 8 or 9.

44
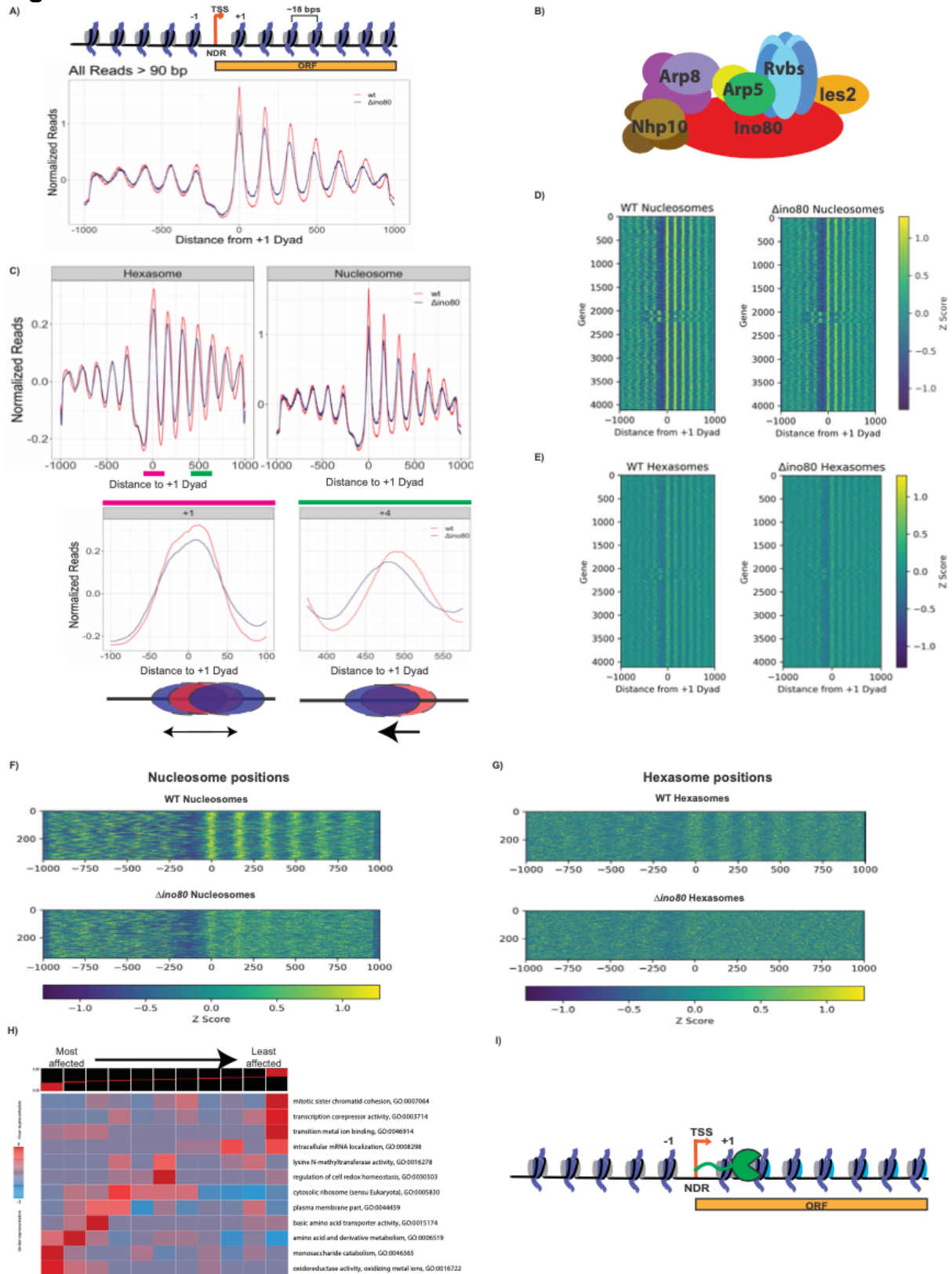
Figures

Figure 2.1. INO80 regulates positions of subnucleosomal particles in vivo.
A) Normalized MNase signal at the TSSs of all genes for WT, in orange, and Δ*ino80*, in dark blue, for all fragment lengths greater than 90 bps. The x-axis represents distance from +1 nucleosome dyad. Upper panel: Schematic of corresponding chromatin architecture in B) Cartoon of the INO80 complex. Only one subunit per module is labelled. C) Upon deletion of Ino80, nucleosomes and hexasomes are less well positioned at +1 location and display shifted positions in gene body. Upper panel: Fragments were binned by sizes representing either hexasomes (100 +/-10 bps) or nucleosomes (147 +/-10 bps), and the average signal at TSSs and in the gene body are plotted for WT and Δ*ino80*. Lower panel: pink and green lines in the hexasome plot from upper panel are magnified to show hexasome footprints at +1 and +4 positions. Below the graphs are cartoons of the respective changes in positioning that occur from WT (red) to Δino80 (blue). D) Heat map of nucleosome footprint signals across all genes for WT and Δ*ino80* cells. E) Same as D, but for the hexasome footprint signals. F) Data for genes where nucleosome positions are most affected by deletion of Ino80. A heat map representing genes that had the lowest Spearman Rho correlation (i.e., most affected by deletion of Ino80) for nucleosome footprint signals ranging from the -100 bps to +1000bps of the +1 dyad between WT and Δ*ino80*. G) Data for the genes in (F) but focusing on hexasome positions. H) An iPAGE heat map of the correlations of nucleosome footprint signal between WT and Δ*ino80* and their annotated GO terms. The genes have been binned into 11 groups, with lowest correlation group (most affected in terms of nucleosome footprints) on the left, and highest correlation group (least affected in terms of nucleosome footprints) on the right. I) Cartoon of RNA Pol II traversing through gene body. The promoter distal dimer that is lost during elongation is depicted in cyan.
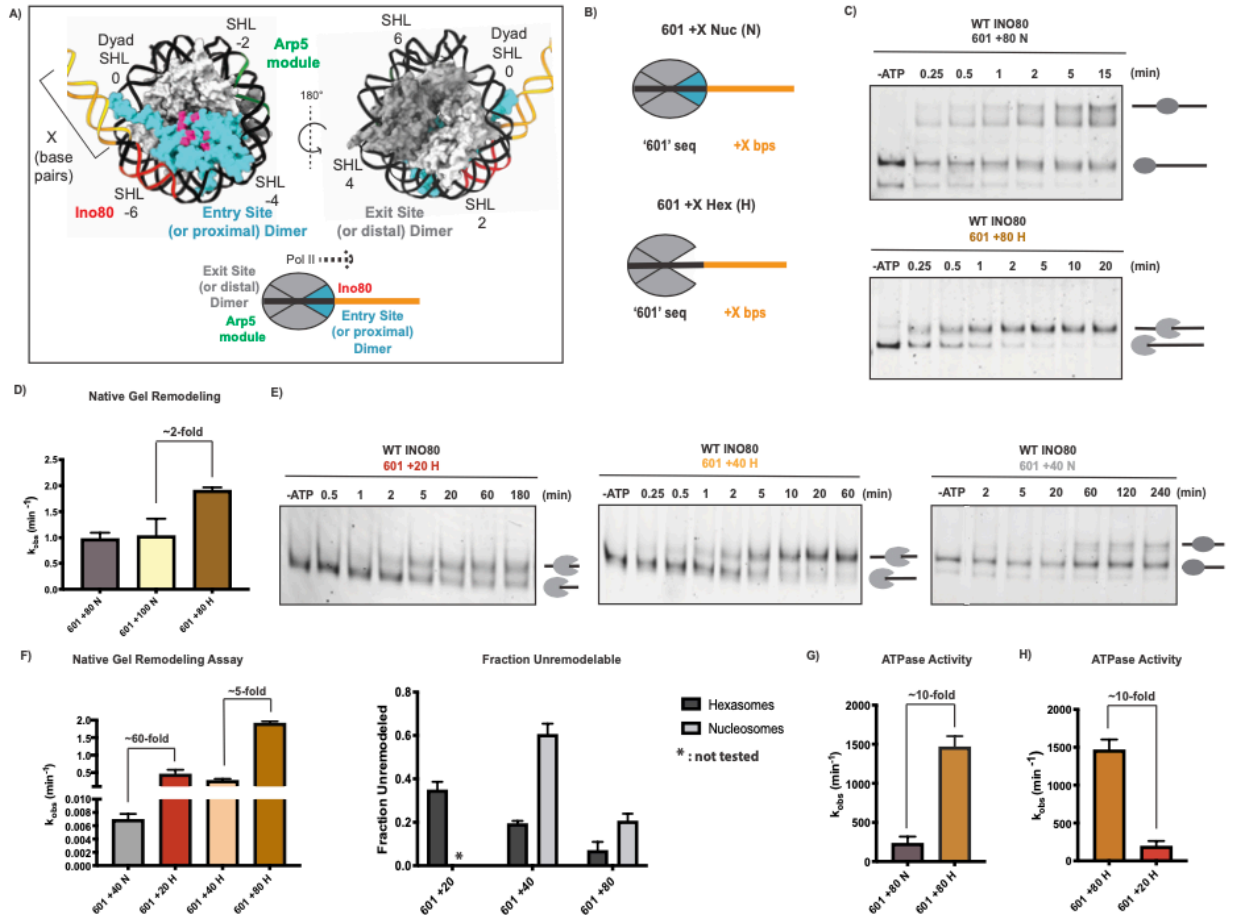
Figure 2.2. Hexasomes are better substrates for INO80 in vitro.
A) Upper panel: two different rotations of nucleosome structure (PDB ID: 1KX5) highlighting the dimer (cyan) at entry site (or proximal to flanking DNA) and its acidic patch(pink). Regions of DNA where Arp5/Ies6 binds (green), Ino80 ATPase binds (red), that are in flanking DNA (yellow), and are in Super Helical Locations (SHL) are indicated. Lower panel: cartoon of nucleosome, indicating the exit site (or distal) and entry site (or proximal) H2A-H2B dimers, and regions where the Arp5/Ies6 and Ino80 ATPase binds. Direction of elongating Pol II based on the loss of the distal dimer is shown with a black dotted line. B) Depiction of 601 nucleosome (N) and hexasome (H) constructs with flanking DNA used in this study. The H2A-H2B dimer missing in hexasomes is in cyan. C) Example native gels showing remodeling by INO80 of 601+80 nucleosomes (top) and 601+80 hexasomes (bottom). Substrates (end-positioned nucleosomes or end-positioned hexasomes) are labelled by cartoons next to the respective bands in gels. D) Quantification of rate constants from multiple repeats of data such as in (C). Rate constant for remodeling of 601 +100 N is also shown. E) Example gels of INO80 remodeling with 601 +20 H (left), 601 +40 H (middle), and 601 +40 N (right). Substrates (end-positioned nucleosomes or end-positioned hexasomes) are labelled by cartoons next to the respective bands in gels. F) Left panel: quantification of rate constants for remodeling of 601 +40 N (grey), 601 +20 H (red), 601 +40 H (peach), and 601 +80 H (tan) by INO80 as assayed using the native gel assay. *Note that the data for 601 +80 H is the same data shown in panel D and is shown again here for ease of comparison*. Right panel: fraction of unremodeled substrate, assayed via the native gel assay and measured at the longest time point (where all reactions

have mostly gone to completion). Hexasomes are in dark grey, nucleosomes are in light grey. G) Observed rate constants of INO80 ATPase activity on 601 +80 N in grey and 601 +80 H in tan. ATPase assays were performed under the same conditions as native gel-based remodeling. H) Rate constants of INO80 ATPase activity on 601 +80 H (tan) (data from G) and 601 +20 H (red). *Note that the data for 601 +80 H is the same data as shown in panel G and is shown again here for ease of comparison.* Error bars represent s.e.m from n>3.

Figure 2.3. The acidic patch that binds to Ies2 is dispensable for INO80 sliding.
A) CryoEM based structure of the core INO80 components bound to the nucleosome (PDB ID: 6FML). B) CryoEM model from (A) showing only the Arp5 (green)/Ies6 (yellow) module and Ies2 (orange) bound to the nucleosome for clarity. Arp5/Ies6 and Ies2 bind to acidic patches (pink) on opposite sides of the nucleosome (PDB ID: 6FML). C) Schematic showing assembly of nucleosomes, with acidic patch mutations (APM) depicted in blue. From (A) Arp5 module (green), binds dimer at entry site, while Ies2 (orange) binds dimer at the exit site. D) Example native gels showing remodeling time courses for nucleosomes shown (C). E) Quantification of rate constants from multiple repeats of data such as that shown in panel D. Error bars represent s.e.m from n>3.

Figure 2.4. The Arp5 module is a key regulatory component for remodeling.
A) Example time courses for remodeling of 601 +80 N (top panel) and 601 +80 H (bottom panel) by
INO80(Δ*arp5*) as assayed by native gel. B) Quantification of INO80(Δ*arp5*) remodeling rate constants
(blue) on 601 +80 N and 601 +80 H from repeats of data such as in (A). *For ease of comparison, the same
WT INO80 data shown in Figure 2.2D and is shown again here (coral).* C) Left panel: schematic showing

the distance parameter in the line-scan data depicted in in the middle and right panels. Middle panel: line scan showing distribution of band intensity (gray value) on a native gel for the last time point for remodeling of 601 +80 N by WT INO80 (coral, 360 min), and INO80(Δarp5) (blue, 360 min). Right panel: line scan showing the distribution of band intensity (gray value) on a native gel for the last time point for remodeling of 601 +80 H by WT INO80 (coral, 360 min), and INO80(Δarp5) (blue, 360 min). D) Top panel: cryoEM structure of the nucleosome (PDB ID: 6FML) showing the entry site dimer (cyan) and the Arp5 module's DNA binding site (green) at SHL-2/-3 (from PDB ID: 6FML). Lower panel: cartoon of the Arp5 module binding the nucleosome (H2A-H2B dimers in cyan; H3-H4 tetramer in orange; DNA in black) at the designated binding site via a DNA binding domain, based on PDB ID: 6FML. E) Top panel: model of the structure of a hexasome missing the entry site dimer. Model shows how the wrapping of the DNA may change upon proximal dimer loss to make Arp5 module's binding site at SHL-2/-3 (in green) more accessible. Lower panel: cartoon model of the Arp5 module binding the hexasome in a different conformation due to the absence of the dimer. Error bars represent s.e.m from n>3.

51
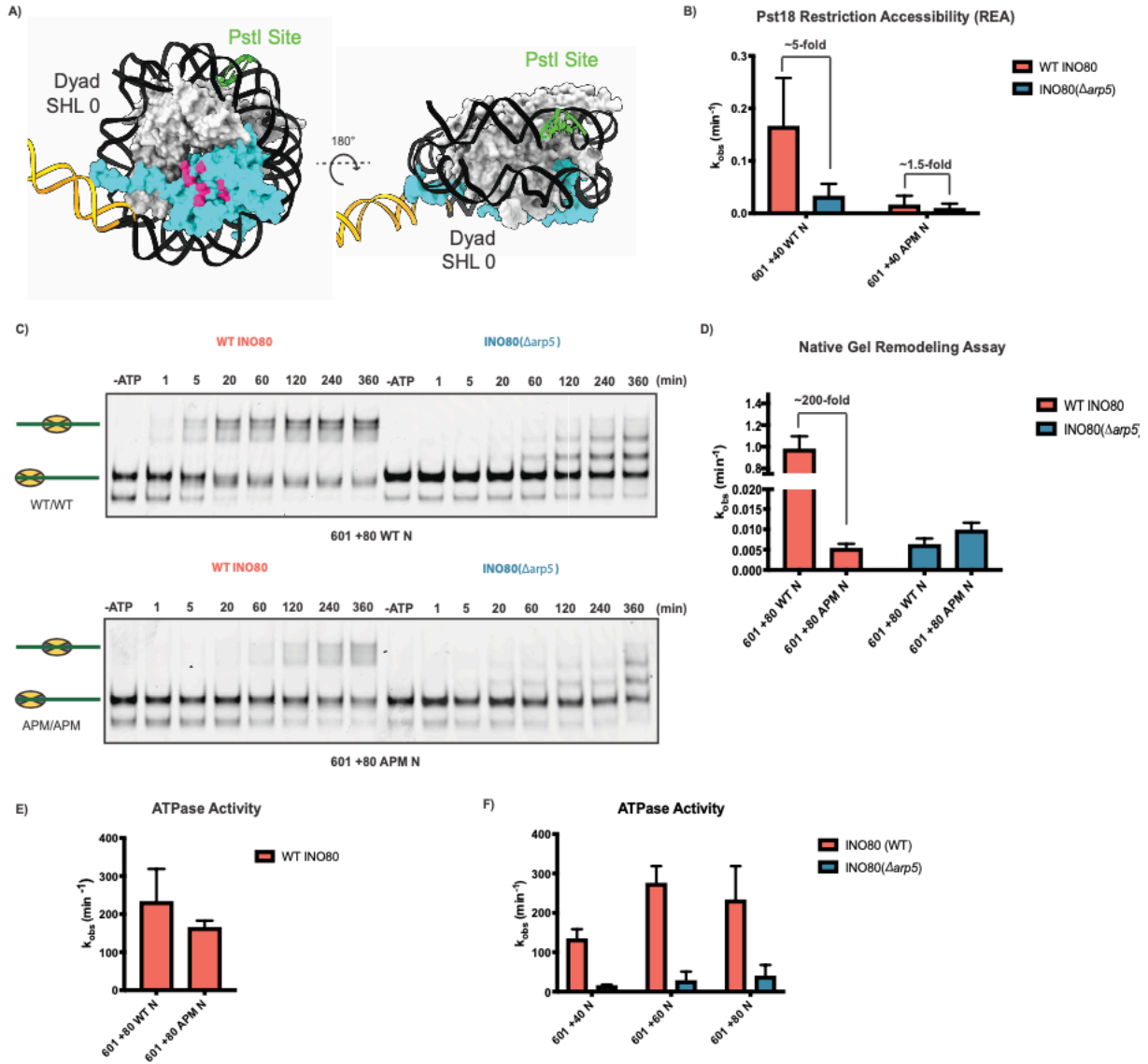
Figure 2.5. The Arp5 module interacts with the acidic patch to regulate INO80 sliding.
A) Model of the nucleosome (PDB: 1KX5) from different angles with location of the engineered PstI restriction site in green. Proximal H2A-H2B dimer is in cyan. B) Rate constants of cutting by PstI for WT and double APM 601+40 N, with saturating ATP and saturating WT INO80 (coral) or INO80($\Delta arp5$) (blue). C) Example native gels showing remodeling of WT (top panel) and double APM (bottom panel) 601 +80 N with WT INO80 (coral) and INO80($\Delta arp5$) (blue). D) Quantification of rate constants from multiple repeats of data such as that shown in panel C. E) Rate constants for INO80 ATPase activity with WT and double APM, 601 +80 N. All ATPase assays were performed under the same conditions as native gel remodeling. F) Observed rate constants for ATPase activity of WT INO80 (coral) and INO80($\Delta arp5$) (blue) on 601 +40 N, 601 +60 N and 601 +80 N. Error bars represent s.e.m from n>3.
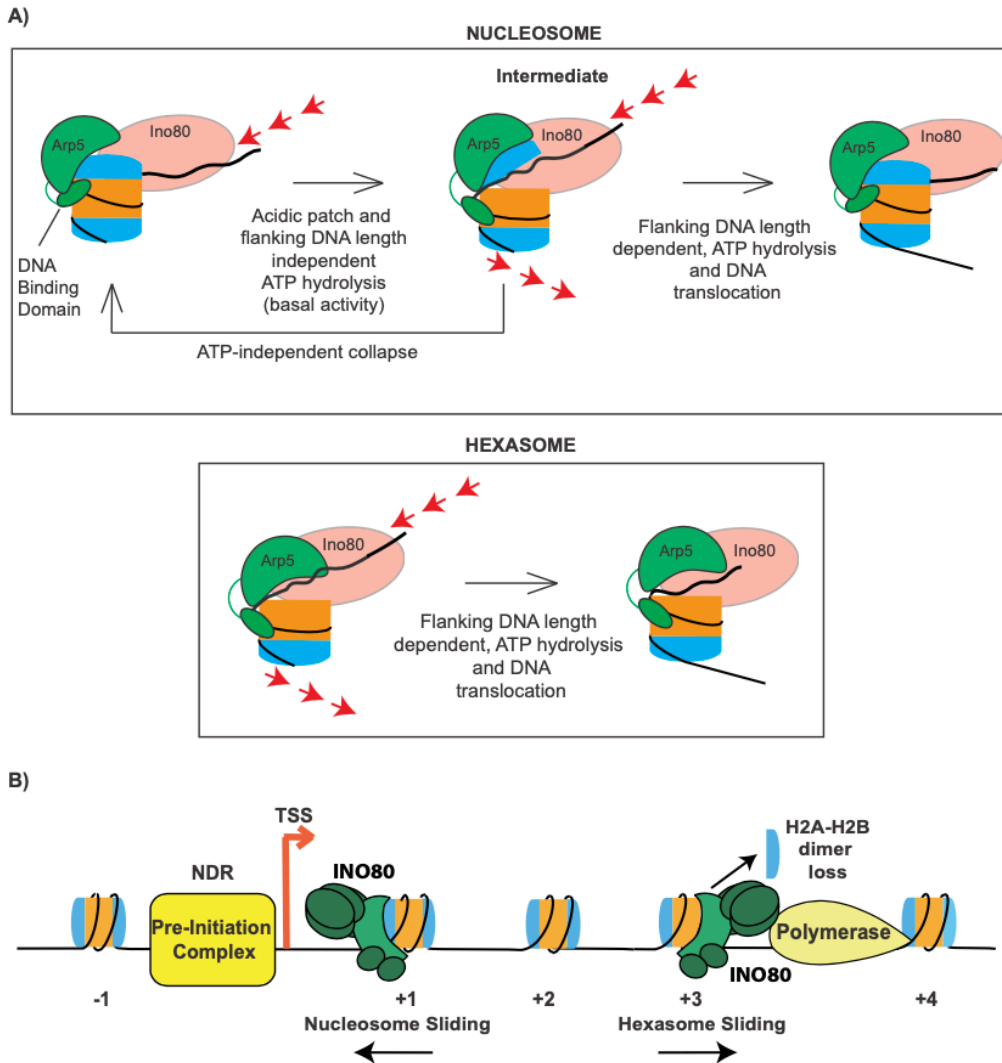
Figure 2.6. Model of the INO80 remodeling mechanism.
A) Cartoon of model for INO80 action on a nucleosome and a hexasome. Nucleosome binding stimulates a basal level of ATP hydrolysis and the Ino80 motor pumps DNA into the nucleosome. This ATPase activity is independent of flanking DNA length and the acidic patch. The torsional strain caused by the pumping of the DNA is partially relieved through transient dislodging of the H2A/H2B dimer. Such dislodging is speculated to occur by the Arp5 module through contacts with the acidic patch and DNA at SHL-2/-3. This transition results in the formation of an intermediate, which can either collapse back in an ATP-independent manner, or transition forward in an ATP-dependent manner to translocate DNA across the nucleosome. Translocation is dictated by flanking DNA length and requires flanking DNA-length dependent ATP hydrolysis. In comparison, for a hexasome, because the dimer is absent and does not inhibit INO80 remodeling, translocation occurs more readily. B) Schematic of INO80 participating in chromatin remodeling at sites of transcription. At the +1 location, INO80 helps position the nucleosome. During elongation as Pol II actively removes the H2A/H2B dimer distal to the promoter, INO80 can act on these subnucleosomal particles to restore proper positioning and help prevent aberrant transcription initiation.

53
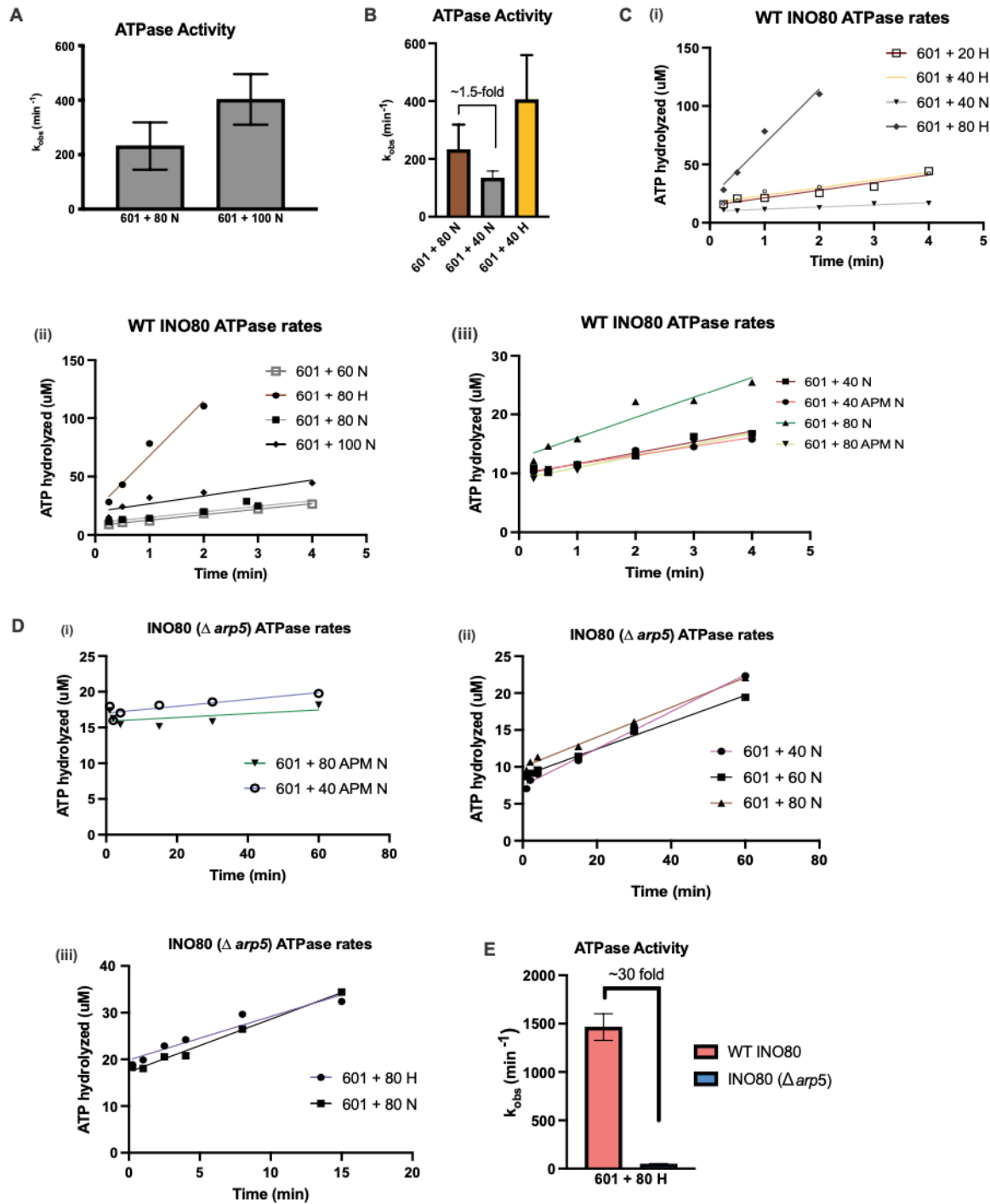
Figure S2.1. INO80 ATPase observed rate constants and representative curves.
A) Observed ATPase rate constants measured for WT INO80 showing the fold difference in activity between 601 +80 N and 601 +100 N is modest, with error bars overlapping. B) Observed ATPase rate constant measured for INO80 with 601+ 80 N, 601+40 N, and 601+40 H. The ATPase assay shows a modest difference (~1.5 fold) in activity between 601 + 80N and 601 +40 N. C) Representative ATPase rate curves for WT INO80 and all nucleosome and hexasome substrates tested in this manuscript. D) Representative ATPase curves for (Δarp5) and all nucleosome and hexasome substrates tested in this manuscript.
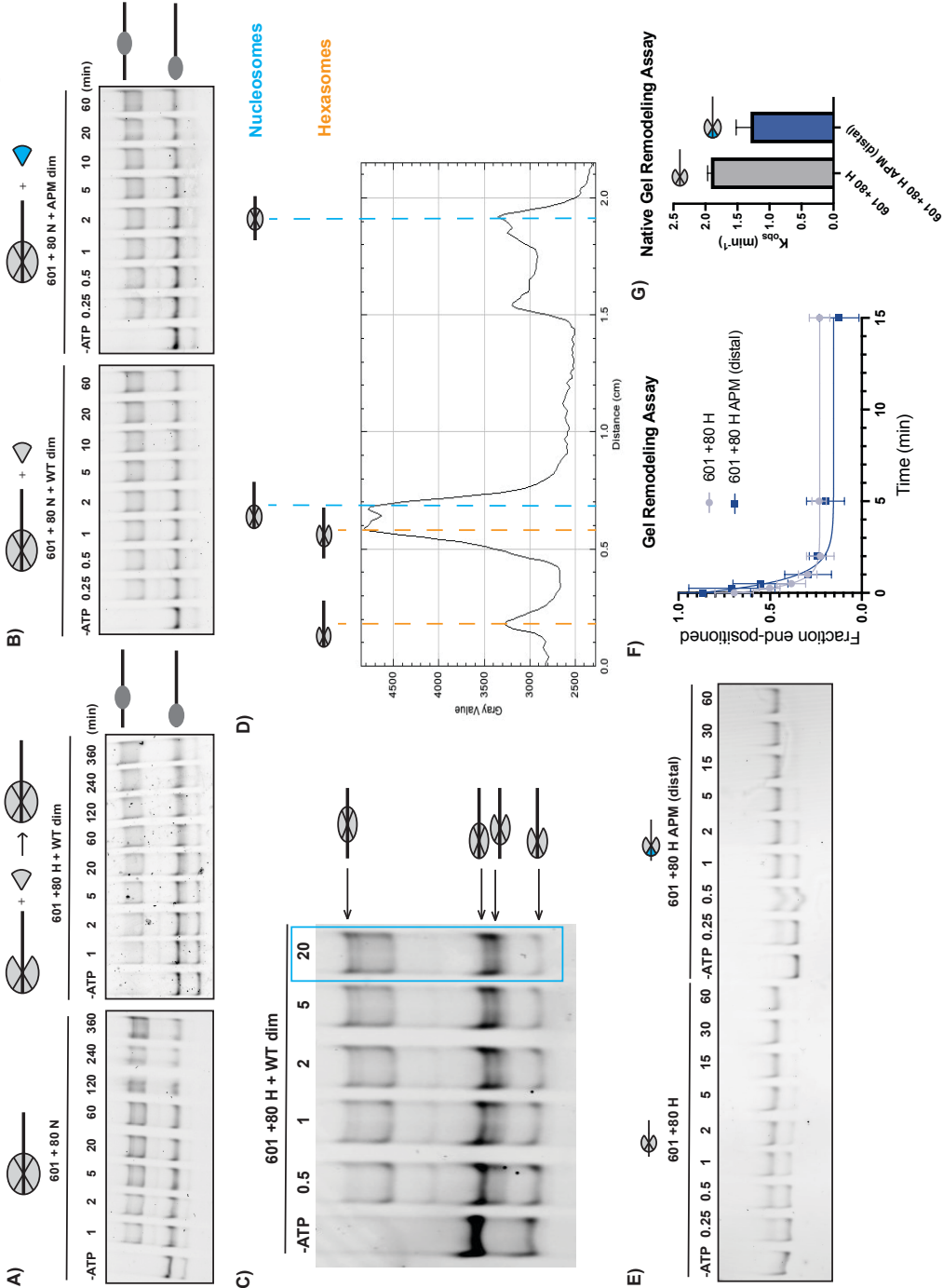
Figure S2.2. Native gel remodeling controls for asymmetric nucleosomes and hexasomes, related to figure 2.4.
A) Native gel remodeling examples of canonically assembled 601 +80 nucleosomes (left) and 601 +80 hexasomes mixed with WT dimer (right). Time points were taken over the course of 6 hours. B) Native gel remodeling examples of nucleosomes with 4-fold excess dimer added. WT dimer has been added to the left panel, and APM dimer (in blue) has been added in the right

panel. C) Native gel remodeling assay of WT hex with WT dimer, indicating the different species of +80 end-positioned hexasomes, +80 remodeled hexasomes, +80 end-positioned nucleosomes and +80 cenetered nucleosomes. The 20 min time point is boxed in blue, and this lane was used to make a line plot in D. The control showing remodeled +80 hexasomes and end-positioned nucleosomes are shown in Figure S2.7. D) A line plot from C at the 20 min time point. The generation of the line plot is described in the main text in Figure 2.4C. This line plot shows that +80 remodeled hexasomes can be distinguished from +80 end-positioned nucleosomes. E) A representative native gel remodeling assay of +80 WT hexasomes and +80 APM (distal) hexasomes. F) Gel remodeling time points (n=3) and their S.E.M. shown for +80 WT hexasomes and +80 APM hexasomes. The remodeling curves are fit to a single exponential as described in the Materials and Methods. G) A bar graph of the rate constants from F.
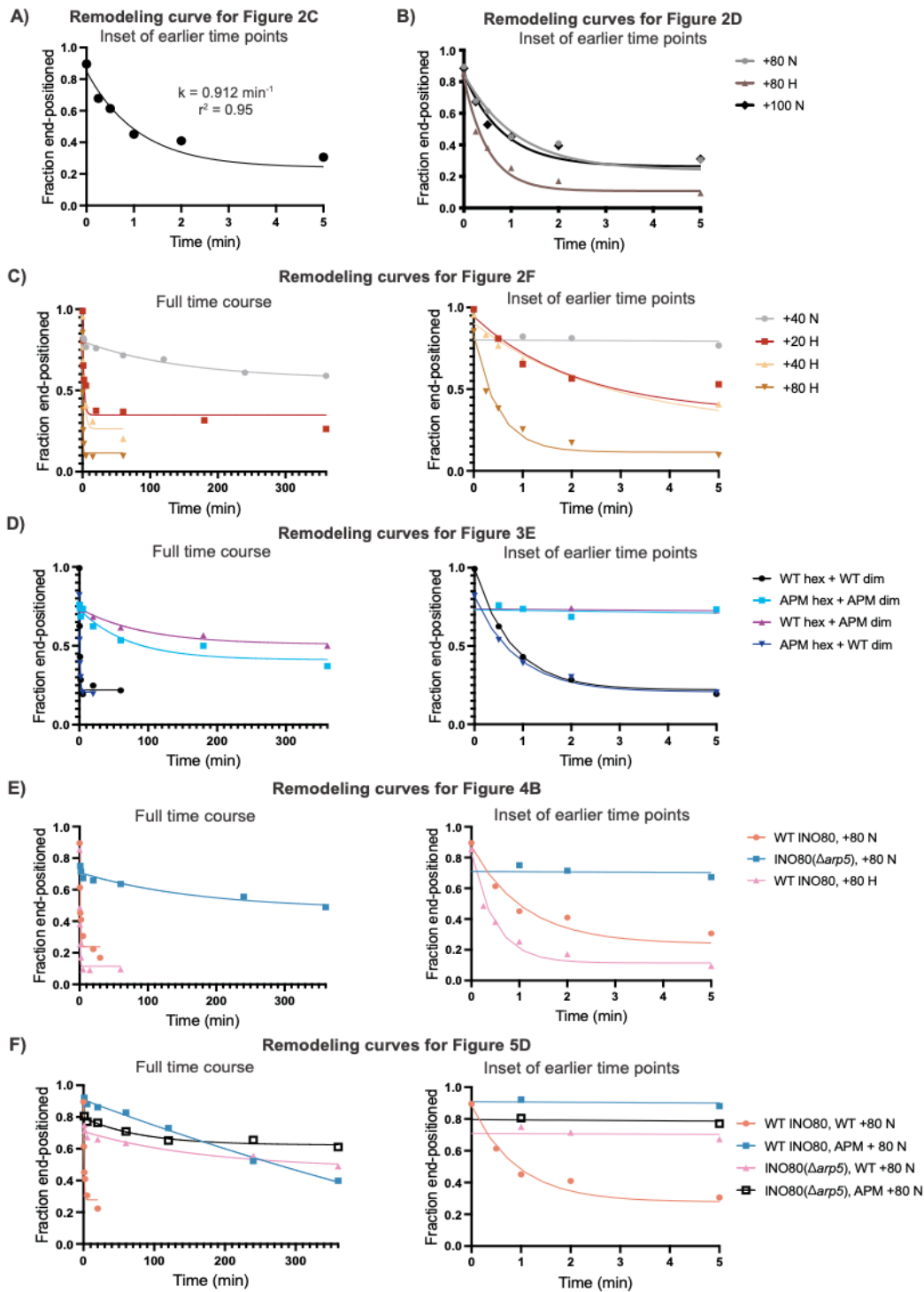
Figure S2.3. Representative gel remodeling time points and fits for all gel remodeling assays.

A) The time course of the gel remodeling assay from Figure 2.2C. The time course is an inset of earlier time points and the points are fit to a single exponential. The rate constant and r2 values are indicated on the graph. B) Representative time courses for Figure 2.2D. INO80 gel remodeling of +80 N in grey, +80 H in brown, and +100 N in black. The time on the x-axis is shortened in this schematic to show the times

where the most remodeling occurs in the reaction.
C) Representative time courses for Figure 2.2F. On the left panel is the full INO80 gel remodeling time course of +40 N in grey, +20 H in maroon, +40 H in peach, and +80 H in tan. On the right panel is an inset of the left panel, showing the first 5 minutes of the reaction. D) Representative time courses for Figure 2.3E. On the left panel is the full INO80 gel remodeling time course of WT hex + WT dim in black, APM hex + APM dim in cyan, WT hex + APM dim in magenta, and APM hex + APM dim in dark blue. On the right panel is an inset of the left panel, showing the first 5 minutes of the reaction. E) Representative time courses for Figure 2.4B. On the left panel is the full INO80 gel remodeling time course of WT INO80 with +80N in orange, INO80(Δarp5) with +80 N in blue, and WT INO80 with +80 H in pink. On the right panel is an inset of the left panel, showing the first 5 minutes of the reaction. F) Representative time courses for Figure 2.5D. On the left panel is the full INO80 gel remodeling time course of WT INO80 with WT +80 N in orange, WT INO80 with APM +80 N in blue, INO80(Δarp5) with WT +80N in pink, and INO80 (Δarp5) with APM +80 N in black. On the right panel is an inset of the left panel, showing the first 5 minutes of the reaction.
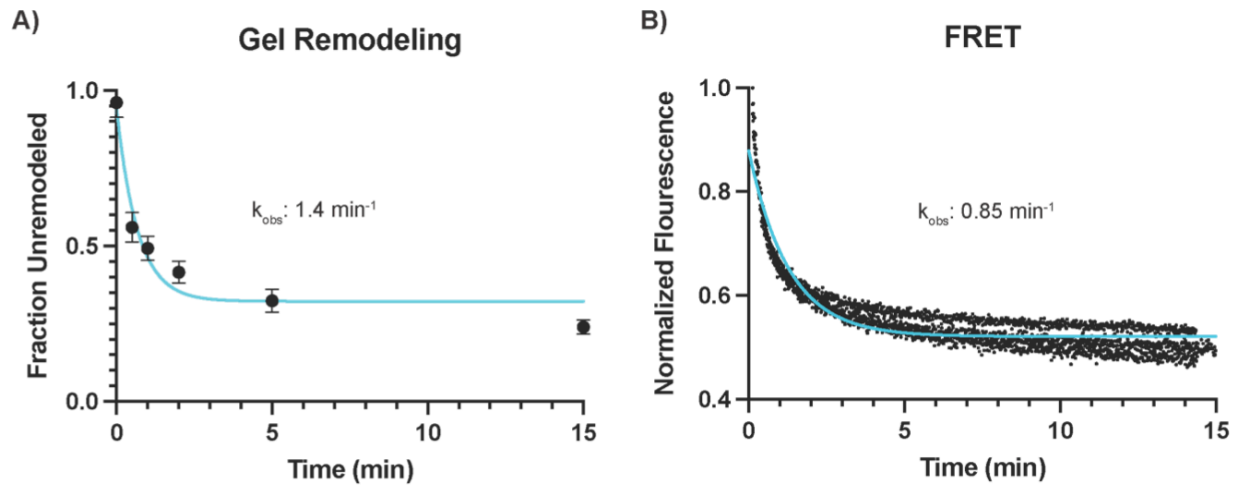
Figure S2.4. Comparison of gel remodeling rate curves and FRET rate curves.
A) Time points of INO80 gel remodeling on +80 N (n=3) with the S.E.M. with the blue line indicating the single exponential fit, which has a r2=0.96. The averaged rate constant is indicated on the graph. B) FRET INO80 remodeling on +80 N traces are depicted in black dots (n=3).The blue line indicates the average of the time course using a single exponential fit, which gives a r2=0.86. The rate constant is indicated on the graph.

59
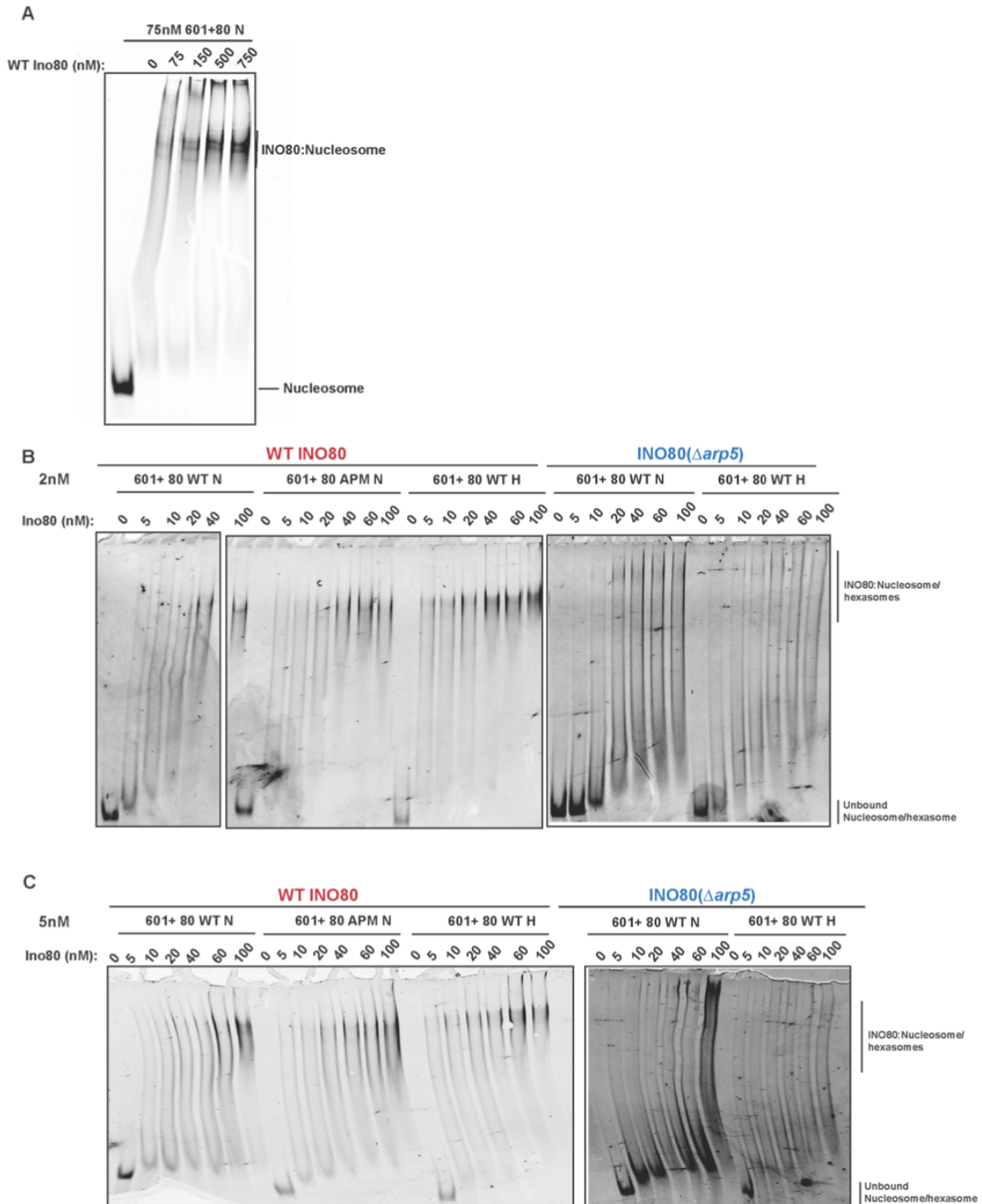
Figure S2.5. Electrophoretic Mobility Shift Assays (EMSA) with WT INO80 and INO80(Δarp5)
A) Native gel showing mobility shift of 75nM nucleosomes in the presence of WT INO80 at 75nM, 150nM, 500nM, and 750nM. B) Native gel showing mobility shift of 2nM of 601 +80 WT and double APM nucleosomes (N) and WT hexasomes (H) in the presence of increasing concentrations of WT INO80 (red) and 2nM of 601 +80 WT nucleosomes (N) and WT hexasomes (H) in the presence of increasing concentrations of INO80(Δarp5) (blue). C) Native

gel showing mobility shift of 5nM of 601 +80 WT and double APM nucleosomes (N) and WT hexasomes (H) in the presence of increasing concentrations of WT INO80 (red) and 5nM of 601 +80 WT nucleosomes (N) and WT hexasomes (H) in the presence of increasing concentrations of INO80($\Delta arp5$) (blue). All samples were prebound at 30°C for 30 minutes and products were separated on 4% acrylamide, 0.5X TBE native gel.
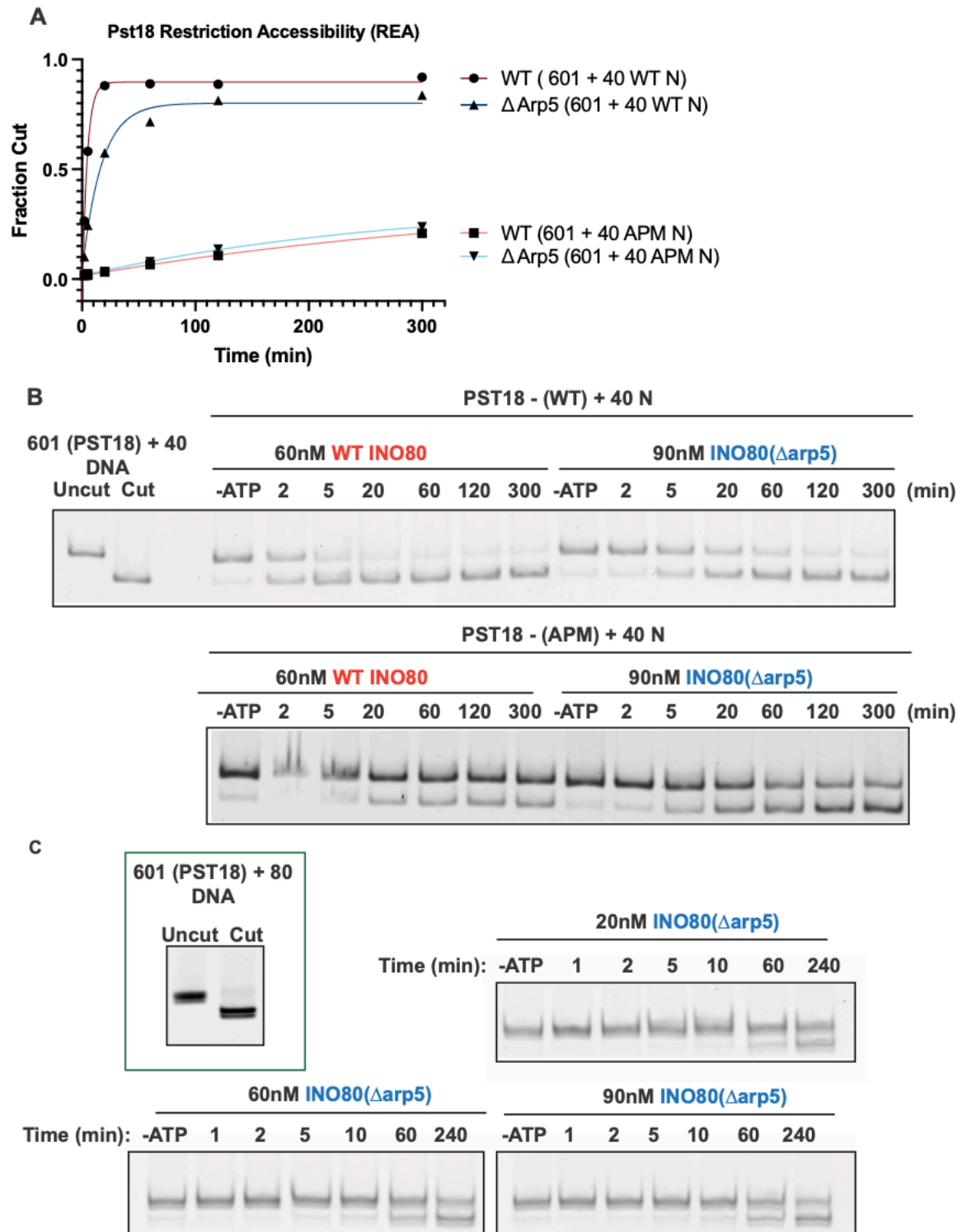
Figure S2.6. Restriction Enzyme Accessibility (REA) Assay for INO80
A) Representative curve for Figure 2.5B. Shows the fraction of DNA cut over a course of time (x-axis) by PstI at PstI site for 601 +40 WT and double APM nucleosomes, in the presence of saturating ATP and saturating WT INO80 (red) and INO80(Δ*arp5*) (blue). B) Example native gel showing the fraction of DNA cut by PstI at PstI site for 601 +40 DNA in absence of INO80 and

601+40 WT and double APM nucleosomes with saturating amounts of INO80 and ATP over a course of time (quantified in S6A). C) Example native gel showing fraction of DNA cut by PstI at Pst1 site for 601+80 DNA (boxed in green) and 601 +80 WT nucleosomes in the presence of saturating ATP and 20nM, 60nM, 90nM INO80(Δ*arp5*) to test saturation of INO80(Δ*arp5*). Uncut and cut DNA products were separated on a 6% acrylamide and 1X TBE native gel.
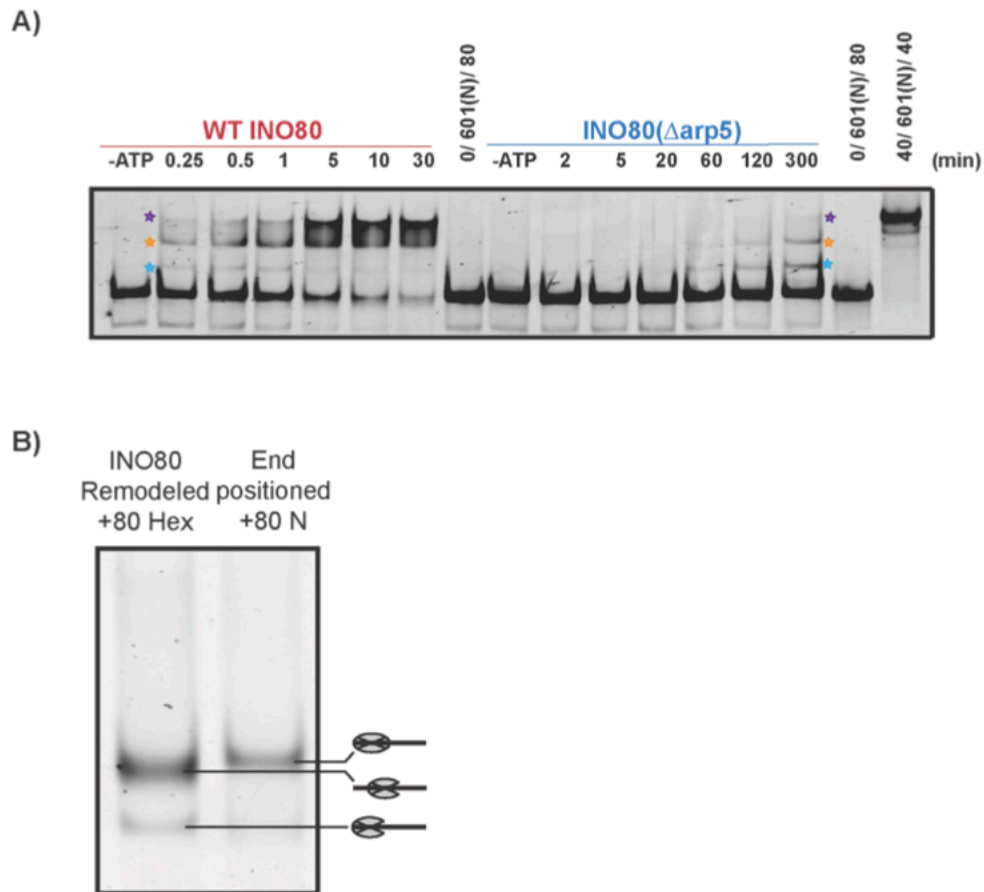
Figure S2.7. Native gel remodeling showing the migration of hexasome and nuclesome substrates and products.
A) Gel remodeling of +80 nucleosomes with WT INO80 and INO80(Δarp5). The centered 40-N-40 control and the end- positioned 0-N-80 is present in the same gel as controls. The purple star denotes the centered product, the orange start denotes another remodeled product that is dependent on the 601 sequence, and the blue star represents an intermediate band. B) A representative gel depicting an endpoint of the remodeled +80 hexasome (H) run next to an end- positioned +80 nucleosome (N). The higher running end-positioned nucleosome, the lower remodeled +80 hexasome, and the even lower end-positioned +80 hexasome (H) are indicated.
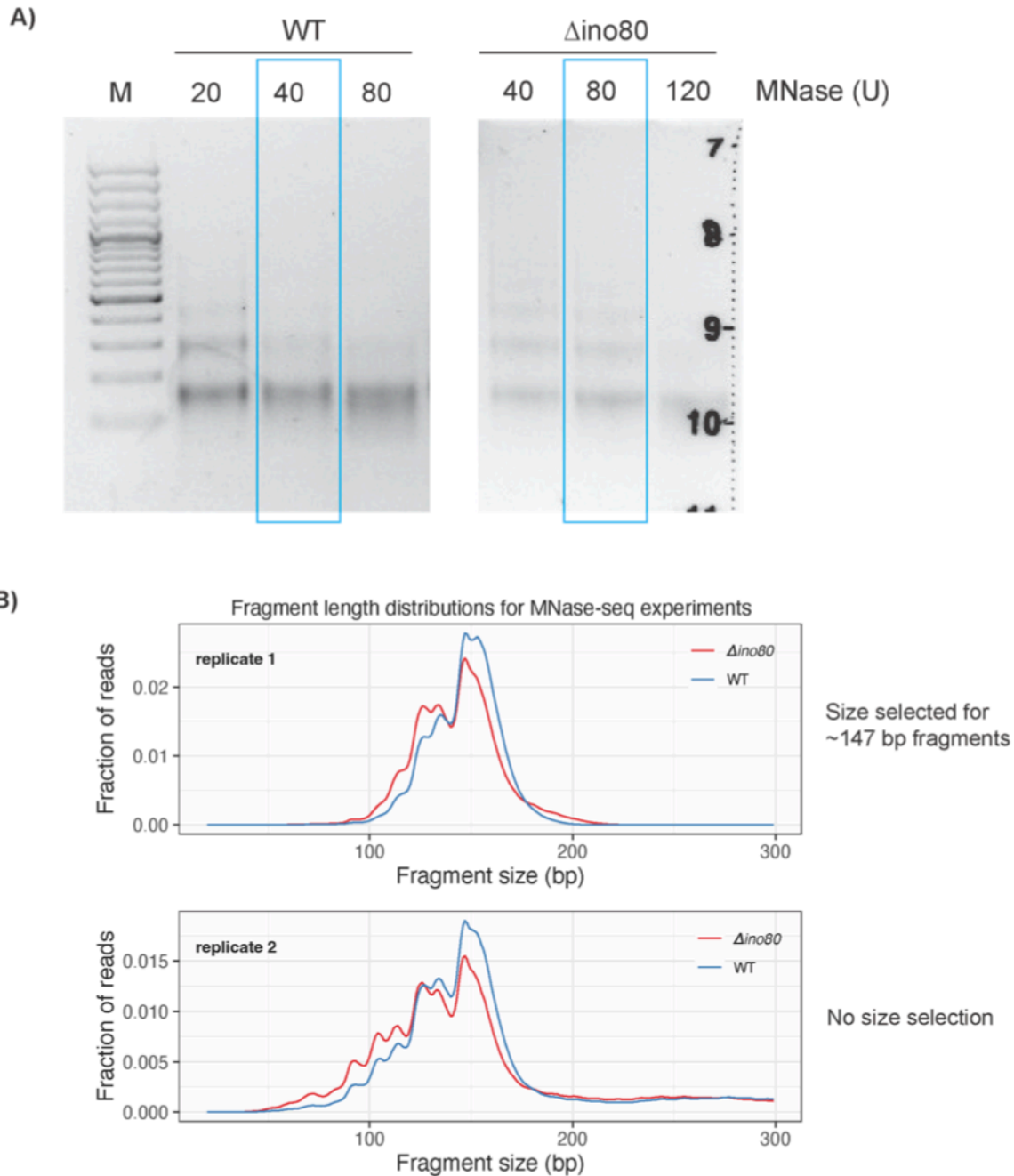
Figure S2.8. MNase digestion and fragment mapping.
A) MNase digestion patterns from WT and Δ*ino80* yeast strains, with increasing amounts of MNase. The conditions chosen for library prep are shown in blue. The samples were selected based on the MNase patterns that were most similar between WT and Δ*ino80* and had ~75% digestion to mononucleosomes, where you culd still see di- tri- nucleosomes present. B) Two replicates of the fragment length distributions from the MNase-seq experiments. The replicate reflects the distribution of fragments when there is no size selection, ensuring more recovery of ~90 bp fragments. While most of the reads map to fragments of ~150bp, there is a significant population of reads mapped to ~90bps, which likely reflects hexasomes.
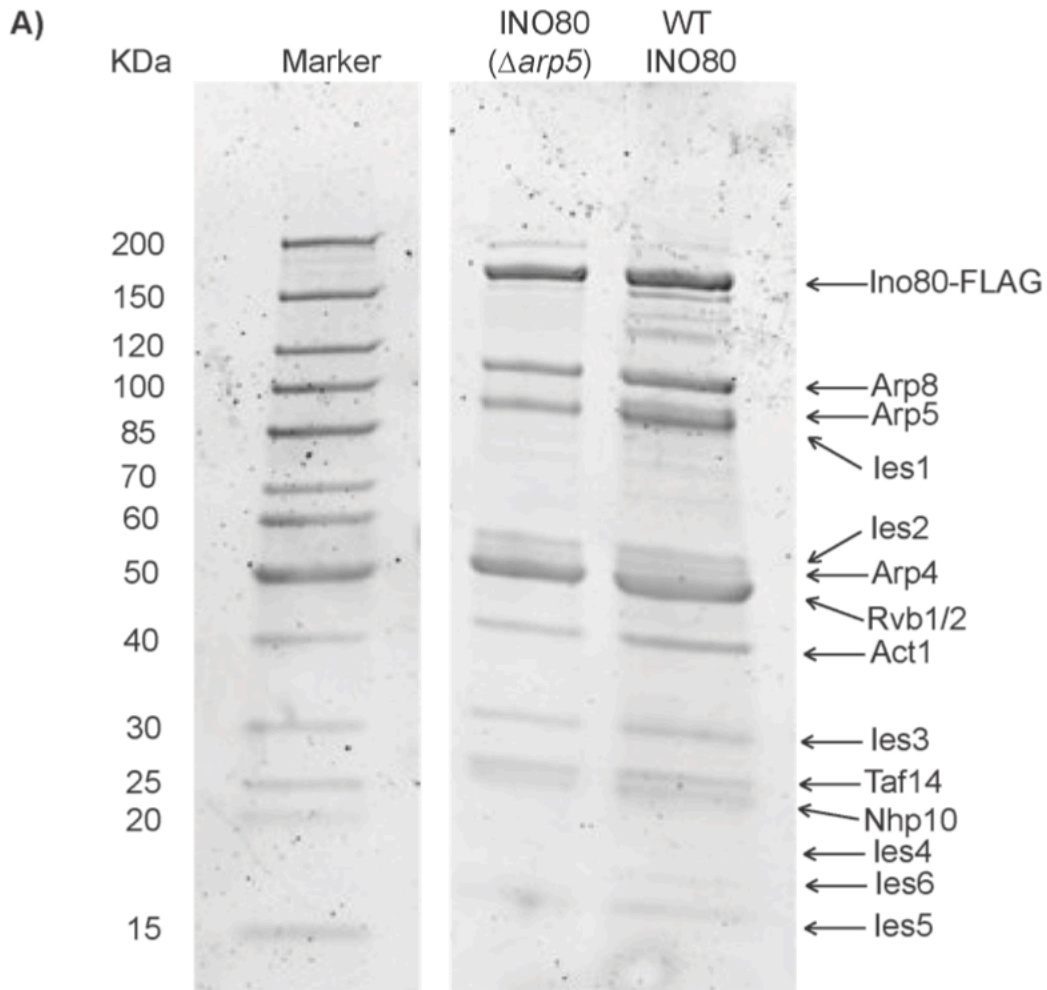
Figure S2.9. SDS-PAGE gel of WT INO80 and INO80(∆arp5) protein purifications.
A) An SDS-PAGE gel showing the FLAG pull down of WT INO80 on the right and INO80 (∆*arp5)* on the left. The ladder was run on the same gel as the purified proteins. The proteins were run on a 4-20% SDS-PAGE gel, stained with SYPRO-Red and scanned with on the GE Typhoon Imager. The molecular weights are denoted on the left, and the INO80 subunits are shown on the right.

Table 2.1 Rate constants of ATPase assays.

Construct	WT INO80 k_{obs} (min^{-1})	S.E.M.	INO80($\Delta arp5$) k_{obs} (min^{-1})	S.E.M.
+40 WT N	133.2	14.6	14.1	2.1
+60 WT N	274.2	25.8	26.9	13.8
+80 WT N	231.9	29.0	38.5	12.0
+100 WT N	402.8	53.7		
+40 APM N	111.7	13.6	0.59	2.1
+80 APM N	163.8	7.7	24.4	9.5
+20 WT H	192.6	40.6		
+40 WT H	404.9	89.1		
+80 WT H	1463.0	79.4	45.9	3.2
+80 APM H	1504.0	96.8		

Table 2.2 Rate constants with the S.E.M. for all gel remodeling based assays.

Construct	WT INO80 k_{obs} (min^{-1})	S.E.M.	INO80($\triangle arp5$) k_{obs} (min^{-1})	S.E.M.
+40 WT N	0.007	0.0005		
+80 WT N	0.977	0.0695	0.006	0.0009
+100 WT N	1.035	0.1908		
+80 APM N	0.005	0.0007	0.010	0.0011
+20 WT H	0.450	0.0751		
+40 WT H	0.273	0.0338		
+80 WT H	1.908	0.0349	*no remodeling detected	*no remodeling detected
+80 WT hex + WT dim	1.639	0.0803		
+80 APM hex + APM dim	0.015	0.0006		
+80 WT hex + APM dim	0.007	0.0018		
+80 APM hex + WT dim	0.998	0.1023		

References

1. S. Henikoff, Mechanisms of Nucleosome Dynamics In Vivo. *Csh Perspect Med*. 6, a026666 (2016).

2. S. Ramachandran, K. Ahmad, S. Henikoff, Transcription and Remodeling Produce Asymmetrically Unwrapped Nucleosomal Intermediates. *Mol Cell*. 68, 1038-1053.e4 (2017).

3. P. T. Lowary, J. Widom, New DNA sequence rules for high affinity binding to histone octamer and sequence-directed nucleosome positioning. *J Mol Biol*. 276, 19–42 (1998).

4. T. N. Mavrich, I. P. Ioshikhes, B. J. Venters, C. Jiang, L. P. Tomsho, J. Qi, S. C. Schuster, I. Albert, B. F. Pugh, A barrier nucleosome model for statistical positioning of nucleosomes throughout the yeast genome. *Genome Res*. 18, 1073–1083 (2008).

5. M. Radman-Livaja, O. J. Rando, Nucleosome positioning: How is it established, and why does it matter? *Dev Biol*. 339, 258–266 (2010).

6. E. Segal, Y. Fondufe-Mittendorf, L. Chen, A. Thåström, Y. Field, I. K. Moore, J.-P. Z. Wang, J. Widom, A genomic code for nucleosome positioning. *Nature*. 442, 772–778 (2006).

7. C. Y. Zhou, S. L. Johnson, L. J. Lee, A. D. Longhurst, S. L. Beckwith, M. J. Johnson, A. J. Morrison, G. J. Narlikar, The Yeast INO80 Complex Operates as a Tunable DNA Length-Sensitive Switch to Regulate Nucleosome Sliding. *Mol Cell*. 69, 677-688.e9 (2018).

69

8. N. Krietenstein, M. Wal, S. Watanabe, B. Park, C. L. Peterson, B. F. Pugh, P. Korber, Genomic Nucleosome Organization Reconstituted with Pure Proteins. *Cell*. 167, 709-721.e12 (2016).

9. A. Klein-Brill, D. Joseph-Strauss, A. Appleboim, N. Friedman, Dynamics of Chromatin and Transcription during Transient Depletion of the RSC Chromatin Remodeling Complex. *Cell Reports*. 26, 279-292.e5 (2019).

10. C. Y. Zhou, S. L. Johnson, N. I. Gamarra, G. J. Narlikar, Mechanisms of ATP-Dependent Chromatin Remodeling Motors. *Annu Rev Biophys*. 45, 153–181 (2016).

11. R. K. McGinty, S. Tan, Nucleosome Structure and Function. *Chem Rev*. 115, 2255–2273 (2015).

12. H. T. Dao, B. E. Dul, G. P. Dann, G. P. Liszczak, T. W. Muir, A basic motif anchoring ISWI to nucleosome acidic patch regulates nucleosome spacing. *Nat Chem Biol*. 16, 134–142 (2020).

13. S. Eustermann, K. Schall, D. Kostrewa, K. Lakomek, M. Strauss, M. Moldt, K.-P. Hopfner, Structural basis for nucleosome remodeling by the INO80 complex. *Nature*. 556, 386–390 (2018).

14. N. Gamarra, S. L. Johnson, M. J. Trnka, A. L. Burlingame, G. J. Narlikar, The nucleosomal acidic patch relieves auto-inhibition by the ISWI remodeler SNF2h. *Elife*. 7, e35322 (2018).

15. R. F. Levendosky, G. D. Bowman, Asymmetry between the two acidic patches dictates the direction of nucleosome sliding by the ISWI chromatin remodeler. *Elife*. 8, e45472 (2019).

16. A. M. Valencia, C. K. Collings, H. T. Dao, R. St. Pierre, Y.-C. Cheng, J. Huang, Z.-Y. Sun, H.-S. Seo, N. Mashtalir, D. E. Comstock, O. Bolonduro, N. E. Vangos, Z. C. Yeoh, M. K. Dornon, C. Hermawan, L. Barrett, S. Dhe-Paganon, C. J. Woolf, T. W. Muir, C. Kadoch, Recurrent SMARCB1 Mutations Reveal a Nucleosome Acidic Patch Interaction Site That Potentiates mSWI/SNF Complex Chromatin Remodeling. *Cell.* 179, 1342-1356.e23 (2019).

17. H. S. Rhee, A. R. Bataille, L. Zhang, B. F. Pugh, Subnucleosomal Structures and Nucleosome Asymmetry across a Genome. *Cell*. 159, 1377–1388 (2014).

18. Y. Qiu, R. F. Levendosky, S. Chakravarthy, A. Patel, G. D. Bowman, S. Myong, The Chd1 Chromatin Remodeler Shifts Nucleosomal DNA Bidirectionally as a Monomer. *Mol Cell*. 68, 76-88.e6 (2017).

19. R. F. Levendosky, A. Sabantsev, S. Deindl, G. D. Bowman, The Chd1 chromatin remodeler shifts hexasomes unidirectionally. *Elife*. 5, e21356 (2016).

20. X. Shen, R. Ranallo, E. Choi, C. Wu, Involvement of Actin-Related Proteins in ATP-Dependent Chromatin Remodeling. *Mol Cell*. 12, 147–155 (2003).

21. X. Shen, G. Mizuguchi, A. Hamiche, C. Wu, A chromatin remodelling complex involved in transcription and DNA processing. *Nature*. 406, 541–544 (2000).

22. S. Brahma, M. I. Udugama, J. Kim, A. Hada, S. K. Bhardwaj, S. G. Hailu, T.-H. Lee, B. Bartholomew, INO80 exchanges H2A.Z for H2A by translocating on DNA proximal to histone dimers. *Nat Commun*. 8, 15616 (2017).

23. W. Yao, D. A. King, S. L. Beckwith, G. J. Gowans, K. Yen, C. Zhou, A. J. Morrison, The INO80 Complex Requires the Arp5-Ies6 Subcomplex for Chromatin Remodeling and Metabolic Regulation. *Mol Cell Biol*. 36, 979–991 (2016).

24. R. Ayala, O. Willhoft, R. J. Aramayo, M. Wilkinson, E. A. McCormack, L. Ocloo, D. B. Wigley, X. Zhang, Structure and regulation of the human INO80–nucleosome complex. *Nature*. 556, 391–395 (2018).

25. K. Yen, V. Vinayachandran, B. F. Pugh, SWR-C and INO80 Chromatin Remodelers Recognize Nucleosome-free Regions Near +1 Nucleosomes. *Cell*. 154, 1246–1256 (2013).

26. K. Brogaard, L. Xi, J.-P. Wang, J. Widom, A map of nucleosome positions in yeast at base-pair resolution. *Nature*. 486, 496–501 (2012).

27. H. Goodarzi, O. Elemento, S. Tavazoie, Revealing Global Regulatory Perturbations across Human Cancers. *Mol Cell*. 36, 900–911 (2009).

28. O. I. Kulaeva, D. A. Gaykalova, N. A. Pestov, V. V. Golovastov, D. G. Vassylyev, I. Artsimovitch, V. M. Studitsky, Mechanism of chromatin remodeling and recovery during passage of RNA polymerase II. *Nat Struct Mol Biol*. 16, 1272–1278 (2009).

29. J. García-Martínez, A. Aranda, J. E. Pérez-Ortín, Genomic Run-On Evaluates Transcription Rates for All Yeast Genes and Identifies Gene Regulatory Mechanisms. *Mol Cell*. 15, 303–313 (2004).

30. V. Pelechano, J. E. Pérez-Ortín, There is a steady-state transcriptome in exponentially growing yeast cells. *Yeast*. 27, 413–422 (2010).

31. W. Yao, S. L. Beckwith, T. Zheng, T. Young, V. T. Dinh, A. Ranjan, A. J. Morrison, Assembly of the Arp5 (Actin-related Protein) Subunit Involved in Distinct INO80 Chromatin Remodeling Activities*. *J Biol Chem*. 290, 25700–25709 (2015).

32. A. Tosi, C. Haas, F. Herzog, A. Gilmozzi, O. Berninghausen, C. Ungewickell, C. B. Gerhold, K. Lakomek, R. Aebersold, R. Beckmann, K.-P. Hopfner, Structure and Subunit Topology of the INO80 Chromatin Remodeler and Its Nucleosome Complex. *Cell*. 154, 1207–1219 (2013).

33. A. J. Morrison, X. Shen, Chromatin remodelling beyond transcription: the INO80 and SWR1 complexes. *Nat Rev Mol Cell Bio*. 10, 373–384 (2009).

34. S. Watanabe, M. Radman-Livaja, O. J. Rando, C. L. Peterson, A Histone Acetylation Switch Regulates H2A.Z Deposition by the SWR-C Remodeling Enzyme. *Science*. 340, 195–199 (2013).

35. F. Wang, A. Ranjan, D. Wei, C. Wu, Comment on "A histone acetylation switch regulates H2A.Z deposition by the SWR-C remodeling enzyme." *Science*. 353, 358–358 (2016).

36. M. Papamichos-Chronakis, S. Watanabe, O. J. Rando, C. L. Peterson, Global Regulation of H2A.Z Localization by the INO80 Chromatin-Remodeling Enzyme Is Essential for Genome Integrity. *Cell*. 144, 200–213 (2011).

37. S. Brahma, M. Ngubo, S. Paul, M. Udugama, B. Bartholomew, The Arp8 and Arp4 module acts as a DNA sensor controlling INO80 chromatin remodeling. *Nat Commun*. 9, 3309 (2018).

38. E. Klopf, L. Paskova, C. Solé, G. Mas, A. Petryshyn, F. Posas, U. Wintersberger, G. Ammerer, C. Schüller, Cooperation between the INO80 Complex and Histone Chaperones

Determines Adaptation of Stress Gene Transcription in the Yeast Saccharomyces cerevisiae. *Mol Cell Biol*. 29, 4994–5007 (2009).

39. A. Lafon, S. Taranum, F. Pietrocola, F. Dingli, D. Loew, S. Brahma, B. Bartholomew, M. Papamichos-Chronakis, INO80 Chromatin Remodeler Facilitates Release of RNA Polymerase II from Chromatin for Ubiquitin-Mediated Proteasomal Degradation. *Mol Cell*. 60, 784–796 (2015).

40. J. Poli, C.-B. Gerhold, A. Tosi, N. Hustedt, A. Seeber, R. Sack, F. Herzog, P. Pasero, K. Shimada, K.-P. Hopfner, S. M. Gasser, Mec1, INO80, and the PAF1 complex cooperate to limit transcription replication conflicts through RNAPII removal during replication stress. *Gene Dev*. 30, 337–354 (2016).

41. A. K. Singh, T. Schauer, L. Pfaller, T. Straub, F. Mueller-Planitz, The biogenesis and function of nucleosome arrays. *Nat Commun*. 12, 7011 (2021).

42. M. L. Kireeva, W. Walter, V. Tchernajenko, V. Bondarenko, M. Kashlev, V. M. Studitsky, Nucleosome Remodeling Induced by RNA Polymerase II Loss of the H2A/H2B Dimer during Transcription. *Mol Cell*. 9, 541–552 (2002).

43. R. Belotserkovskaya, S. Oh, V. A. Bondarenko, G. Orphanides, V. M. Studitsky, D. Reinberg, FACT Facilitates Transcription-Dependent Nucleosome Alteration. *Science*. 301, 1090–1093 (2003).

44. B. G. Kuryan, J. Kim, N. N. H. Tran, S. R. Lombardo, S. Venkatesh, J. L. Workman, M. Carey, Histone density is maintained during transcription mediated by the chromatin remodeler RSC and histone chaperone NAP1 in vitro. *Proc National Acad Sci*. 109, 1931–1936 (2012).

45. E. A. Alcid, T. Tsukiyama, ATP-dependent chromatin remodeling shapes the long noncoding RNA landscape. *Gene Dev*. 28, 2348–2360 (2014).

46. N. Slavov, B. A. Budnik, D. Schwab, E. M. Airoldi, A. van Oudenaarden, Constant Growth Rate Can Be Supported by Decreasing Energy Flux and Increasing Aerobic Glycolysis. *Cell Reports*. 7, 705–714 (2014).

47. A. J. Morrison, J.-A. Kim, M. D. Person, J. Highland, J. Xiao, T. S. Wehr, S. Hensley, Y. Bao, J. Shen, S. R. Collins, J. S. Weissman, J. Delrow, N. J. Krogan, J. E. Haber, X. Shen, Mec1/Tel1 Phosphorylation of the INO80 Chromatin Remodeling Complex Influences DNA Damage Checkpoint Responses. *Cell*. 130, 499–511 (2007).

48. J. Rodriguez, J. N. McKnight, T. Tsukiyama, *Curr Protoc Mol Biology*, in press , doi:10.1002/0471142727.mb2128s108.

49. V. Ramani, R. Qiu, J. Shendure, High Sensitivity Profiling of Chromatin Structure by MNase-SSP. *Cell Reports*. 26, 2465-2476.e4 (2019).

50. Y. Voichek, K. Mittelman, Y. Gordon, R. Bar-Ziv, D. L. Smit, R. Shenhav, N. Barkai, Epigenetic Control of Expression Homeostasis during Replication Is Stabilized by the Replication Checkpoint. *Mol Cell*. 70, 1121-1133.e9 (2018).

Chapter 3: Structure analysis of S. cerevisiae INO80 bound to hexasome, reveals mechanistic insights on how this unique conserved chromatin remodeling machine is more similar to its closely related chromatin remodeling counterparts.

Abstract

Unlike other chromatin remodelers, the INO80 complex preferentially mobilizes hexasomes, which can form during transcription. Why INO80 prefers hexasomes over nucleosomes remains unclear. Here, we report the cryogenic electron microscopy structures of *S. cerevisiae* INO80 with a hexasome. Unexpectedly, INO80 is rotated by ~180° placing its ATPase subunit, Ino80, at superhelical location (SHL)-2 instead of SHL-6/-7 as seen on a nucleosome. Our results indicate that INO80 action on hexasomes resembles action by other remodelers on nucleosomes, such that the Ino80 ATPase is maximally active at SHL-2. In contrast, INO80 action on nucleosomes, appears heavily regulated by auto-inhibition and steric clashes that prevent Ino80 from readily accessing SHL-2. These novel mechanistic adaptations for preferential hexasome sliding imply that sub-nucleosomal particles play significant regulatory roles.

Introduction

In eukaryotes central nuclear processes such as gene expression, DNA replication and DNA repair are coordinated with dynamic changes in chromatin states (*1-3*). ATP-dependent chromatin remodeling enzymes play essential roles in catalyzing such changes. These enzymes, which often operate as multi-subunit complexes, are broadly categorized into four major families: SWI/SNF, ISWI, CHD, and INO80 (*4, 5*). Each of these classes contains a core remodeling ATPase subunit and several auxiliary subunits that regulate the core ATPase. It has typically been presumed that the preferred substrate of these enzymes is a nucleosome, the smallest unit of chromatin, containing ~ 147 bp of DNA wrapped around an octamer of histone proteins (*6*). Consistent with this assumption, these four classes possess activities that slide the histone octamer, exchange histone variants and transfer entire octamers (*5, 7*).

The INO80 complex, has been shown to play roles in regulating transcription, DNA replication and DNA repair (*8-11*). How INO80's biochemical activities relate to its diverse biological roles is not well understood. Interestingly, unlike remodelers from other families, whose core ATPase subunits bind at the internal nucleosome location of superhelical location (SHL)2, Ino80, the core ATPase subunit of the INO80 complex, binds near the edge of the nucleosome at SHL-6/-7 (figure. S3.1A)(*12-14*). It has been speculated that this key difference in nucleosome engagement reflects a fundamentally different remodeling mechanism (*15, 16*). Indeed, we showed that the preferred substrate of the *S. cerevisiae* INO80 complex is not a nucleosome but a sub-nucleosomal particle that is missing a histone H2A-H2B dimer (*17*). Such subnucleosomal particles, called hexasomes, are generated during transcription and may also be formed during DNA replication and repair (*18-21*). Further, INO80's activity on nucleosomes is more dependent on flanking DNA length than its activity on hexasomes (*17, 22*). These results suggested that INO80 has the versatility to act on hexasomes or nucleosomes based on the density of nucleosomes and sub-nucleosomal particles at a given locus. Yet, fundamental mechanistic questions remain. It is not clear how INO80 can act on both nucleosomes and hexasomes, which differ substantially in their structures. Additionally, why INO80 has different flanking DNA length dependencies on hexasomes versus nucleosomes is also unclear.

Here, we report single particle cryogenic-electron microscopy (cryo-EM) structures of endogenously purified *S. cerevisiae* INO80 bound to a hexasome and a nucleosome. Surprisingly, our structures show that INO80 binds hexasomes analogous to how other remodelers bind nucleosomes, with the core ATPase, Ino80, binding at SHL-2. In our INO80-hexasome structures the Arp5 module engages the H3-H4 interface and the Arp8 module interacts with DNA unwrapped from the histone core. In our INO80-nucleosome structures the Arp5 module engages the H2A-H2B acidic patch and the Arp8 module engages flanking DNA. These structural

snapshots uncover the mechanistic strategies INO80 uses to slide hexasomes and imply a highly regulated mechanism for sliding nucleosomes.

Results

Overall structure of the INO80-hexasome complex

To visualize how INO80 binds to a hexasome or a nucleosome by single particle cryo-EM, we prepared hexasomes and nucleosomes on DNA templates containing the 147 bp 601 nucleosome positioning sequence with 80 bp of additional DNA as described previously (601+80 H and 601+80 N, Figure 3.1A, and figure S3.1 A and B) (*17, 23, 24*). These hexasomes are asymmetric and lack the entry-site proximal H2A-H2B. We define the entry and exit DNA sites as the sites closest and farthest from the flanking DNA, respectively. Further, given the additional DNA that is unwrapped in a hexasome, we define flanking DNA as the additional DNA beyond the 147 bp of the 601 sequence, and free DNA as the DNA that is not bound to histones. Thus, 601+80 N has 80 bp of free DNA while 601+80 H has ~ 115 bp of free DNA because of the additional ~35 bp of DNA that is unwrapped from removal of an H2A-H2B dimer. INO80-hexasome and INO80-nucloeosome complexes were formed by mixing hexasomes or nucleosomes with endogenously purified *S. cerevisiae* INO80 without adding nucleotide and subjected to single particle cryo-EM (Figures S3.1, C to H, and S3.2-S3.5).

We determined the cryo-EM structure of the INO80-hexasome complex at a global resolution of 2.6Å and a local resolution for the hexasome at 2.9Å, allowing accurate model building for most of the complex (Figures 3.1B, 3.1C, S3.2, S3.4A-F, and S3.5). The overall shape of INO80 is similar to previously published structures of the INO80-nucleosome complex obtained with human (*12*) and *Chaetomium thermophilum* (*14*) INO80. Similar to these previous studies we grouped all visible subunits of the INO80 complex into four modules: Rvb module (Rvb1/Rvb2), Arp8 module

79

(Arp8/Arp4/Actin), Ino80 module (Ino80/Ies2) and Arp5 module (Arp5/Ies6). The Nhp10 module is present in the complex but is not visible in our structure, suggesting its flexibility.

The well-resolved Rvb module contains the heterohexamer formed by the Rvb1 and Rvb2 that serves as a scaffold to assemble other subunits (Figure 3.1B, S3.5A). Although no nucleotide was added during sample preparation, clear density for ADP is seen in all nucleotide binding pockets of Rvb1/Rvb2 (Figure S3.5C). The resolution of the Arp8 module is low, but sufficient for placing the previous crystal structure (PDB: 5NBN (*25*)) into the density map (Figure S3.2B, and S3.6, A and B). The Ino80 ATPase is composed of three major regions: the N-terminal domain (NTD), the HSA region (Ino80^{HSA}) and the ATPase domain (Ino80^{ATPase}). Among them, the HSA links Ino80 with the Arp8 module and is only partially resolved. The two RecA lobes in the ATPase domain (N-lobe and C-lobe) are interrupted by a large insertion, which can clearly be seen threaded through the Rvb1/Rvb2 hexamer similar to previous INO80-nucleosome structures (*12, 14*). While the C-lobe is clearly resolved, the N-lobe resolution is only sufficient for docking in the atomic model. As a result, the nucleotide binding state of Ino80^{ATPase} is unclear. The core of the Arp5 subunit is well resolved with its DNA binding domain Arp5^{DBD} interacting with hexasomal DNA at SHL+2 (Figure S3.6, C and D) and with density for an ATP molecule in the nucleotide binding pocket (Figure S3.5D). Furthermore, similar to the previously published INO80-nucleosome structure (*12, 14*), the C-terminal HIT-like domain of Ies6 forms a stable contact with Rvb1/2, while the rest of Ies6 wraps around Arp5 (Figure S3.6E).

While the overall INO80 architecture appears similar to prior studies as well as our own INO80-nucleosome structures (discussed below), a major difference is that the INO80 complex is rotated ~180° on a hexasome compared to a nucleosome (Figure 3.1, D and E). The hexasome bound by INO80 is well defined (Figures S3.4F and S3.5B), retaining the canonical structural features of a hexasome seen in previous structures (*26-28*). We identified two primary interaction points

80

between INO80 and the hexasome: Ino80[ATPase] binds the hexasome near SHL-2, and the Arp5/Ies6 module binds near SHL+2 (Figure 3.1E and 3.2). This Ino80[ATPase] binding location is different from the location of Ino80[ATPase] on nucleosomes, shown to be at SHL-6 or SHL-7 in prior cryo-EM structures and biochemical studies (*12-14*). However, the position of Ino80[ATPase] on the hexasome is consistent with structures of other major chromatin remodelers such as *S. cerevisiae* ISW1 (*29-31*), Chd1 (*32-34*), RSC (*35-37*) and in particular the SWR1 complex (*38*), which is from the same sub-family as the INO80 complex. In all of these structures the ATPase domains interact with nucleosomal DNA at either SHL+2 or SHL-2 (Figure 3.1E). Below, we first explore in more detail the engagement of Ino80 with a hexasome, then describe our INO80-nucleosome structures and finally compare changes observed for the Arp8 and Arp5 modules.

Binding of Ino80 ATPase domain at SHL-2 correlates with unwrapping of hexasomal DNA

In addition to the INO80-hexasome reconstruction described above, which contains the largest portion of particles in our dataset, we obtained two more reconstructions by focused classification centered on the hexasome (Figures 3.2A and S3.2). The overall resolutions of these two reconstructions are 3.0Å (class 1) and 2.8Å (class 2), with the local resolution of the hexasome at 6.7Å and 3.2Å, respectively, sufficient to position the atomic model of a hexasome (Figures S3.4, A to D). Comparison of these two reconstructions with the one described above, which we name as class 3, shows that the conformation of the INO80 complex in all classes is largely similar but the two major contact sites on the hexasome are different (Figures 3.2 and S3.7A). In class 1, Ino80[ATPase] interacts with hexasomal DNA at SHL-3 and the Arp5/Ies6 module binds near SHL+1. In class 2, Ino80[ATPase] and the Arp5/Ies6 module interact with the hexasome at SHL-2.5 and SHL+1.5, respectively. Thus, we see that Ino80[ATPase] can bind to hexasomal DNA at SHL-3 (class 1), -2.5 (class 2), and -2 (class 3) positions (Figures 3.2A and S3.7A).

81

One available atomic model of a hexasome was determined with a short peptide bound (pdb code: 6ZHY, (*27*)), which we approximate as representing an unbound hexasome. Loss of an H2A-H2B dimer in a hexasome causes an additional ~35 bp of DNA to unwrap from the histone core (Figures 3.1A and S3.1B). Interestingly, comparison of the hexasome structures found in our reconstructions with this unbound hexasome reveal different levels of further DNA unwrapping. In class 1, the hexasome structure is almost identical with the unbound hexasome, without detectable additional DNA unwrapping. The level of DNA unwrapping increases as the Ino80^{ATPase} binding position changes from SHL-3 (class 1) to SHL-2 (class 3) (Figures 3.2B and S3.7B). For comparison, the Chd1 remodeler which binds to a nucleosome at SHL-2/+2 also leads to DNA unwrapping (*32-34, 39*), suggesting that binding at a location most conducive to DNA translocation is correlated with DNA unwrapping.

S. cerevisiae INO80-nucleosome structures uncover two conformations

The prior INO80-nucleosome structures were determined with human and *C. thermophilum* INO80, while we use *S. cerevisiae* INO80. To control for any species related differences, we also determined structures of *S. cerevisiae* INO80 bound to a nucleosome without added nucleotide. 3D classification reveals two major conformations, with overall resolutions of 3.5Å for class 1 and 3.4Å for class 2, and the local resolutions for the nucleosomal region of 3.5Å and 3.3Å, respectively (Figures 3.3, S3.3, and S3.4, G to J, and S3.8A). The INO80 structure is almost identical between these two states, with a rmsd of 0.4Å. The overall architecture of *S. cerevisiae* INO80 on a nucleosome is also similar to that in previous INO80-nucleosome structures (*12, 14*).

Interestingly, when aligning the two structures based on their respective nucleosome dyads, Ino80^{ATPase} in class 1 is located at SHL-7, similar to its location in the human INO80-nucleosome structure (*12*), while in class 2, it binds at SHL-6, similar to the *C. thermophilum* INO80-

nucleosome structure (*14*) (Figure 3.3B). Correspondingly, the Arp5/Ies6 module interacts with the nucleosome near SHL-4 and SHL-3, respectively. This finding is also consistent with previous findings showing that nucleosomal DNA between SHL-7 and SHL-6 is protected by INO80 (*13*). Interestingly, the C-terminal tail of Ies6 is better resolved in class 2, and makes a close interaction with H2B, correlating with a shift of H2B towards Ies6 by ~1Å, as measured from the position of Y118 in H2B (Fig 3.3C). The differences between these two conformations are also seen when comparing the published structures of human and *C. thermophilum* INO80-nucleosome complexes (*12, 14*). However, unlike in both human and *C. thermophilum* INO80-nucleosome structures, we see much less DNA unwrapping for each INO80-nucleosome class. We speculate that this may be a consequence of these prior structures missing additional flanking DNA binding subunits such as the Nhp10 module in *S. cerevisiae* INO80.

The role of the Arp8 module in flanking DNA length dependence

Prior studies have suggested that the Arp8 module binds flanking DNA (*40*). To understand the role of this module in hexasome and nucleosome sliding we compared its location in our structures. In both the INO80-hexasome and INO80-nucleosome structures, we can resolve the Arp8 module after focused classification but with lower resolution (figures S3.2B, S3.3B, S3.6, A and B, and S3.8B). Nonetheless, the quality of the density maps allows us to place the previous atomic model of the Arp8 module (PDB: 5NBN (*25*)) into the cryo-EM density maps and to build an atomic model together with the rest of INO80. In all cases, we find that the Arp8 module requires ~40 bp of DNA for appropriate engagement. In class 1 of the INO80-hexasome structure, Arp8 engages with the ~35 bp of DNA unwrapped from removal of the H2A-H2B dimer and an additional 5 bp of flanking DNA. In class 3 of the INO80-hexasome structure, the Arp8 module engages entirely with 40 bp of unwrapped DNA that now includes additional DNA unwrapped

83

relative to the unbound hexasome (Figure 3.4A). In contrast in class 2 of the INO80-nucleosome structure, the Arp8 module engages entirely with flanking DNA (Figure 3.4A).

The Arp 8 module's interaction with ~40 bp of DNA is interesting because *S. cerevisiae* INO80 slides 601+40 nucleosomes ~100-fold more slowly than 601+80 nucleosomes (*17, 22*). Our structural data suggests that 40 bp may be the minimum amount of DNA needed for the Arp8 module to bind and that proper Arp8 module engagement is essential for maximal remodeling activity. We therefore asked if deleting the Arp8 module inhibits nucleosome sliding. Surprisingly, while deleting the Arp8 module modestly decreased sliding of 601+80 nucleosomes (~2.5-fold), it increased nucleosome sliding of 601+40 nucleosomes by ~ 50-fold (Figures 3.4B and S3.9A). These results suggest that rather than playing a stimulatory role, the Arp8 module plays an auto-inhibitory role when the flanking DNA is 40 bp or less. We next asked if Arp8 plays a similar role in the context of hexasomes. We found that deletion of the Arp8 module increased sliding of 601+40 hexasomes by a smaller (~ 4.5-fold) amount compared to nucleosomes (Figre 3.4C and S3.9B). This result indicates that the Arp8 module plays a smaller autoinhibitory role in the context of hexasomes. We further explore the implications of these findings in the Discussion.

Altered interactions by the Arp5 module

In prior INO80-nucleosome structures and the structures obtained here, the Arp5 module makes interactions with the acidic patch of the entry-site proximal H2A-H2B dimer using its grappler domain (Figure S3.8, C and F) and with nucleosomal DNA between SHL-2 and -3 using its DNA binding domain (DBD) (Figure S3.8D) (*12, 14*). Ies6 wraps around Arp5 and interacts with the H2A-H2B dimer and DNA at SHL-2. In contrast, on a hexasome, the Arp5^{DBD} binds DNA between SHL+1 and +3 (Figure S3.6, C and D) and the Arp5^{grappler} appears to interact with the exposed H3-H4 tetramer and flanking DNA at the entry site (figure S3.6F). Ies6 maintains similar

interactions with Arp5, but no longer interacts with the H2A-H2B dimer as it is missing in a hexasome. Its interaction with DNA changes to the SHL+1/+2 location. These comparisons showcase how the Arp5/Ies6 regions used in the context of a nucleosome are repurposed for different interactions in a hexasome.

To better understand why Ino80 may not bind a nucleosome at SHL-2, we modeled the missing H2A-H2B dimer into our INO80-hexasome structure. We see distinct clashes of the Arp5 module with the entry side proximal H2A-H2B dimer and with part of the DNA that wraps around the H2A-H2B dimer near SHL-2 (figure S3.10). These clashes could be avoided if the H2A-H2B dimer is sufficiently dislodged. To test for this possibility, we did two types of experiments. In the first experiment we used a site-specific disulfide cross-link between the two H2A molecules (N38C), which inhibits complete loss of H2A-H2B (*41*), to test if this cross-link slows down nucleosome remodeling. In the second experiment we used an H2A mutant (R81A) that destabilizes the interface between H2A-H2B and H3-H4 (*42*), to test if this mutation speeds up nucleosome remodeling (figure S3.11, A and B). The cross-link did not show a significant decrease in nucleosome sliding and the destabilizing mutation did not show a significant increase in nucleosome sliding (figure S3.11, C to G). These results indicate that, if the dimer dislodgement occurs, it involves only a subtle conformational rearrangement. In the absence of major dimer dislodgement, another way to avoid these clashes could be by substantial rearrangement of the Arp5 module. We further explore the implications of these possibilities in the Discussion.

Discussion

Compared to other ATP-dependent chromatin remodeling enzymes, the mechanism of INO80 is less clear due its different binding mode on a nucleosome and due to its newly discovered preference for remodeling hexasomes. Here through a collection of high-resolution structures of

INO80 bound to hexasomes and nucleosomes we uncover unexpected conformational changes that reconcile previous differences between INO80 and other remodelers while also raising new mechanistic questions. Overall, INO80 binds to a hexasome and nucleosome in almost opposite orientations. There is more DNA unwrapping when the Ino80 ATPase domain binds at SHL-2 (hexasome) than at SHL-7 (nucleosome). These findings suggest that INO80 slides hexasomes from a position analogous to where other remodelers slide nucleosomes. In comparison, we propose that INO80 slides nucleosomes from a location that may resemble the hexasome sliding mode but is harder to access. Below we discuss these models and their implications for the biological roles of INO80.

Implications of the INO80-hexasome structure for nucleosome sliding by INO80

The most prevalent ground-state conformation of the INO80-hexasome complex (class 3) has the Ino80^{ATPase} at SHL-2 and approximately ~ 15 bp of unwrapped DNA from the entry site in addition to the ~ 35 bp of DNA that is unwrapped from removal of a H2A-H2B dimer. The placement of the Ino80^{ATPase} at SHL-2 is consistent with how the ATPase subunits of all other remodelers bind the nucleosome. Together with our prior finding that hexasomes are remodeled faster than nucleosomes, these results strongly suggest that the class 3 structure represents the sliding competent conformation of INO80 on hexasomes (Figure 3.5A). In contrast, the dominant ground state conformations of INO80 bound to a nucleosome have the Ino80^{ATPase} bound at either SHL-6 or SHL-7 consistent with previous findings. These differences raise the question of whether the INO80-nucleosome structures represent sliding competent conformations or whether a rearrangement of Ino80 to SHL-2 is essential prior to nucleosome sliding.

Previous cross-linking studies have shown that detachment of nucleosomal DNA from H2A-H2B close to the entry site occurs during INO80 remodeling (*13*). Our data shows that progressively

more DNA is unwrapped as the Ino80^{ATPase} moves closer to SHL-2. We see this in our three hexasome structures. Together these results raise the possibility that DNA unwrapping is coupled to Ino80 accessing its most sliding-competent state. Prior foot-printing studies have shown that while binding of INO80 to nucleosomes mainly protects nucleosomal DNA at SHL-3 and from SHL-5 to SHL-6, there is modest but detectable protection at SHL-2 (*13*). Interestingly, nicks and gaps between SHL-7 and SHL -2 have been shown to inhibit nucleosome sliding (*13, 43*). These results are consistent with the possibility that the Ino80^{ATPase} translocates on DNA towards SHL-2 to access its most sliding-competent state. Additionally single-molecule FRET studies have identified an ATP-dependent pause phase prior to nucleosome sliding (*22*), suggesting the presence of an ATP-dependent conformational change preceding sliding. The pause could represent the translocation of Ino80^{ATPase} from SHL-6/-7 towards SHL-2.

However, simply placing the INO80 complex as is on nucleosomes with Ino80^{ATPase} at SHL-2 results in clashes of the Arp5 module with DNA at the entry side proximal H2A-H2B dimer and with the DNA that wraps around the H2A-H2B dimer near SHL-2 (figure S3.10). Two mutually compatible ways this clash can be avoided are if (i) the flanking DNA is further unwrapped analogous to the INO80-hexasome structures and (ii) the interactions between the Arp5 module and the proximal H2A-H2B dimer are rearranged. The rearrangement of the Arp5/Ies6 interactions with the H2A-H2B dimer could in principle involve some dislodgement as previously proposed (*17*). However, our biochemical data suggest that any dimer dislodgement that occurs is subtle. The small change in H2B conformation seen between the class 1 and class 2 INO80-nucleosome structures is compatible with such a subtle rearrangement. In the extreme version of this model, the Ino80^{ATPase} translocates all the way to SHL-2 to adopt a sliding competent state (Figure 3.5B). However, it is also possible that the Ino80 subunit cannot move all the way to SHL-2 and initiates nucleosome sliding from a position between SHL-2 and SHL-6. In this model, the

conformational rearrangement of INO80 would add a rate-limiting step that slows remodeling of nucleosomes compared to hexasomes.

Implications for hexasome sliding by INO80

Our structures provide the first direct view into how INO80 engages a hexasome. Given the location of Ino80^{ATPase} at SHL-2 in these structures, we propose that the microscopic DNA translocation steps carried out by Ino80 would resemble those carried out by the ISWI, CHD and SWI/SNF complexes. However, the regulation of these steps would be different due to the unique interactions made by INO80 with hexasomes. For example, we observe an additional 15 bp of DNA is unwrapped (up to SHL-2.5) in class 3 compared to an unbound hexasome. These loosened histone DNA interactions could allow more ready translocation from SHL-2 compared to the subtle changes at SHL-2 observed when other remodelers bind nucleosomes (*16*). Additionally, we observe that the Arp5/Ies6 module makes substantially different contacts in the hexasome compared to a nucleosome. Thus, unlike in a nucleosome, where the Arp5 grappler contacts the H2A-H2B acidic patch, in a hexasome, the grappler contacts the exposed H3-H4 surface. We propose that these and other new contacts made by the Arp5/Ies6 module provide an anchor that allows the Ino80 motor to pump DNA through the hexasome. Further, our previous results showed that the Arp5/Ies6 module plays a more critical role in sliding hexasomes compared to nucleosomes (*17*). The different Arp5/Ies6 contacts seen on a hexasome also help explain these differential effects of the Arp5/Ies6 module on hexasome versus nucleosome sliding.

Role of the Arp8 module in flanking DNA length dependence and hexasome preference

INO80 activity on nucleosomes and hexasomes is sensitive to the flanking DNA length. However, the dependence on flanking DNA is steeper for nucleosomes than hexasomes (*17, 22*). Thus

while 601+80 nucleosomes are remodeled ~100-fold faster than 601+40 nucleosomes, 601+80 hexasomes are remodeled only ~ 5-fold faster than 601+40 hexasomes (*17*). The basis for these different flanking DNA dependencies is not well-understood. The Arp8 module is proposed to bind flanking DNA raising the possibility that it contributes to the flanking DNA length dependence (*40*). In this context, the greater amount of free DNA in hexasomes can in principle explain why they are remodeled faster than nucleosomes and why their sliding is less dependent on flanking DNA length (Figure 3.4A). However, the structures and biochemical data presented here suggest a more complex picture as discussed below.

The location of the Arp8 module is different on hexasomes than nucleosomes. On nucleosomes the Arp8 module binds ~ 40 bp entirely on the flanking DNA (Figure 3.4A). In the most prevalent INO80-hexasome state (class 3), the Arp8 module is bound entirely to the unwrapped DNA (Figure 3.4A). These structures raise the possibility that ~40 bp of free DNA is needed for the Arp8 module to bind and activate the Ino80 ATPase. This would be similar to the role of the HAND-SANT-SLIDE (HSS) domain of ISWI family remodelers, which binds flanking DNA. Indeed, deletion of the HSS slows down ISWI remodeling (*44*). However, deletion of the Arp8 module specifically accelerates sliding of 601+40 nucleosomes and 601+40 hexasomes, eliminating most of the flanking DNA length dependence for both substrates (Figure 3.4, B and C). These results indicate that the Arp8 module imposes flanking DNA length dependence by specifically inhibiting sliding of substrates with short flanking DNAs.

The Arp8 module interacts with the HSA region of Ino80 which is proposed to bind flanking DNA on nucleosomes. We therefore speculate that, without sufficient flanking DNA, the Arp8 module plays an inhibitory role by preventing the HSA region from effectively contacting the DNA. Increasing flanking DNA length may provide additional binding surfaces for the Arp8 module to bind, releasing auto-inhibition. In the context of a hexasome, given the ~35 bp of free DNA, less

89

flanking DNA would be needed compared to nucleosomes to relieve such inhibition, resulting in lower sensitivity to flanking DNA length. Consistent with the possibility that Arp8 regulates the HSA, deletion of the N-terminal extension of Arp8 increases interactions of HSA with nucleosomal flanking DNA (*40*). Interestingly deletion of the Arp8 N-terminus also changes how the Arp5 module engages the H2A-H2B dimer, implying coupling between the Arp8 and Arp5 modules.

In the context of nucleosomes, effective engagement of the HSA may stimulate movement of the Ino80 ATPase towards SHL-2 and also stimulate nucleosome sliding once INO80 accesses a sliding competent state. In the context of hexasomes, HSA engagement may mainly stimulate hexasome sliding. The role of the Arp8 module is reminiscent of the auto-inhibitory role shown for the Nhp10 module (*22*). The similarity raises the possibility that the Arp8 and Nhp10 modules collaborate to impose flanking DNA length dependence (*40, 45, 46*).

Biological Implications

The activity of INO80 is exquisitely tuned for discriminating in favor of hexasomes over nucleosomes. Such a highly regulated mechanism raises the question of why INO80 needs to be inhibited in sliding nucleosomes within gene bodies and instead promoted to slide hexasomes. We speculate that the answer relates to the impact of RNA polymerase on nucleosomes. When RNA polymerase moves through a nucleosome it can completely and asymmetrically dislodge an H2A-H2B dimer while also moving the resultant hexasome towards the promoter (*17, 19, 20, 47, 48*). Rapid restoration of hexasome positions may be essential to prevent cryptic transcription. Other remodelers such as ChdI and ISWI are known to provide nucleosome sliding functions within gene bodies. INO80's hexasome specific role may reflect a division of labor amongst remodelers in a crowded chromatin context (*49*). Similar crowded chromatin contexts containing hexasomes are also likely to occur as nucleosomes are being reassembled behind the replication

fork and during DNA repair events when nucleosomes are disrupted and clustered away from DNA damage sites.

Materials and Methods

Expression and purification of INO80

FLAG-tagged Ino80 *S. cerevisiae* strains were grown in YPD at 30 °C to saturation. INO80 complexes was then purified by FLAG immunoprecipitation based on previously published methods (*17, 22, 50*) with minor modifications. A second 30-minute elution step was added to increase yield. INO80 (Δarp8) was purified from an *S. cerevisiae* strain in which the *arp8* gene was deleted.

Preparation of nucleosomes and hexasomes

Recombinant *Xenopus laevis* histones were expressed in *E. coli* and purified as previously described (*51, 52*). DNA was amplified from a plasmid containing a Widom 601 sequence and labeled with a Cy3 fluorophore modified primer (IDT). Large scale PCR was performed and products were separated on an 8% polyacrylamide gel and cut out. The gel slice containing the DNA was crushed, soaked in 1X TE overnight, and filtered through a 0.45 mm filter. The DNA was ethanol precipitated and dissolved in 1X TE.

Nucleosomes and hexasomes were assembled using salt gradient dialysis (*23, 51*). Nucleosomes were purified by ultracentrifugation with a 10-30% glycerol gradient. Hexasomes were purified using a Mini PrepCell (BioRad) with a 7% acrylamide gel based on the previous published method. Briefly, asymmetry of the 601 DNA sequence yields weaker affinity of one side of the DNA sequence for the H2A/H2B dimer versus the other side. Placing the flanking DNA adjacent to the weaker side allows the assembly of hexasomes with the H2A/H2B dimer missing proximal to the

longer flanking DNA. The hexasomes are further purified away from nucleosomes through a prep-cell as described in Levendosky and Bowman.

Native gel-based remodeling assay

All remodeling reactions were done under single-turnover conditions (enzyme in excess of nucleosomes) with saturating INO80 and ATP. The reactions were carried out at 30 °C. Briefly, 60 nM INO80 WT or 90 nM INO80(Δarp8) was incubated with 15 nM nucleosomes or hexasomes (60 nM INO80 (Δarp8) and 10 nM nucleosomes were used for remodeling assays on +40N) in reaction buffer (40 mM Tris-HCl, pH7.5, 50 mM KCl, 1.1mM free $MgCl_2$, 0.02% NP-40, and 7% glycerol) for 10 minutes at 30 °C before adding 1mM ATP· $MgCl_2$ to start the reaction. The no ATP control was taken at the last time point of the reaction. The reaction samples taken at specific time points were quenched with excess plasmid DNA and ADP. Samples were resolved on a native PAGE gel (6% acrylamide, 0.5X TBE) ran for 3 hours at 125V. Gels were scanned on a Typhoon Imager (GE Life Sciences) and quantified by densitometry using ImageJ. The fraction of nucleosome products was determined by the ratio of slower-migrating nucleosomes (everything above unremodeled nucleosomes) to the total nucleosome intensity. Using Prism 7 (GraphPad) data was fit to a single-phase exponential decay model (Equation 1),

$$y = (y_0 - p)e^{-k_{obs}t} + p$$

where y_0 is the initial fraction product, k_{obs} is the observed rate constant, and p is the fraction product at the plateau.

Amine functionalized GO grids preparation

Preparations and functionalization of Graphene Oxide (GO) grids were performed following the previously described protocol (*53, 54*). After depositing GO onto 300 Mesh, R1.2/1.3 Au Quantifoil grids, GO covered grids were submerged in 10 mM ethylenediamine (Sigma-Aldrich E26266) solution diluted in dimethyl sulfoxide (DMSO) and incubated for 5 h at room temperature. The

92

grids were washed thoroughly twice with DMSO without ethylenediamine, twice with autoclaved water, twice with ethanol, and dried under ambient conditions. Amino modified grids were stored dry at −20 °C until use.

Electron microscopy sample preparation and data collection

Freshly prepared INO80 was mixed with either hexasome or nucleosome in 1:1 molar ratio, and then incubated at 30 °C for 30 min, after which the buffer was exchanged to EM buffer (25mM HEPES, pH 7.5, 100mM KCl, 2mM $MgCl_2$, 2mM DTT, 1% glycerol).

Negative staining of the complex was performed with 0.75% uranium formate, following an established protocol (*55*). Grids were examined using an FEI T12 microscope operated at 120 kV, and images were recorded using a 4k x 4k charge-coupled device (CCD) camera (UltraScan 4000, Gatan).

To prepare cryo-grids, samples (3μl at 0.2 μM) were loaded onto the amine modified GO grids, and then blotted for 4 s before being plunge-frozen in liquid ethane cooled by liquid nitrogen using a FEI Vitrobot IV with the sample chamber set at 8°C and 100% humidity. The blotting force was 0, using ø 55/20 mm blotting filter paper from TED PELLA. Grids were examined and screened using an FEI Tecnai Arctica operated at 200 kV and equipped with a Gatan K3 camera. All cryo-EM datasets were collected on a Titan Krios at the UCSF Cryo-EM Center for Structural Biology operated at an acceleration voltage of 300 kV and equipped with a BioQuantum energy filter (slit width set to 20 eV) and a K3 direct electron detector (Gatan).

All cryo-EM data were collected using SerialEM (*56*). All images were acquired with a nominal magnification of 105 K, resulting in a pixel size of 0.4175 Å. Defocus range was set from -1.0 μm to -2.0 μm. For the INO80-hexasome sample, 18,991 images were collected, each was dose-

fractionated to 117 movie frames with a total exposure time of 5.9 s, resulting in a total dose of ~67 electrons per $Å^2$. For the INO80-nucleosome sample, 8,653 images were collected, each was dose-fractionated into 80 movie frames with a total exposure time of 2.024 s, resulting in a total dose of ~43 electrons per $Å^2$.

Image processing

For the dataset of the INO80-hexasome sample, a total of 18,991 movie stacks were motion corrected and dose weighted using MotionCor2 (*57*). The CTF parameters were estimated and all subsequent 2D and 3D classification were performed using cryoSPARC (*58*). 500 micrographs were randomly selected to generate a template. In brief, 624,536 particles were picked by cryoSPARC blob picker and were subject to ab-initio reconstruction and multi-round heterogenous refinement. From one good class showing clear features of INO80 bound to the hexasome, we generated 16 different projection images for template picking, yielding 7,831,514 particles from all micrographs. After multiple rounds of heterogenous refinement, a final 1,220,910 particles were selected to calculate a reconstruction of the INO80-hexasome complex with a global resolution of 2.8 Å. This reconstruction showed clear structural features of INO80, but the hexasome was not well resolved.

This particle stack was then exported to RELION (*59*). A mask containing the Arp5-Ies6 module and hexasome was generated. 3D classification of background subtracted particles producing a new map of 560,912 particles with clear Arp5-Ies6 and hexasome features. Then, a 3D reconstruction of the entire INO80-hexasome complex was calculated from this same subset of particles and further refined, in which the densities of both INO80 and hexasome are improved compared with the previous round. We then performed another round of background subtraction with a mask on the hexasome, followed by classification with local alignment focused entirely on

94

the hexasome. Three major classes were identified, among which the main difference is the hexasome orientation, mainly reflecting different binding positions of INO80 on the hexasome.

For each class, we then further refined the whole complex and hexasome to higher resolutions by using either cryoSPARC or cisTEM (*60*). The final 3D maps were sharpened by DeepEMhancer (*61*), except for the hexasome of class 1. Lastly, reconstructions of INO80 and the hexasome were assembled together into a composite map for model building and figure generating. For both class 1 and class 3, we also generated a mask around the flanking DNA for further focused 3D classification, producing a clear density that allows docking of the crystal structure of Arp8-N-actin-Arp4 into the density map (figure S3.2B).

For the dataset of the INO80-nucleosome sample, a total of 8,653 movie stacks were motion corrected and dose weighted using MotionCor2. The CTF parameters were estimated and all subsequent 2D and 3D classification were performed using cryoSPARC. 3,625,796 particles were picked by cryoSPARC template picker. The remaining parts of image processing were performed following the procedure described above.

Model building

For the model building, the initial model was generated by fitting the available coordinates into our cryo-EM density maps by using Chimera (*62*). These coordinates include the INO80 core (with its sequence changed to that of *S. cerevisiae* by alphafold (*63*) and ccp4em), the crystal structure of Arp8-N-actin-Arp4 and the model of a hexasome (PDB: 6FML, 5NBN, 6ZHY (*14, 25, 27*)). The inconsistent parts were then manually built and refined in coot (*64*). The structures were refined using Phenix (*65*) with secondary structure constraints. Model building of INO80-nucleosome complexes was performed following the same procedure, except that the atomic model of a nucleosome (PDB: 1KX5) (*66*) was used.

Acknowledgements

Data and materials availability: For the core INO80 of the INO80-Hexasome complex (class 1, class 2 and class 3) and the core INO80 of the INO80-Nucleosome complex (class 1 and class 2), the coordinates are deposited in the Protein Data Bank with the accession codes 8ETS, 8ETU, 8ETW, 8EU9, and 8EUF; the cryo-EM density maps are deposited in the Electron Microscopy Data Bank (EMDB) with the accession codes EMD-28597, EMD-28599, EMD-28601, EMD-

96

28609, and EMD-28613. For the hexasome of the INO80-Hexasome complex (class 1, class 2 and class 3) and the nucleosome of the INO80-Nucleosome complex (class 1 and class 2), the coordinates are deposited in the Protein Data Bank with the accession codes 8ETT, 8ETV, 8EU2, 8EUE, and 8EUJ; the cryo-EM density maps are deposited in the Electron Microscopy Data Bank (EMDB) with the accession codes EMD-28598, EMD-28600, EMD-28602, EMD-28612, and EMD-28614.
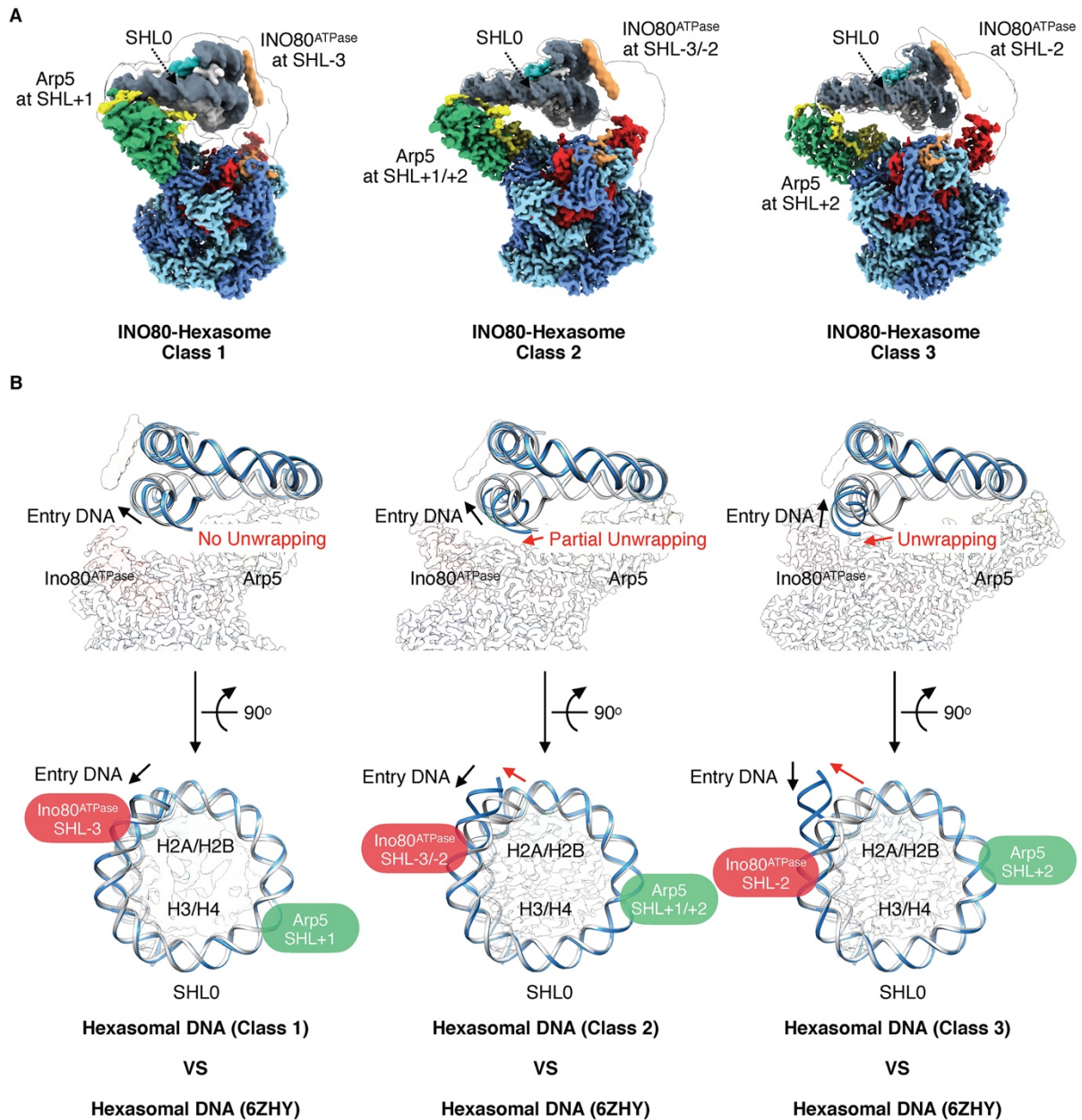
Figures
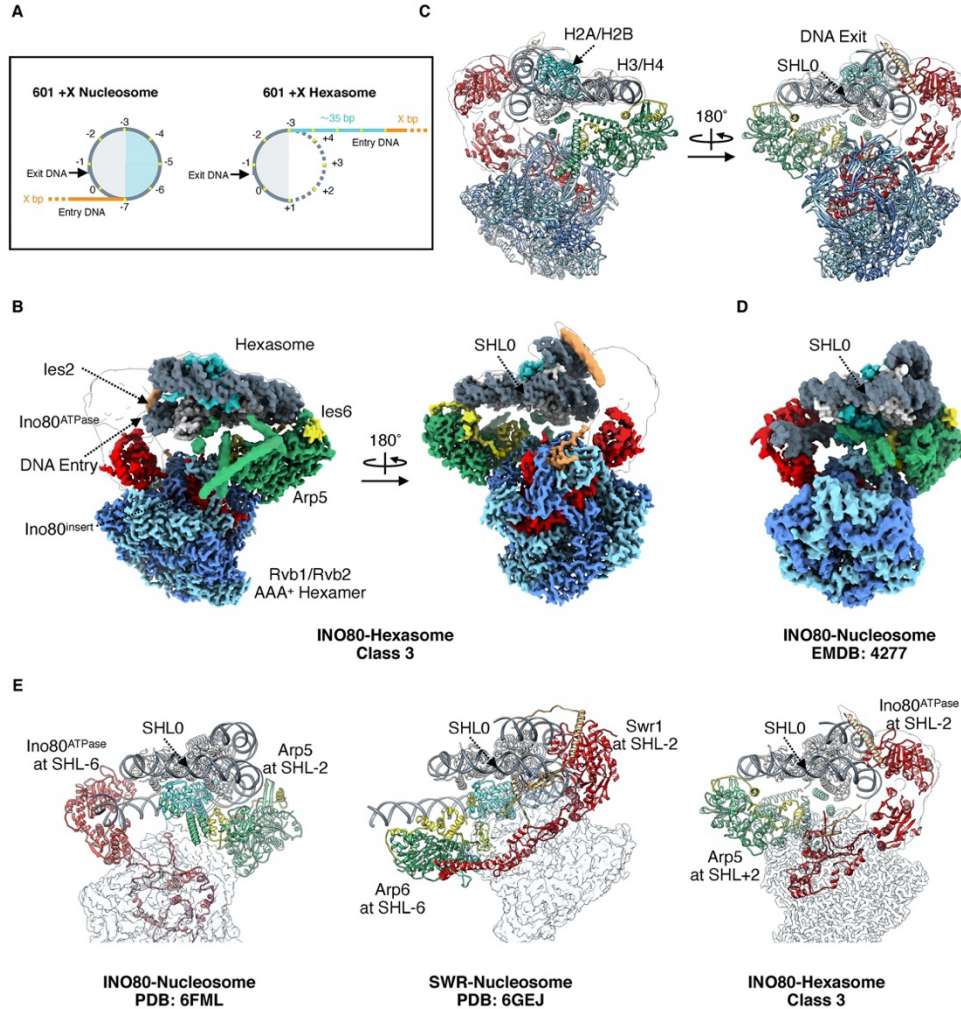
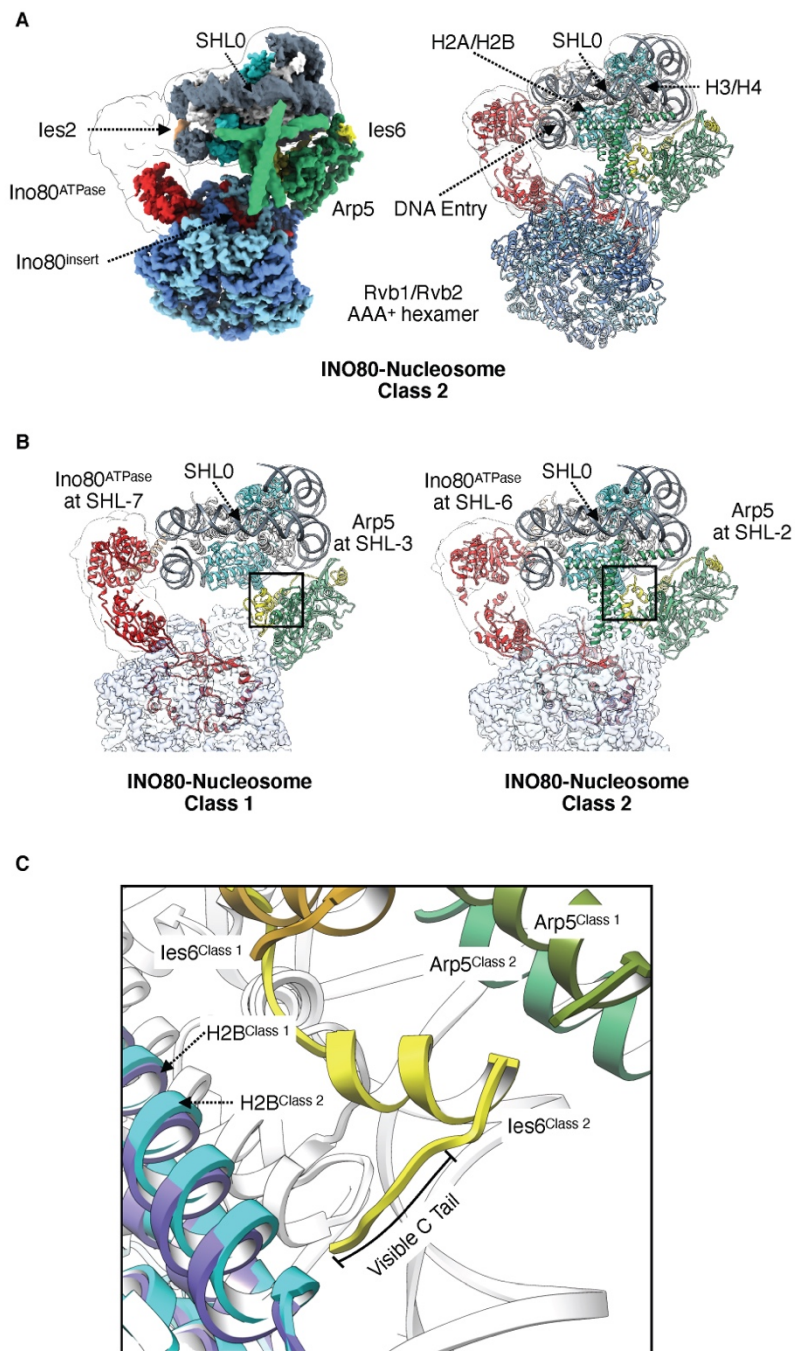**Figure 3.1. Structure of the INO80-hexasome complex reveals large rotation.**
(A) Cartoon illustration of a 601+X Nucleosome (left) and 601+X Hexasome (right). H2A/H2B dimer proximal to the flanking DNA (entry side dimer) is cyan, H3-H4 is light gray, 601 DNA is slate gray, flanking DNA is orange, additional free DNA is cyan, super helical locations are labeled by yellow dots, DNA from the bottom gyre is represented by a dotted line. (B) Cryo-EM density map of the INO80-hexasome complex. Two views are vertically rotated 180° from each other. (C) Atomic model of the INO80-hexasome complex, viewed in the same orientation as the map in (B). (D) Cryo-EM density map of *Chaetomium thermophilum* INO80-nucleosome complex (EMDB: 4277 (*14*)) displayed with its nucleosome dyad and H3-H4 tetramer aligned with that of the hexasome in the right panel of (B). Note that INO80 on a hexasome rotates ~180° from where it sits on a nucleosome when keeping the nucleosome/hexasome dyad and H3-H4 aligned. Colors in (B) – (D): Rvb1: cornflower blue; Rvb2: sky blue; Arp5: medium sea green; Ies6: yellow; Ino80: red; Ies2: sandy brown; H2A/H2B: cyan; H3-H4: white; DNA: slate gray. (E) Structural comparisons of INO80-nucleosome complex (left), SWR-nucleosome complex (middle) and INO80-hexasome complex (right), with nucleosome/hexasome dyad and H3-H4 aligned with each other. Arp5 or Arp6: medium sea green; Ies6 or Swc6: yellow; Ino80 or Swr1: red; Ies2 or Swc2: sandy brown; H2A/H2B near flanking DNA: cyan; H3-H4: white; H2A/H2B near exit DNA: white; DNA: slate gray.

Figure 3.2. Conformational snapshots of INO80-hexasome complexes.
(A) Cryo-EM density maps of the INO80-hexasome complex in three different conformations. Maps are aligned by the hexasome orientation. Ino80^{ATPase} and Arp5 binding sites are labeled. Colors are the same as panel B of Figure 3.1 (B) Comparison of DNA from each INO80-hexasome class (dodger blue) with DNA from the unbound hexasome (PDB: 6ZHY, light gray), showing degree of DNA unwrapping (upper row) and binding locations of Ino80^{ATPase} and Arp5 (bottom row).

99

Figure 3.3. Structure of the INO80-nucleosome complex.
(A) Cryo-EM density map (left) and atomic model (right) of S. cerevisiae INO80-nucleosome complex in class 2. Colors are the same as panel B of Figure 3.1. (B) Two conformational snapshots of INO80-nucleosome complex, aligned by the nucleosome. Binding location of Ino80ATPase and Arp5 are labeled. (C) Enlarged view of the boxed areas in (B) shows overlay of nucleosome atomic models in the two conformations. In class 2, H2B near flanking DNA is shifted slightly and the C terminal tail of Ies6 becomes visible. Entry-site H2A/H2B in class 1:

100

medium purple; Entry-site H2A/H2B in class 2: cyan; Ies6 in class 1: goldenrod; Ies6 in class 2: yellow; Arp5 in class 1, forest green, Arp5 in class 2, medium sea green.
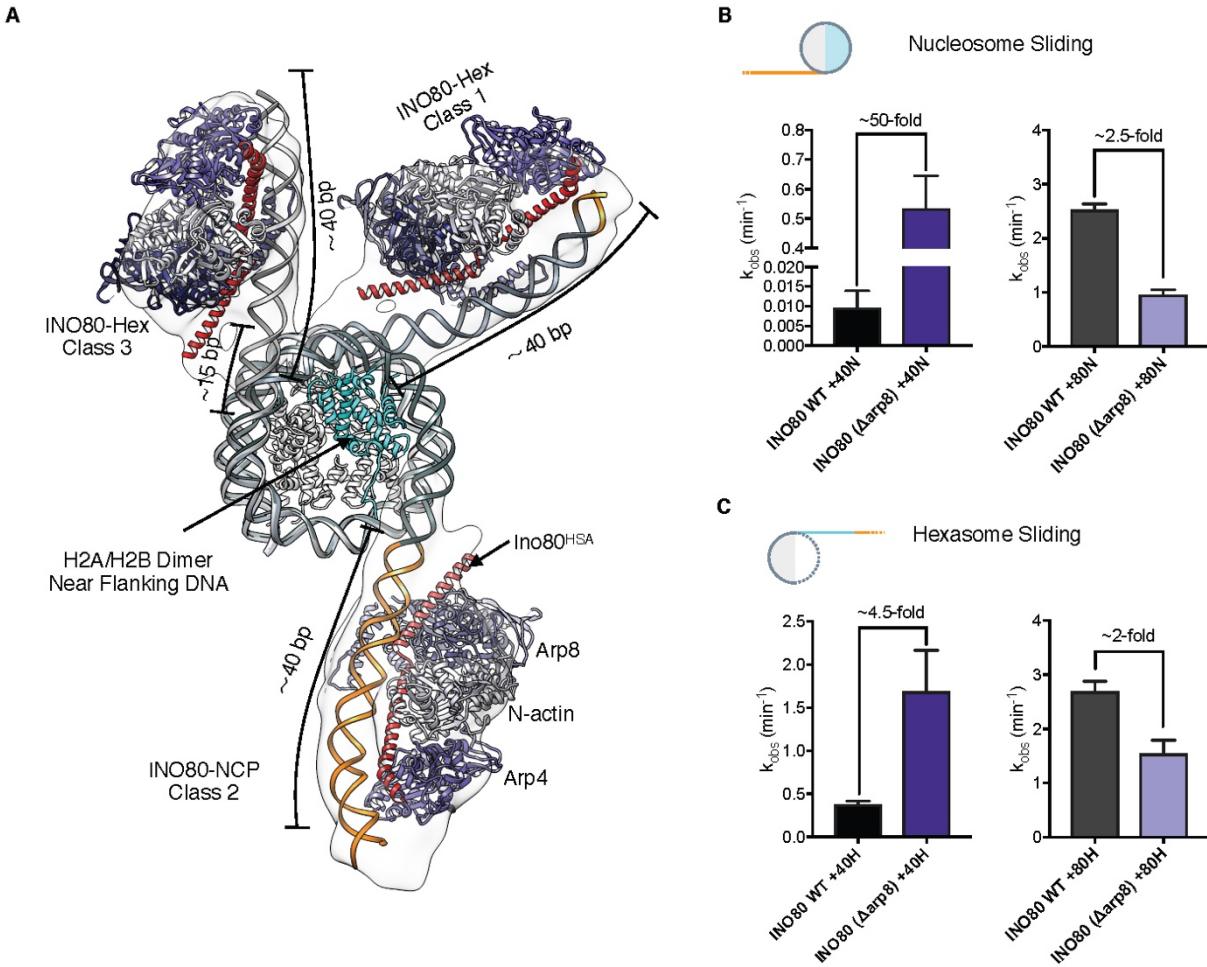
Figure 3.4 The Arp8 module engages different regions of DNA in nucleosomes versus hexasomes.

(A) Overlay of atomic models of the hexasome (class 1 and class 3) and the nucleosome (class 2) with the Arp8 module. The H3-H4 tetramer of three structures are aligned. Colors: 601 DNA: slate gray, flanking DNA: orange, H2A/H2B that is missing in hexasome: cyan; Arp8: dark purple; N-actin: lavender; Arp4: medium purple. Ino80 HSA domain: red; (B) Observed rate constants for sliding of +40 and +80 nucleosomes by INO80 WT and INO80 (Δ arp8) determined by native gel-based remodeling assays; (C) Rate constants for sliding of +40 and +80 hexasomes by INO80 WT and INO80 (Δ arp8) determined by native gel-based remodeling assays. All assays were performed under single-turnover conditions with saturating and excess enzyme and ATP. Data in (B) and (C) represent the mean +/- SEM for three replicates.
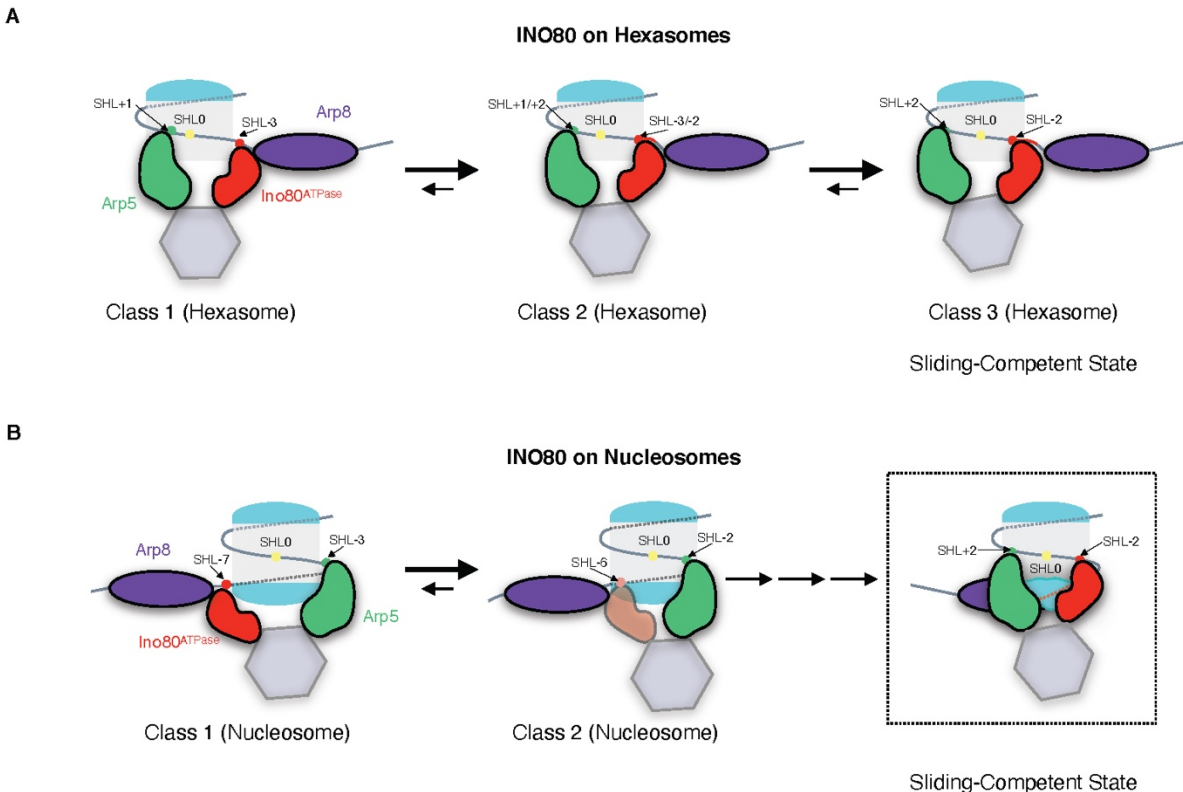
Figure 3.5. Model of INO80-induced hexasome and nucleosome sliding.
(A) Hexasome sliding: Ino80 can bind a hexasome with $Ino80^{ATPase}$ at SHL-3 or -3/-2 and the Arp5 module at SHL+1 or +1/+2. However, the dominant location of $Ino80^{ATPase}$ is at SHL-2 where we propose INO80 becomes sliding-competent. We speculate that the structures in class 1 and class 2 represent intermediates that represent some translocation of Ino80 on hexasomal DNA. (B) Nucleosome sliding: Ino80 binds a nucleosome with $Ino80^{ATPase}$ at SHL-7 or -6 and the Arp5 module at SHL-3 or -2. We speculate that Ino80 translocates along DNA toward SHL-2 where INO80 becomes sliding-competent. This translocation may cause minor destabilization of the entry-site H2A/H2B, unwrapping of DNA from the same destabilized H2A/H2B, and repositioning of the Arp5 module.

103

Figure S3.1. INO80-nucleosome and INO80-hexasome.
(A) and (B): Models of 601+X Nucleosome (A) and 601+X Hexasome (B). 601 DNA: slate;
flanking DNA: orange. The additional free DNA in hexasome is colored with cyan;
(C) SDS PAGE gel of purified *S. cerevisiae* INO80 complex;
(D) Negative staining of the INO80-hexasome sample;
(E) Representative cryo-EM micrograph of the INO80-hexasome complex;
(F) Negative staining of the INO80-nucleosome complex;
(G) Representative cryo-EM micrograph of the INO80-nucleosome complex;
(H) Representative 2D average image of the INO80-nucleosome complex.

104

A

18,991
Movie Stacks

500 Images
Blob Picker

Motion Correction

All Images
Template Picker

624,536 Particles

Ab-Initio
Reconstruction

Heterogeneous
Refinement

Heterogeneous
Refinement

7,831,514 Particles

Create
Template

INO80 Core
Complex

INO80-Hexasome
Complex

1,220,910 Particles

Signal Subtraction

Export to RELION

3D Classification

560,912 Particles

3D
Refinement

Revert to
Original Particles

6.68 Å

Class 1
76,874 Particles

Revert
Refinement

CryoSPARC
DeepEMhancer

3D
Refinement

3.04 Å

Signal Subtraction

3D Classification

3D
Refinement

cisTEM
DeepEMhancer

3.16 Å

Class 2
130,147 Particles

Revert
Refinement

CryoSPARC
DeepEMhancer

2.80 Å

3D
Refinement

cisTEM
DeepEMhancer

2.93 Å

Class 3
233,675 Particles

Revert
Refinement

cisTEM
DeepEMhancer

2.64 Å

B

Mask focused

3D Classification

105
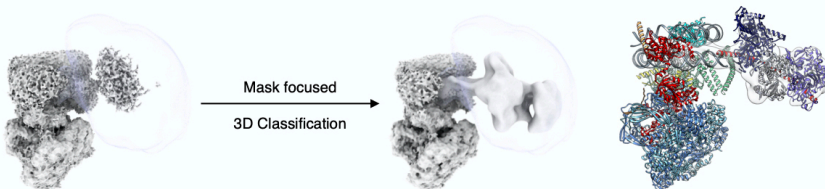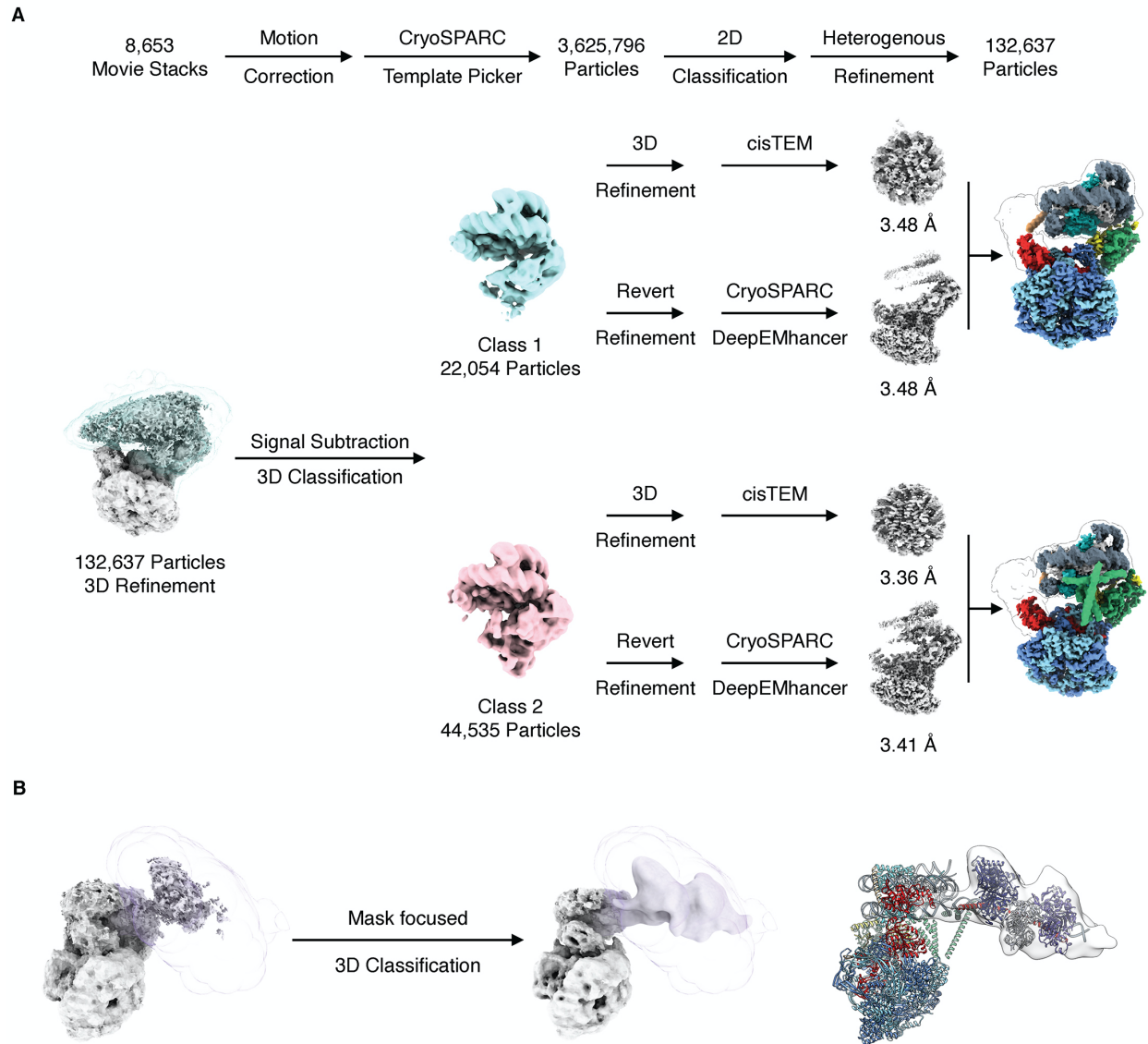
**Figure S3.2. Image processing of the INO80-hexasome dataset.**
(A) A flow-chart outlining the processing of the INO80-hexasome cryo-EM dataset;
(B) Focused classification near flanking DNA produced density of Arp8 module.

Figure S3.3. Image processing of the INO80-nucleosome.
(A) A flow-chart describing processing of the INO80-nucleosome complex cryo-EM dataset;
(B) Focused classification near flanking DNA produced density of Arp8 module.
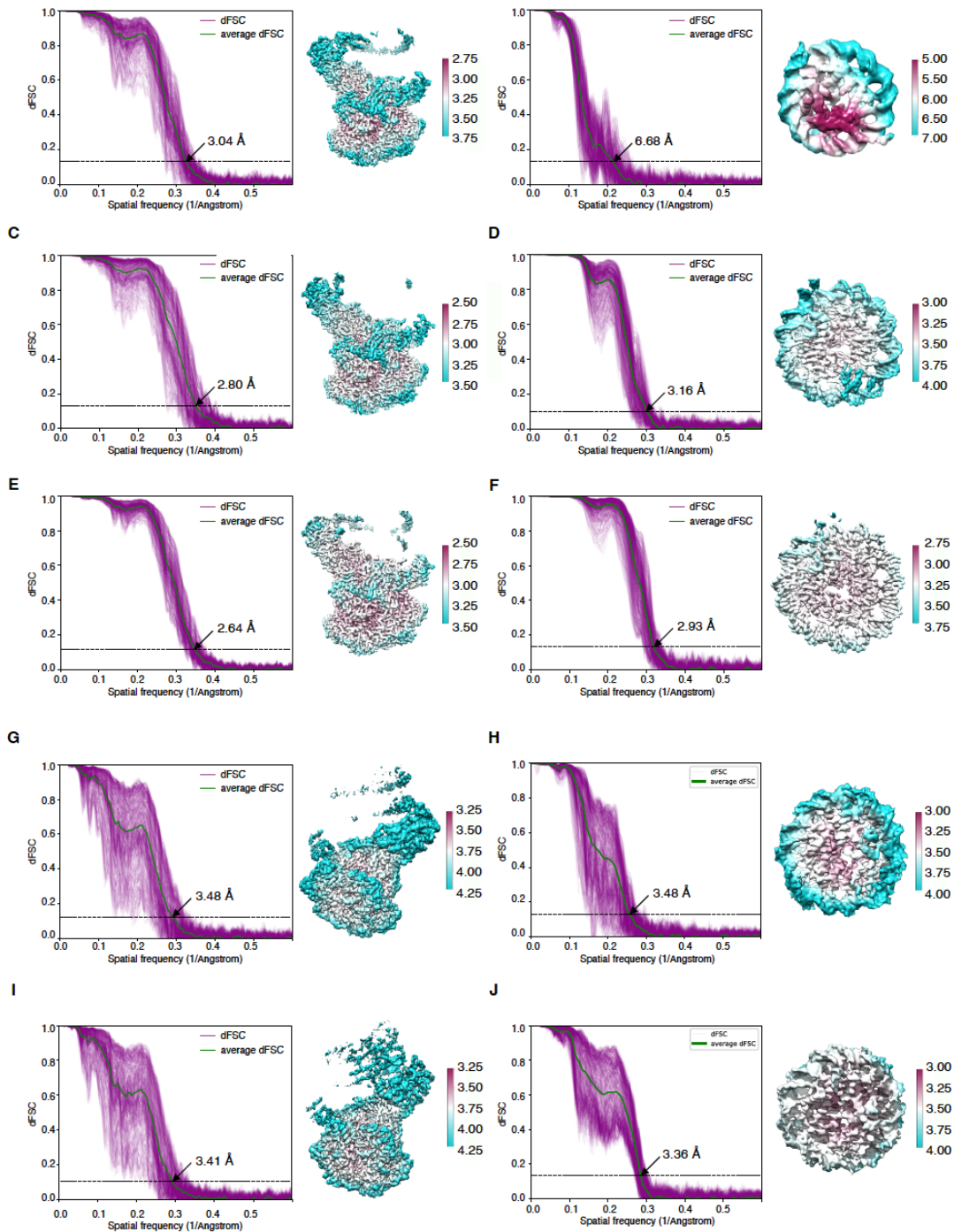
**Figure S3.4. Resolution estimation of the cryo-EM structures.**
All panels contain direction FSC with global resolution estimated from FSC=0.143 criterion
marked (left), cryo-EM map colored with local resolution (right) and resolution scale bar.
(A) and (B) Class 1 of INO80-hexasome complex (A) and the corresponding hexasome (B);
(C) and (D) Class 2 of INO80-hexasome complex (C) and the corresponding hexasome (D);
(E) and (F) Class 3 of INO80-hexasome complex (E) and the corresponding hexaxome (F);
(G) and (H) Class 1 of INO80-nucleosome complex (G) and the corresponding nucleosome (H);
(I) and (J) Class 2 of INO80-nucleosome complex (I) and the nucleosome (J).
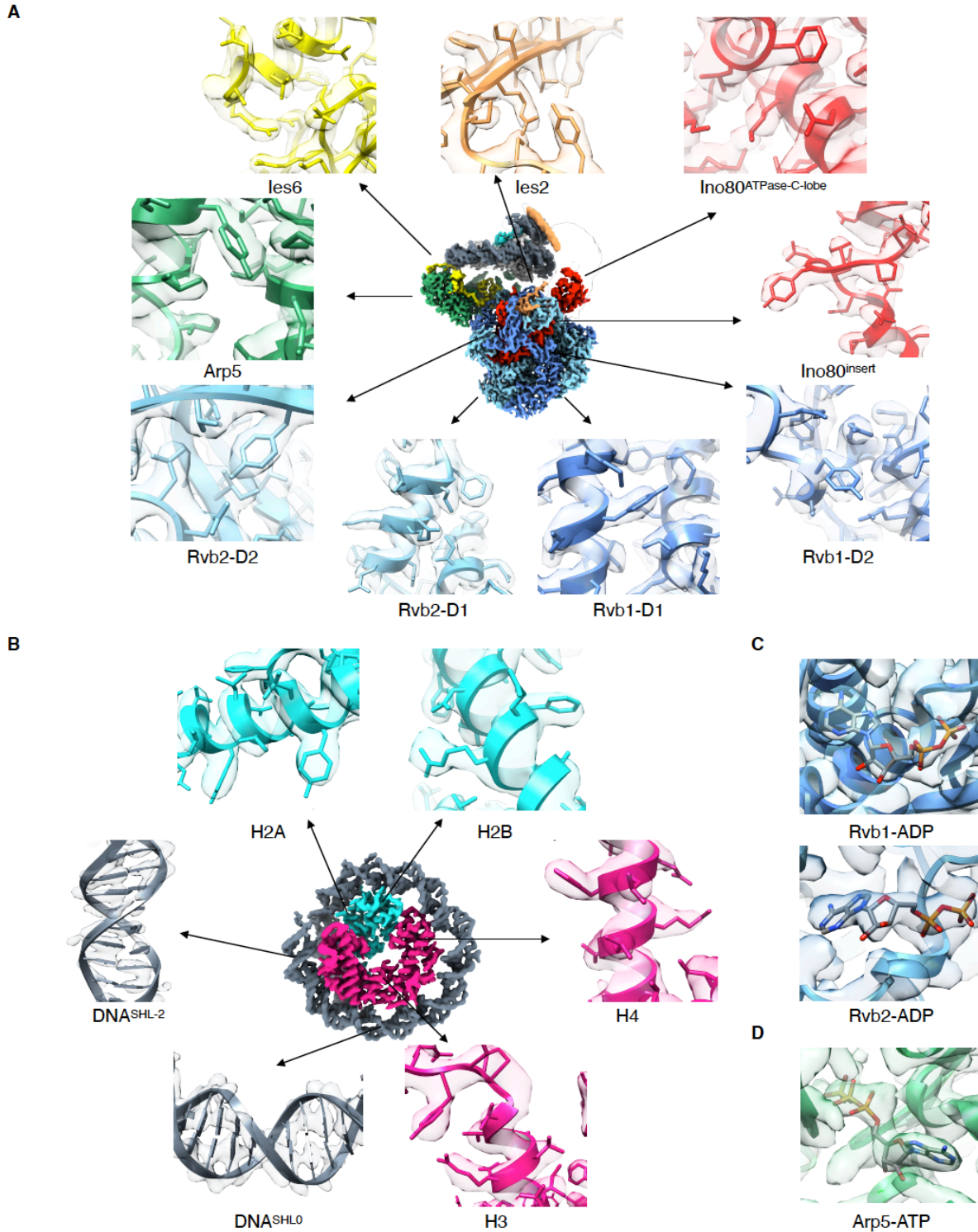
Figure S3.5. Representative densities of INO80-hexasome complex.
(A) Representative densities of INO80 from class 3 of the INO80-hexasome complex;
(B) Representative densities of the hexasome region from class 3 of the INO80-hexasome complex; (C) Nucleotide densities seen in all six nucleotide binding pockets of Rvb1/Rvb2 hetero-hexamer are modeled as ADP;
(D) Nucleotide density seen in the Arp5 nucleotide binding pocket is modeled as ATP.

109
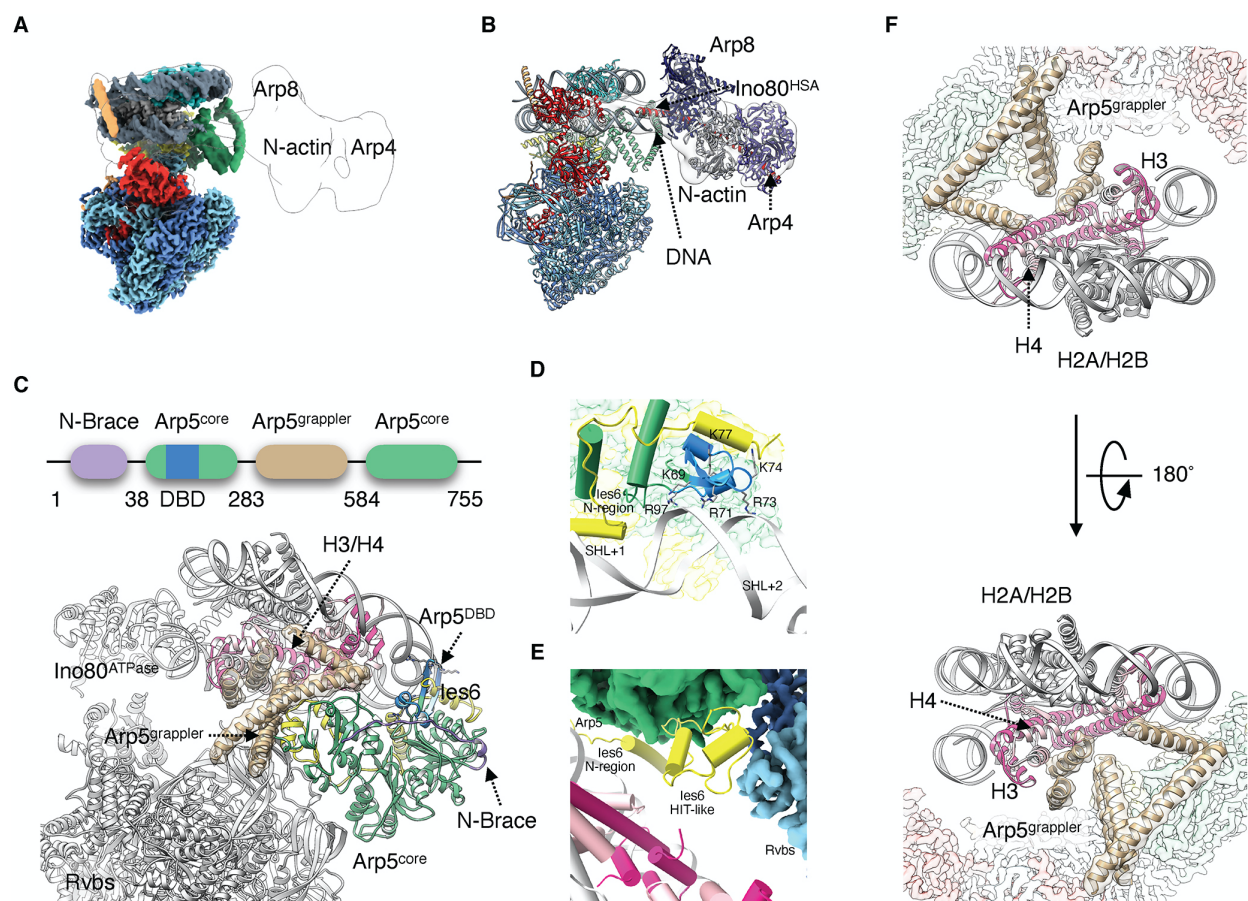
Figure S3.6. Arp5 and Arp8 modules in the INO80-hexasome structure.
(A) Cryo-EM map of the class 3 INO80-hexasome complex with density of the Arp8 module shown as transparent;
(B) Atomic model from the class 3 INO80-hexasome complex shown in the same view as (A), with the crystal structure of the Arp8 module (PDB:5NBN) docked into the density map;
(C) Domain arrangement (upper) and atomic model (bottom) of the Arp5 module. Colors: N-brace of Arp5: medium purple; DNA binding domain of Arp5: dodger blue; Core domain of Arp5: medium sea green; Grappler of Arp5: tan; Ies6: yellow; H3: deep pink; H4: pink;
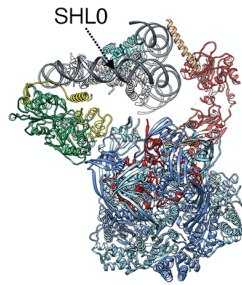(D) An enlarged view showing interactions between Arp5[DBD] and DNA;
(E) An enlarged view showing interactions between Ies6, Arp5 and Rvb1/Rvb2;
(F) Two enlarged views rotated 180° from each other showing interactions between Arp5[grappler] and the hexasome.
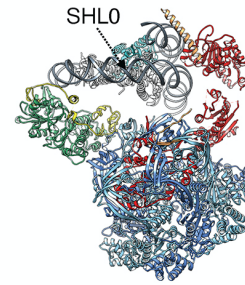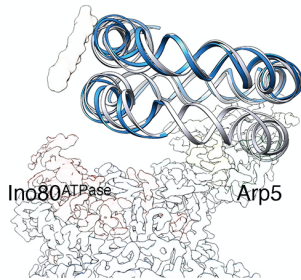
A

SHL0

**INO80-Hexasome
Class 1**

SHL0
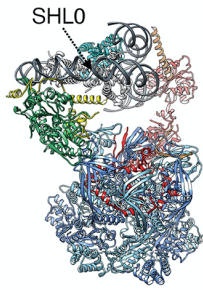
**INO80-Hexasome
Class 2**

SHL0

**INO80-Hexasome
Class 3**

B

Ino80^ATPase — Arp5

Hexasomal DNA (Class 1)

VS

Nucleosomal DNA (1KX5)

Ino80^ATPase — Arp5
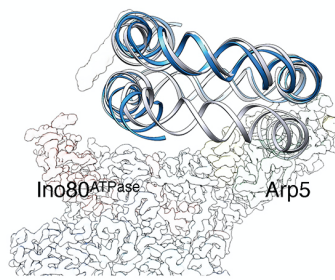
Hexasomal DNA (Class 2)

VS

Nucleosomal DNA (1KX5)

Ino80^ATPase — Arp5
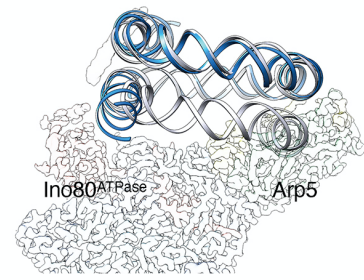
Hexasomal DNA (Class 3)

VS

Nucleosomal DNA (1KX5)

Figure S3.7. Comparison of three INO80-hexasome conformational snapshots.
(A) Comparison of atomic models of the three classes of the INO80-hexasome complexes,
where the hexasome dyads are aligned using the H3-H4 tetramers;
(B) Comparison of the hexasome in the INO80-hexasome complex with the crystal structure of a
free nucleosome aligned by the histone core. Hexasomal DNA: dodger blue; Nucleosomal DNA:
lavender.
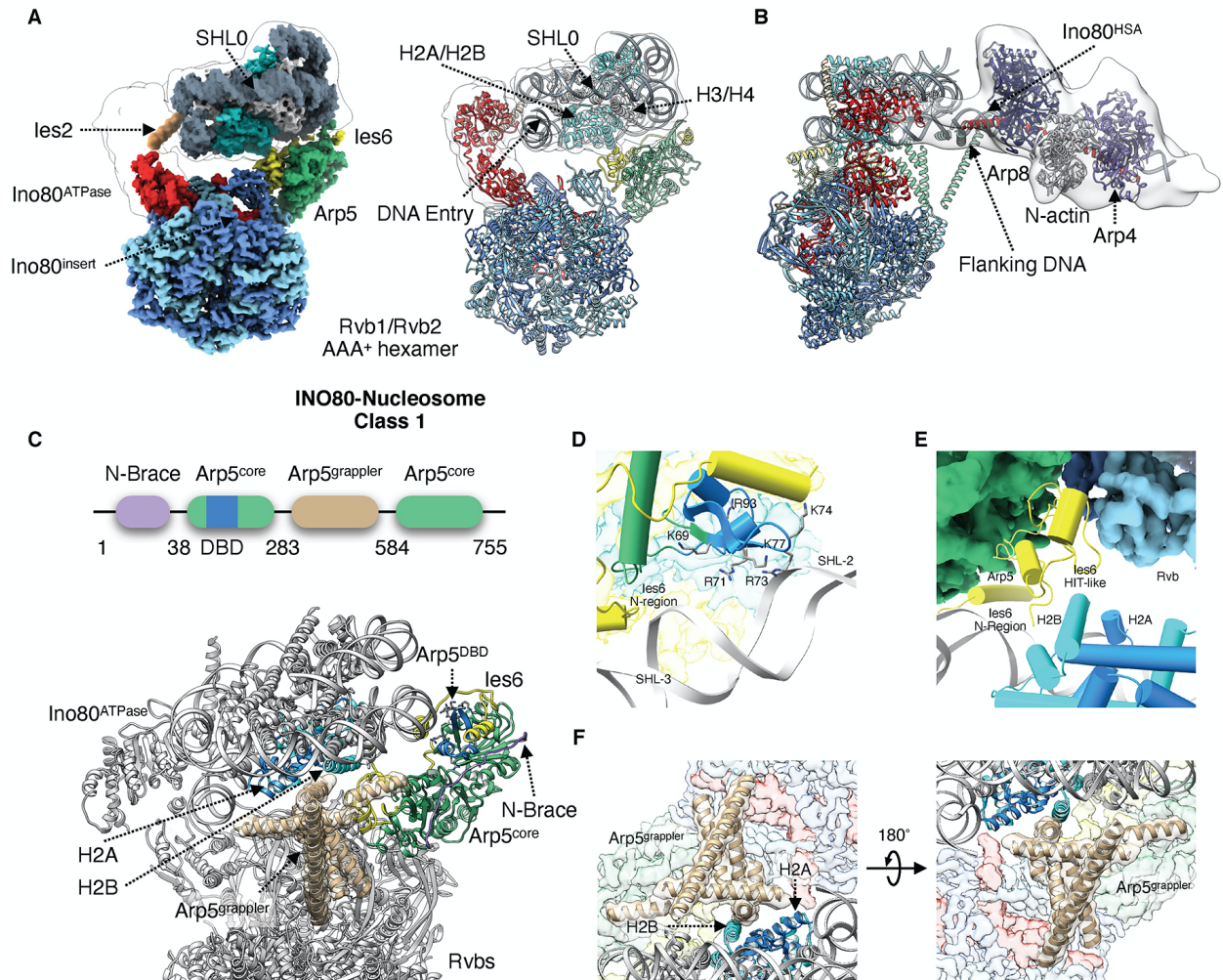
Figure S3.8. Structure of the INO80-nucleosome.
(A) Cryo-EM map and atomic of the class 1 *S. cerevisiae* INO80-nucleosome complex;
(B) Atomic model of the class 1 INO80-nucleosome complex with the crystal structure of the Arp8 module docked into the density map;
(C) Domain arrangement (upper) and atomic model (bottom) of the Arp5 module. Colors: N-brace of the Arp5: medium purple; DNA binding domain of Arp5: dodger blue; Core domain of Arp5: medium sea green; Grappler of Arp5: tan; Ies6: yellow; H2A: dodger blue; H2B: cyan;
(D) An enlarged view showing interactions between Arp5^{DBD} and DNA;
(E) An enlarged view showing interactions between Ies6, Arp5 and Rvb1/Rvb2;
(F) Two enlarged views rotated 180° from each other showing interactions between Arp5^{grappler} and the nucleosome.
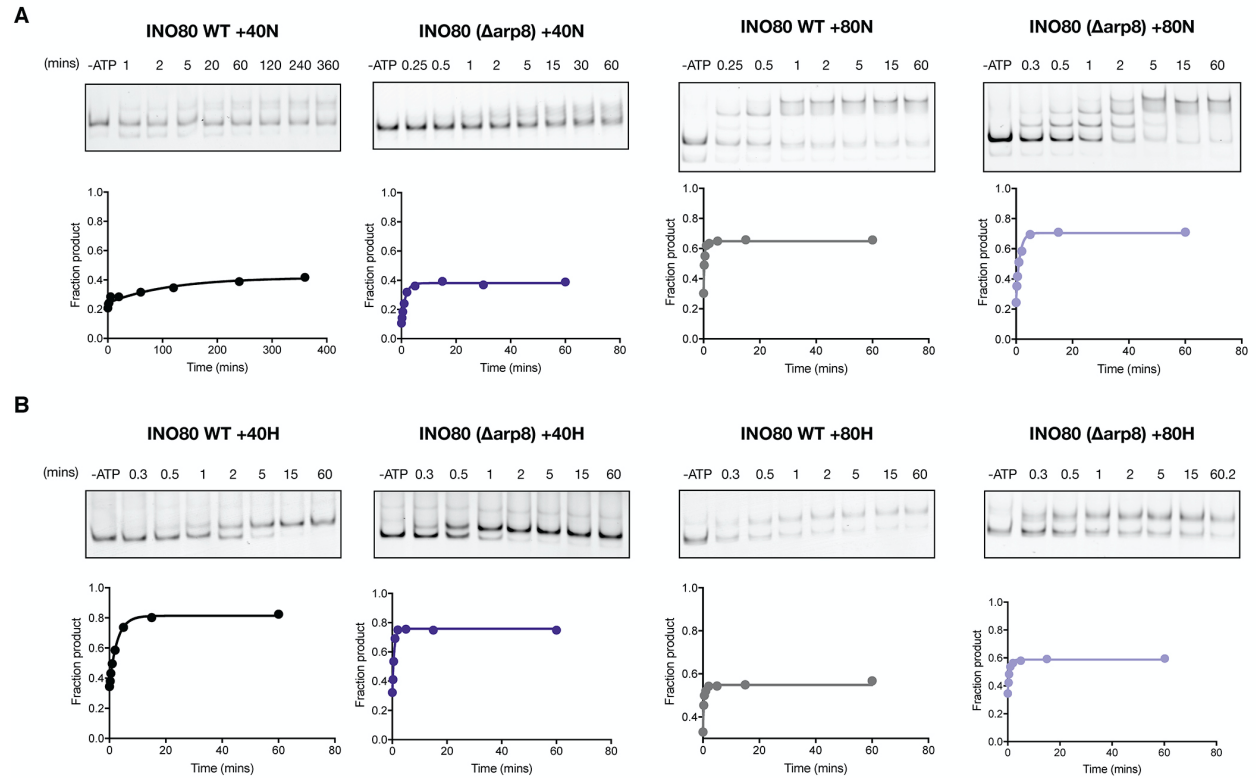
Figure S3.9. Remodeling activity of WT INO80 and INO80 (Δarp8) on nucleosomes and hexasomes.
 (A) Example gels and time courses of native gel-based remodeling assays of WT INO80 or INO80 (Δarp8) on nucleosomes with +40 or +80 base pairs of flanking DNA; (B) Example gels and time courses of native gel remodeling assays of WT INO80 or INO80 (Δarp8) on hexasomes with +40 or +80 base pairs of flanking DNA. Data was quantified by determining the fraction of product species over total species at each timepoint.

113
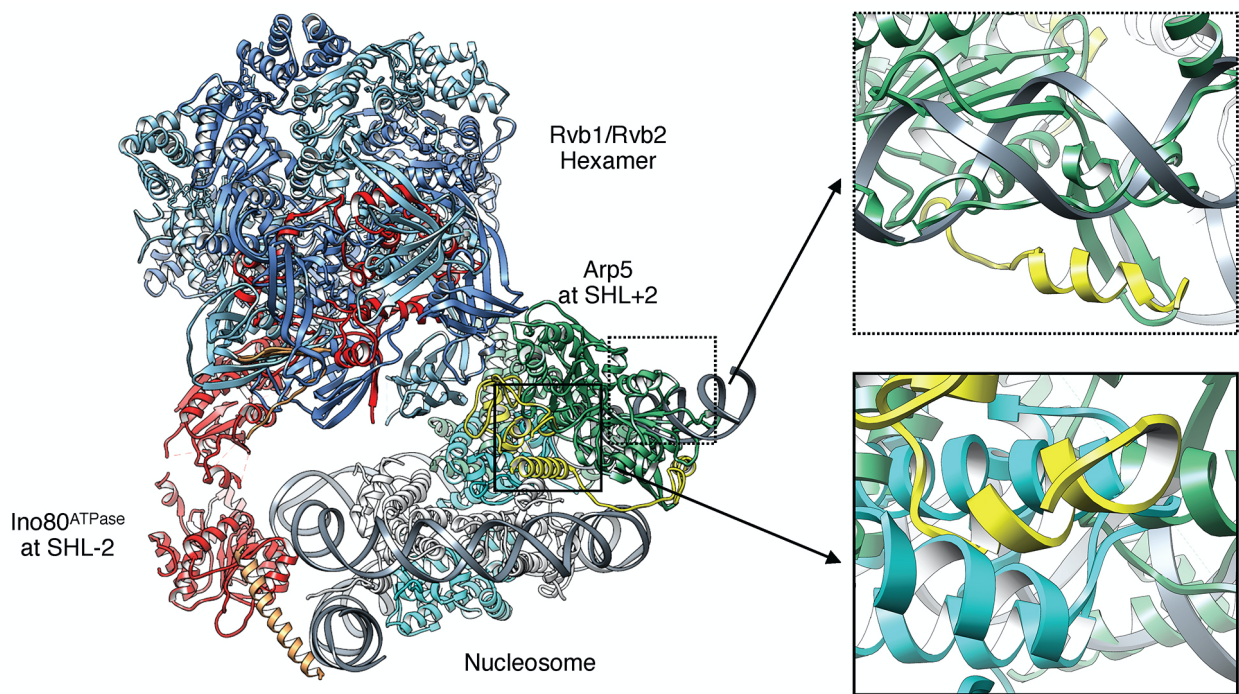
Figure S3.10. Modeling INO80 on a nucleosome with Ino80ATPase at SHL-2 results in clashes.
A hypothetic model of INO80 on a nucleosome made by directly positioning Ino80^{ATPase} at SHL-2 reveals clashes between the Arp5 module and the entry-side H2A-H2B (bottom panel) and between the Arp5 module and DNA that wraps around entry-side H2A-H2B (top panel).
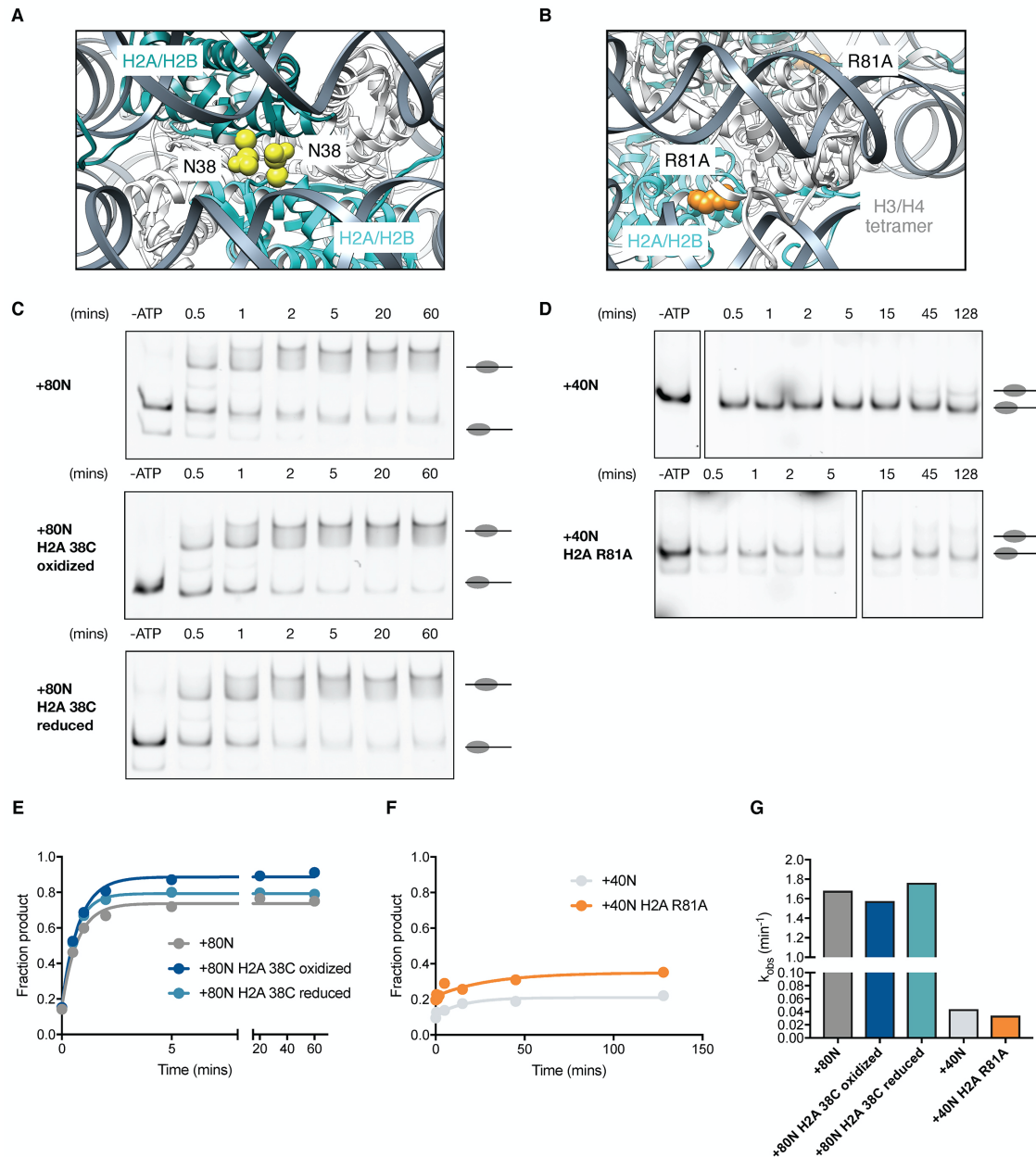
Figure S3.11. Crosslinking H2A or destabilizing dimer-tetramer interface does not significantly affect INO80 remodeling activity.
(A) Location of H2A N38 residues that are mutated to cysteine for cross-linking experiments (PDB: 1KX5); (B) Location of H2A R81 residues that are mutated to alanines. These mutations were shown to have destabilizing effects on the nucleosome (PDB: 1KX5); (C-D) Example gels of native gel-based remodeling assays of (C) WT INO80 on wildtype nucleosomes with 80 base pairs of flanking DNA (+80N) or +80N containing oxidized or reduced H2A N38C residues; (D) WT INO80 on wildtype nucleosomes with 40 base pairs of flanking DNA (+40N) or +40N containing H2AR81A (+40N R81A); (E) Example time courses of native gel-based remodeling assays shown in (C); (F) Example time courses of native gel-based remodeling assays shown in (D); Average observed rate constants determined from fitting a single-phase exponential decay model to two replicates. All assays were performed under single-turnover conditions with saturating enzyme and ATP.

References

1. R. Bar-Ziv, Y. Voichek, N. Barkai, Chromatin dynamics during DNA replication. *Genome Res* **26**, 1245-1256 (2016).

2. A. E. Ehrenhofer-Murray, Chromatin dynamics at DNA replication, transcription and repair. *Eur J Biochem* **271**, 2335-2349 (2004).

3. M. R. Hubner, D. L. Spector, Chromatin dynamics. *Annu Rev Biophys* **39**, 471-489 (2010).

4. C. R. Clapier, B. R. Cairns, The biology of chromatin remodeling complexes. *Annu Rev Biochem* **78**, 273-304 (2009).

5. C. Y. Zhou, S. L. Johnson, N. I. Gamarra, G. J. Narlikar, Mechanisms of ATP-Dependent Chromatin Remodeling Motors. *Annu Rev Biophys* **45**, 153-181 (2016).

6. K. Luger, A. W. Mader, R. K. Richmond, D. F. Sargent, T. J. Richmond, Crystal structure of the nucleosome core particle at 2.8 A resolution. *Nature* **389**, 251-260 (1997).

7. C. R. Clapier, J. Iwasa, B. R. Cairns, C. L. Peterson, Mechanisms of action and regulation of ATP-dependent chromatin-remodelling complexes. *Nat Rev Mol Cell Biol* **18**, 407-422 (2017).

8. Y. Bao, X. Shen, INO80 subfamily of chromatin remodeling complexes. *Mutat Res* **618**, 18-29 (2007).

9. A. J. Morrison, X. Shen, Chromatin remodelling beyond transcription: the INO80 and SWR1 complexes. *Nat Rev Mol Cell Biol* **10**, 373-384 (2009).

10. J. Poli, S. M. Gasser, M. Papamichos-Chronakis, The INO80 remodeller in transcription, replication and repair. *Philos Trans R Soc Lond B Biol Sci* **372**, (2017).

11. X. Shen, G. Mizuguchi, A. Hamiche, C. Wu, A chromatin remodelling complex involved in transcription and DNA processing. *Nature* **406**, 541-544 (2000).

12. R. Ayala *et al.*, Structure and regulation of the human INO80-nucleosome complex. *Nature* **556**, 391-395 (2018).

13. S. Brahma *et al.*, INO80 exchanges H2A.Z for H2A by translocating on DNA proximal to histone dimers. *Nat Commun* **8**, 15616 (2017).

14. S. Eustermann *et al.*, Structural basis for ATP-dependent chromatin remodelling by the INO80 complex. *Nature* **556**, 386-390 (2018).

15. J. Markert, K. Luger, Nucleosomes Meet Their Remodeler Match. *Trends Biochem Sci* **46**, 41-50 (2021).

16. L. Yan, Z. Chen, A Unifying Mechanism of DNA Translocation Underlying Chromatin Remodeling. *Trends Biochem Sci* **45**, 217-227 (2020).

17. L. J. Hsieh *et al.*, A hexasome is the preferred substrate for the INO80 chromatin remodeling complex, allowing versatility of function. *Mol Cell* **82**, 2098-2112 e2094 (2022).

18. S. Henikoff, Mechanisms of Nucleosome Dynamics In Vivo. *Cold Spring Harb Perspect Med* **6**, (2016).

19. M. L. Kireeva *et al.*, Nucleosome remodeling induced by RNA polymerase II: loss of the H2A/H2B dimer during transcription. *Mol Cell* **9**, 541-552 (2002).

20. O. I. Kulaeva, F. K. Hsieh, V. M. Studitsky, RNA polymerase complexes cooperate to relieve the nucleosomal barrier and evict histones. *Proc Natl Acad Sci U S A* **107**, 11325-11330 (2010).

21. S. Ramachandran, K. Ahmad, S. Henikoff, Transcription and Remodeling Produce Asymmetrically Unwrapped Nucleosomal Intermediates. *Mol Cell* **68**, 1038-1053 e1034 (2017).

22. C. Y. Zhou *et al.*, The Yeast INO80 Complex Operates as a Tunable DNA Length-Sensitive Switch to Regulate Nucleosome Sliding. *Mol Cell* **69**, 677-688 e679 (2018).

23. R. F. Levendosky, G. D. Bowman, Asymmetry between the two acidic patches dictates the direction of nucleosome sliding by the ISWI chromatin remodeler. *Elife* **8**, (2019).

24. R. F. Levendosky, A. Sabantsev, S. Deindl, G. D. Bowman, The Chd1 chromatin remodeler shifts hexasomes unidirectionally. *Elife* **5**, (2016).

25. K. R. Knoll *et al.*, The nuclear actin-containing Arp8 module is a linker DNA sensor driving INO80 chromatin remodeling. *Nat Struct Mol Biol* **25**, 823-832 (2018).

26. L. Farnung, M. Ochmann, G. Garg, S. M. Vos, P. Cramer, Structure of a backtracked hexasomal intermediate of nucleosome transcription. *Mol Cell* **82**, 3126-3134 e3127 (2022).

27. L. C. Lehmann *et al.*, Mechanistic Insights into Regulation of the ALC1 Remodeler by the Nucleosome Acidic Patch. *Cell Rep* **33**, 108529 (2020).

28. K. Mayanagi *et al.*, Structural visualization of key steps in nucleosome reorganization by human FACT. *Sci Rep* **9**, 10183 (2019).

29. J. P. Armache *et al.*, Cryo-EM structures of remodeler-nucleosome intermediates suggest allosteric control through the nucleosome. *Elife* **8**, (2019).

30. S. Chittori, J. Hong, Y. Bai, S. Subramaniam, Structure of the primed state of the ATPase domain of chromatin remodeling factor ISWI bound to the nucleosome. *Nucleic Acids Res* **47**, 9400-9409 (2019).

31. L. Yan, H. Wu, X. Li, N. Gao, Z. Chen, Structures of the ISWI-nucleosome complex reveal a conserved mechanism of chromatin remodeling. *Nat Struct Mol Biol* **26**, 258-266 (2019).

32. L. Farnung, S. M. Vos, C. Wigge, P. Cramer, Nucleosome-Chd1 structure and implications for chromatin remodelling. *Nature* **550**, 539-542 (2017).

33. I. M. Nodelman *et al.*, Nucleosome recognition and DNA distortion by the Chd1 remodeler in a nucleotide-free state. *Nat Struct Mol Biol* **29**, 121-129 (2022).

34. R. Sundaramoorthy *et al.*, Structure of the chromatin remodelling enzyme Chd1 bound to a ubiquitinylated nucleosome. *Elife* **7**, (2018).

35. A. B. Patel *et al.*, Architecture of the chromatin remodeler RSC and insights into its nucleosome engagement. *Elife* **8**, (2019).

36. F. R. Wagner *et al.*, Structure of SWI/SNF chromatin remodeller RSC bound to a nucleosome. *Nature* **579**, 448-451 (2020).

37. Y. Ye *et al.*, Structure of the RSC complex bound to the nucleosome. *Science* **366**, 838-843 (2019).

38. O. Willhoft *et al.*, Structure and dynamics of the yeast SWR1-nucleosome complex. *Science* **362**, (2018).

39. J. M. Tokuda *et al.*, The ATPase motor of the Chd1 chromatin remodeler stimulates DNA unwrapping from the nucleosome. *Nucleic Acids Res* **46**, 4978-4990 (2018).

40. S. Brahma, M. Ngubo, S. Paul, M. Udugama, B. Bartholomew, The Arp8 and Arp4 module acts as a DNA sensor controlling INO80 chromatin remodeling. *Nat Commun* **9**, 3309 (2018).

41. T. D. Frouws, P. D. Barth, T. J. Richmond, Site-Specific Disulfide Crosslinked Nucleosomes with Enhanced Stability. *J Mol Biol* **430**, 45-57 (2018).

42. K. Lehmann *et al.*, Effects of charge-modifying mutations in histone H2A alpha3-domain on nucleosome stability assessed by single-pair FRET and MD simulations. *Sci Rep* **7**, 13303 (2017).

43. F. Mueller-Planitz, H. Klinker, P. B. Becker, Nucleosome sliding mechanisms: new twists in a looped history. *Nat Struct Mol Biol* **20**, 1026-1032 (2013).

44. F. Mueller-Planitz, H. Klinker, J. Ludwigsen, P. B. Becker, The ATPase domain of ISWI is an autonomous nucleosome remodeling machine. *Nat Struct Mol Biol* **20**, 82-89 (2013).

45. A. J. Morrison *et al.*, INO80 and gamma-H2AX interaction links ATP-dependent chromatin remodeling to DNA damage repair. *Cell* **119**, 767-775 (2004).

46. K. Yen, V. Vinayachandran, B. F. Pugh, SWR-C and INO80 chromatin remodelers recognize nucleosome-free regions near +1 nucleosomes. *Cell* **154**, 1246-1256 (2013).

47. O. I. Kulaeva *et al.*, Mechanism of chromatin remodeling and recovery during passage of RNA polymerase II. *Nat Struct Mol Biol* **16**, 1272-1278 (2009).

48. H. S. Rhee, A. R. Bataille, L. Zhang, B. F. Pugh, Subnucleosomal structures and nucleosome asymmetry across a genome. *Cell* **159**, 1377-1388 (2014).

49. T. Gkikopoulos *et al.*, A role for Snf2-related nucleosome-spacing enzymes in genome-wide nucleosome organization. *Science* **333**, 1758-1760 (2011).

50. X. Shen, Preparation and analysis of the INO80 complex. *Methods Enzymol* **377**, 401-412 (2004).

51. P. N. Dyer *et al.*, Reconstitution of nucleosome core particles from recombinant histones and DNA. *Methods Enzymol* **375**, 23-44 (2004).

52. K. Luger, T. J. Rechsteiner, T. J. Richmond, Expression and purification of recombinant histones and nucleosome reconstitution. *Methods Mol Biol* **119**, 1-16 (1999).

53. E. Palovcak *et al.*, A simple and robust procedure for preparing graphene-oxide cryo-EM grids. *J Struct Biol* **204**, 80-84 (2018).

54. F. Wang *et al.*, Amino and PEG-amino graphene oxide grids enrich and protect samples for high-resolution single particle cryo-electron microscopy. *J Struct Biol* **209**, 107437 (2020).

55. M. Ohi, Y. Li, Y. Cheng, T. Walz, Negative Staining and Image Classification - Powerful Tools in Modern Electron Microscopy. *Biol Proced Online* **6**, 23-34 (2004).

56. D. N. Mastronarde, Automated electron microscope tomography using robust prediction of specimen movements. *Journal of Structural Biology* **152**, 36-51 (2005).

57. S. Q. Zheng *et al.*, MotionCor2: anisotropic correction of beam-induced motion for improved cryo-electron microscopy. *Nat Methods* **14**, 331-332 (2017).

58. A. Punjani, J. L. Rubinstein, D. J. Fleet, M. A. Brubaker, cryoSPARC: algorithms for rapid unsupervised cryo-EM structure determination. *Nat Methods* **14**, 290-296 (2017).

59. S. H. Scheres, RELION: implementation of a Bayesian approach to cryo-EM structure determination. *J Struct Biol* **180**, 519-530 (2012).

60. T. Grant, A. Rohou, N. Grigorieff, cisTEM, user-friendly software for single-particle image processing. *Elife* **7**, (2018).

61. R. Sanchez-Garcia *et al.*, DeepEMhancer: a deep learning solution for cryo-EM volume post-processing. *Commun Biol* **4**, 874 (2021).

62. E. F. Pettersen *et al.*, UCSF Chimera--a visualization system for exploratory research and analysis. *J Comput Chem* **25**, 1605-1612 (2004).

63. J. Jumper *et al.*, Highly accurate protein structure prediction with AlphaFold. *Nature* **596**, 583-589 (2021).

64. P. Emsley, K. Cowtan, Coot: model-building tools for molecular graphics. *Acta Crystallogr D Biol Crystallogr* **60**, 2126-2132 (2004).

65. P. V. Afonine *et al.*, Towards automated crystallographic structure refinement with phenix.refine. *Acta Crystallogr D Biol Crystallogr* **68**, 352-367 (2012).

66. C. A. Davey, D. F. Sargent, K. Luger, A. W. Maeder, T. J. Richmond, Solvent mediated interactions in the structure of the nucleosome core particle at 1.9 a resolution. *J Mol Biol* **319**, 1097-1113 (2002).

Chapter 4: Unpublished Data

Studying how INO80 ATPase Activity is Stimulated.

a. INO80 ATPase activity on nucleosomes is minimally affected by changes in flanking DNA length.

Previously, it has been shown that the flanking DNA modulates the remodeling activity of INO80 but not the ATPase activity. However, for the remodeling experiments conducted in Chapters 2 and 3, different conditions were used compared to published data. The remodeling experiments for WT INO80, ΔArp8 or ΔNph10 were conducted with either 60 nM or 90 nM enzyme, respectively. For all three complexes either 10 nM nucleosomes or 15 nM hexasomes were used with saturating amounts of ATP (1 mM). To measure ATPase activity under these conditions, a ^{32}P-radioactive ATPase assay was used to measure the liberation of inorganic phosphate (^{32}Pi) over time. Due to technical limitations of the assay, saturating amounts of ATP used in the remodeling experiments could not be used. Therefore, I performed ATPase assays at varying ATP concentrations to determine the rate constant k_{obs} (ATP) for the different INO80 complexes (WT, ΔNhp10, ΔArp5, ΔArp8, ΔIes2) within the detection limits of the assay (Figure 4.1A). For WT INO80, ΔNhp10, ΔArp5, and ΔArp8, 200 μM ATP was determined to be saturating for nucleosomes with 40, 60, and 80 bp of flanking DNA (Figure 4.1A). However, for ΔIes2 the ATPase activity was close to background, making it difficult to quantify the k_{obs}. The K_m for ATP was determined to be ~40 μM for WT INO80, ΔNhp10, ΔArp8, and ΔArp5 for nucleosomes with 40, 60, and 80 bp of flanking DNA (Figure 4.1A). Furthermore, with saturating ATP, less than an ~2-fold difference in k_{obs} was observed between +40 and +80 nucleosomes (Figure 4.1B). Additionally, removing Arp8 and Nhp10 modestly affected the k_{obs}, suggesting that these modules do not contribute to ATP hydrolysis by INO80 during nucleosome remodeling (Figure 4.1B). However, by removing Arp5, INO80's ATPase activity was reduced by 10-fold (Figure 4.1B, C). Similar to ΔIes2, it was challenging to detect ATP hydrolysis by ΔArp5, because it was slightly above the background activity for INO80 alone(Figure 4.1 A-C). For future studies it would be ideal to use alternative methods to measure ATP hydrolysis of ΔArp5 and ΔIes2 INO80.

b. INO80 is stimulated by core nucleosomes.

The results from the previous section suggest that flanking DNA does not contribute to ATP hydrolysis by INO80. However, whether there is a minimum amount of flanking DNA required for stimulation of INO80's ATPase activity is unknown. Therefore, I tested whether INO80 would be stimulated by nucleosomes that did not have any flanking DNA (i.e., core nucleosomes). I performed the ATPase assay with 160nM Ino80, 15nM core nucleosomes and 320 μM ATP. Interestingly, INO80's ATPase activity was stimulated by core nucleosomes and the k_{obs} was~2-fold less compared to nucleosomes with 80 bp of flanking DNA (Figure 4.1E). Previous studies have reported that INO80's affinity for nucleosomes decreases upon shortening the flanking DNA. Hence it is unclear whether saturating amounts of INO80 were utilized for the ATPase experiment using core nucleosomes . Future studies will need to be conducted to determine saturating concentrations of INO80 for core nucleosomes to properly assess differences in ATPase activity.

c. Supplementing additional H2A-H2B dimer does not stimulate ATPase activity of INO80.

The INO80 family is composed of SWR and INO80 complexes. The sole known function of SWR is to exchange the canonical H2A-H2B dimer for the non-canonical H2A.Z-H2B dimer. There is a controversy within the field of whether INO80 solely slides nucleosomes or whether it can also actively exchange the non-canonical H2A.Z-H2B dimer for the canonical H2A-H2B dimer. Previous studies have shown that if INO80 does facilitate exchange, it is inefficient as less than 20% percent of the nucleosomes are exchanged. One hypothesis is that INO80's exchange activity is an "off-pathway" activity. If INO80 actively exchanges dimers, I would suspect INO80's ATPase would be further stimulated by the presence of a nucleosome and dimer, like observed with SWR. I performed the ATPase assay with 60nM Ino80, 15nM nucleosomes, 30mM dimer and 320 μM ATP. I found that supplementing the H2A-H2B dimer did not increase the ATPase

activity of INO80 on nucleosomes containing H2A-H2B dimers and 80 bp of flanking DNA. Previous studies have suggested that INO80 is primarily involved in exchanging the H2A.Z/H2B dimer containing nucleosomes for H2A/H2B dimers (Figure 4.1D). Therefore, further experiments will need to be conducted to test whether excess H2A/H2B dimers in the presence of H2A.Z/H2B containing nucleosomes stimulate the ATPase activity of INO80.

Nucleosome intermediates generated by INO80

d. Assessing nucleosome intermediates using the Restriction Enzyme Accessibility Assay (PST18) :

Previously, our lab showed that during remodeling by INO80 at least one nucleosomal intermediate is formed which was captured by a restriction enzyme accessibility (REA) assay. The REA assay reports on changes in the accessibility of nucleosomal DNA. In chapter 2, we discussed how the generation of PST18 accessibility (PstI site incorporated 18 bps away from the exit site) was affected during remodeling by ΔArp5 INO80. We also tested what role Arp8 and Ies2 play in generating the PST18 accessible intermediate. Generally, removing Ies2 and Arp5 reduced the accessibility of the PST18 site to cutting by PstI on nucleosomes with 40 bp of flanking DNA (Figure 4.2A,B). Removing Ies2 disables the ability of INO80 to generate the PST18 accessible nucleosome intermediate with either 40 or 80 bp of flanking DNA. Removing Arp8 does not significantly affect the generation of the PST18 accessible nucleosome intermediate for nucleosomes with 40bp or 80bp of flanking DNA (Figure 4.2 A-C).

    i. INO80 requires an ATP independent pre-binding step of 10 minutes with nucleosomes. This was observed with nucleosomes with 80bp of flanking DNA. Because INO80 doesn't efficiently remodel nucleosomes with 40bp or less flanking DNA, we asked if we could capture the dependence of the pre-binding step via REA. I measured the INO80 and ATP-dependent accessibility of the PST18 site with and without prebinding. I observed no

significant difference in cutting at the PST18 site using nucleosomes with 80bps of flanking DNA (Figure 4.2D). This suggested that the REA assay does not capture the changes that occur during the pre-binding step.

ii. Caveats with REA: The k_{obs} for PstI cutting of naked DNA is comparable to the maximal gel-based sliding remodeling rate constant of WT INO80 on nucleosomes with 80 bps of flanking DNA in the current REA buffer, as described in Chapter 2. Under the current REA buffer, the k_{obs} for cutting naked DNA was 1.6 min^{-1}, which is ~4.5 fold slower compared to the cutting rate constant in the PstI buffer (New England Biolabs Buffer 3.1 :10mM NaClm 5mM Tris-HCL, 1mM MgCl2, and 10μg/mL BSA) (Figure 4.2E). Thus the REA assay cannot directly measure any steps that show rates constants greater than ~1.6 min^{-1} (Figure 4.2E). However, the remodeling rate of INO80 on nucleosomes with 80 bp of flanking DNA, measured via native gel-based sliding assay, is ~1 min^{-1}. This rate constant is slower or comparable to the rates constant for cutting naked DNA, indicating that rates constant derived from the Pst1 accessibility assay for PST18 on nucleosomes does not reflect the actual rates constant for formation of the intermediate. This comparison may explain why the difference between the k_{obs} for INO80 obtained using REA 40 bps and 80 bps of flanking DNA as previously published in our lab is not as great compared the difference in remodeling rate constants measured by the FRET and gel-based sliding assays. The reaction conditions for REA need to be optimized to enable accurate capturing of the rate constant for intermediate formation.

e. **Assessing nucleosome intermediates using the Restriction Enzyme Accessibility Assay (PST129)**

i. INO80 does not require ATP to unpeel the DNA away from the nucleosome core.

   1. In Chapter 3, the cryo-EM structure of INO80 bound to nucleosomes revealed that there is DNA unwrapping at SHL-6, where the Ino80 ATPase is positioned. This structure was solved with no ATP analogs present, suggesting that DNA unwrapping by INO80 is independent of ATP hydrolysis. To biochemically test this notion, I assembled nucleosomes with a Pst1 cut site located at PST129 (18bps) into the nucleosome at the DNA entry site of the nucleosome (Figure 4.3A). Unlike with PST18, INO80 can generate PST129 accessible nucleosomes in the absence of ATP(Figure 4.3B). This result corroborates the DNA unpeeling observed in the cryo-EM structure and indicates that INO80 needs to unwrap the DNA prior to activating the ATPase, on path to remodelling the nucleosome.

ii. The H2A-H2B dimer acidic patch contributes to PST129 accessibility in absence of ATP.

   1. Next, I wanted to test the role the acidic patch contributed to accessibility of PST129 on nucleosomes. There was no detectable change in PST129 accessibility in nucleosomes when both H2A-H2B dimer acid patches were mutated (APM) in the presence of ATP. Interestingly, in the absence of ATP, there was a decrease in PST129 accessibility for APM nucleosomes. This suggests the H2A-H2B dimer acidic patch contributes to DNA unwrapping prior to sliding. The Arp5 module contacts this H2A-H2B acidic patch, so

I assessed if the change in PST129 accessibility in the APM nucleosomes was dependent on the Arp5 contacts. Removing Arp5 does not change PST129 accessibility (Figure 4.3B). This suggests that the generation of the ATP independent PST129 accessible nucleosome may require the H2A-H2B acidic patch in an Arp5 independent manner. This is unlike the PST18 accessible nucleosomal intermediate, as mentioned in Chapter 2.

iii. Caveats with cutting the PST129 DNA.

    1. To have a better understanding of the PST129 REA data, I wanted to assess the cutting rate of Pst1 on naked DNA under our REA conditions to determine if the cutting rate is comparable to the sliding rate constant or comparable to the rate constant for cutting at the PST18 site. Unfortunately I discovered Pst1 does not fully cut the PST129 DNA (Figure 4.3C). Additionally, there is significant difference in cutting when Pst1 is incubated with the DNA for over 30 seconds compared to 10 minutes (Figure 4.3C). This data suggests that the PST129 DNA is challenging for Pst1 to cleave. This indicates that the cutting rates observed for PST129 are slower than the rate at which DNA is exposed on nucleosomes.

f. **Assessing nucleosome intermediates using the Restriction Enzyme Accessibility Assay (PST137)**

i. In 2018, two cryo-EM structures of human and fungal INO80 bound to a nucleosome, revealed that INO80 unwrapped ~15 bp of DNA way from the octamer core. To interrogate the role of DNA unwrapping, in the context of the INO80 reaction, I cloned a PstI cut site 137bp into the 601 sequence. This PST cut site is ~10bp from the DNA entry site, which should increase

in accessibility once WT INO80 engages the nucleosome (Figure 4.4A). I generated PST137 nucleosomes with 40bps of flanking DNA and tested PstI accessibility at the PST137 site. I compared accessibility of this site in nucleosomes either with or without INO80. Approximately 50% of the DNA is cut in both conditions, and INO80 does not appear to change DNA accessibility (Figure 4.4) These results suggest that PST137 does not report on DNA unwrapping facilitated by INO80. Therefore, future studies will need to be performed to determine a PST1 site that better reports on INO80 driven DNA wrapping.
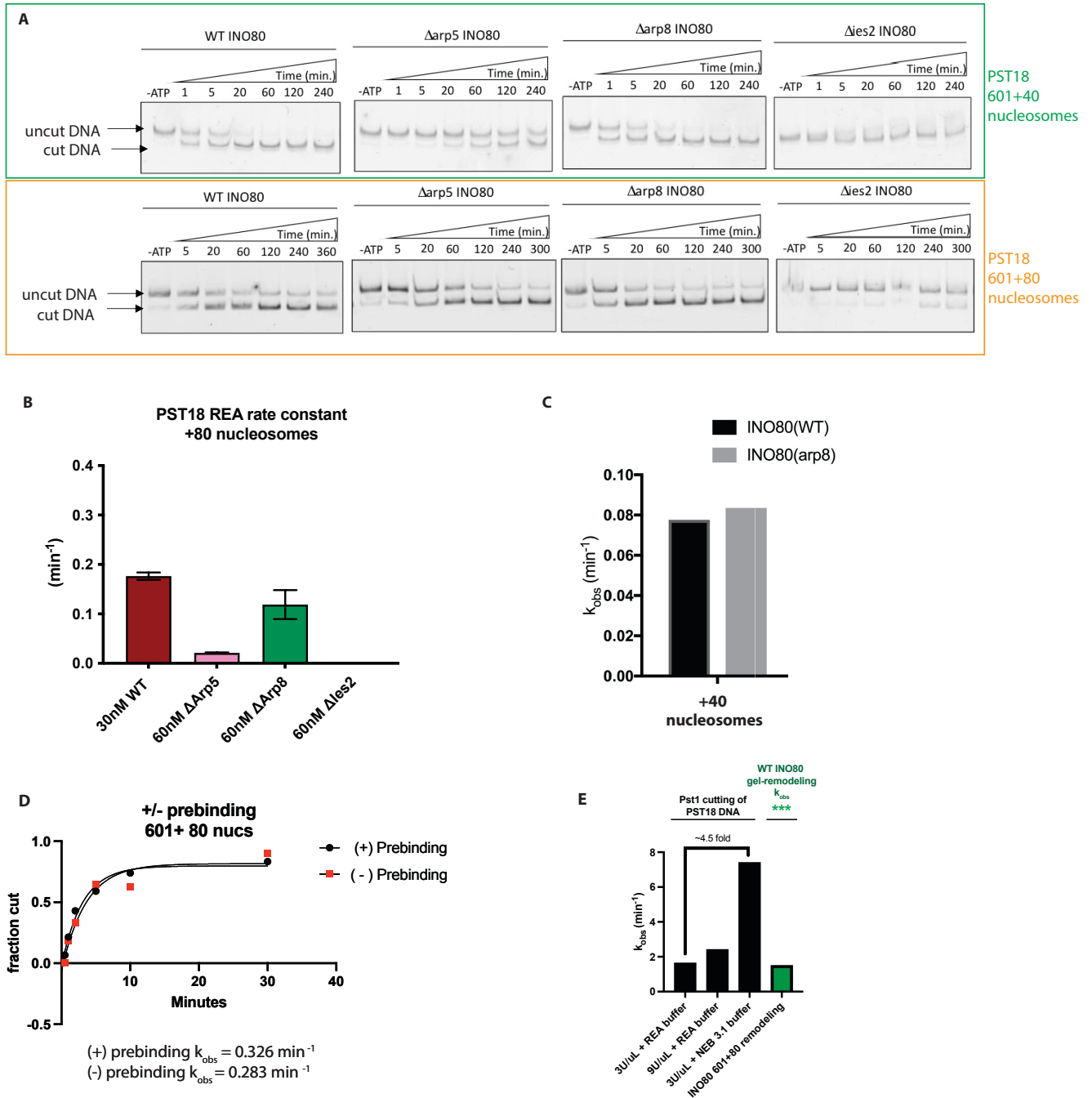
Figures
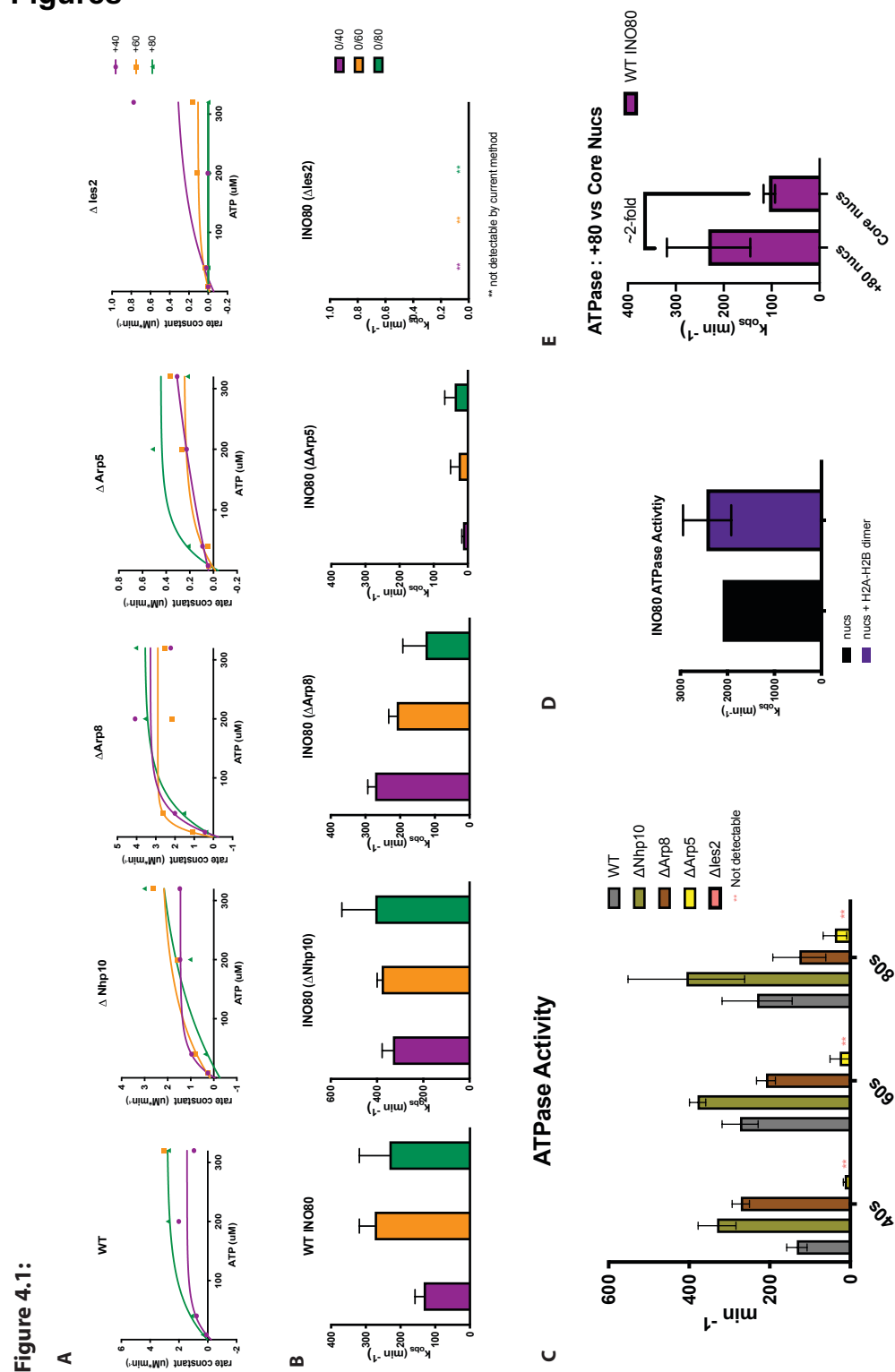
Figure 4.1: Stimulation of the INO80 ATPase Activity.
A) Determining what concentration of ATP is saturating for INO80. Measured the observed rate
constant and plotted, in the y-axis, rate constant (μM*min^{-1}) versus ATP (μM) in the x-axis.

Measured the rate constant for (WT INO80, ΔNhp10, ΔArp5, ΔArp8, and ΔIes2 with nucleosomes with either 40 (purple curve), 60 (orange curve), or 80bp (green curve). The ATP concentrations tested were 8μM, 40μM, 200μM, 320μM, and 500 μM. B) Observed rate constants for INO80 (WT, ΔNhp10, ΔArp5, ΔArp8, and ΔIes2) ATPase activity on nucleosomes with 40 (purple bar), 60 (orange bar), or 80 (green bar) bps of flanking DNA. Assay were performed with saturating amounts of Ino80 (60 or 90nM), 15nM nucleosomes, and 320μM ATP. C) Observed rate constants from (Figure4.1B) compiled. D) Observed rate constants of WT INO80 ATPase activity with nucleosome versus nucleosomes supplemented with H2A-H2B dimer. This assay was performed with 60nM Ino80, 15nM nucleosomes with 80 bps of flanking, 30nM of H2A-H3B dimer when supplemented, and 320μM ATP. E) Observed rate constants of INO80 ATPase activity on nucleosomes with 80bps of flanking DNA vs core nucleosomes. This assay performed with 60nM of WT Ino80 (with nucleosomes with 80bps flanking DNA) or 160nM WT Ino80 (with core nucleosomes), 15nM nucleosomes, and 320μM ATP. It is not clear if 160nM of INO80 was saturating with 15nM of core nucleosomes.
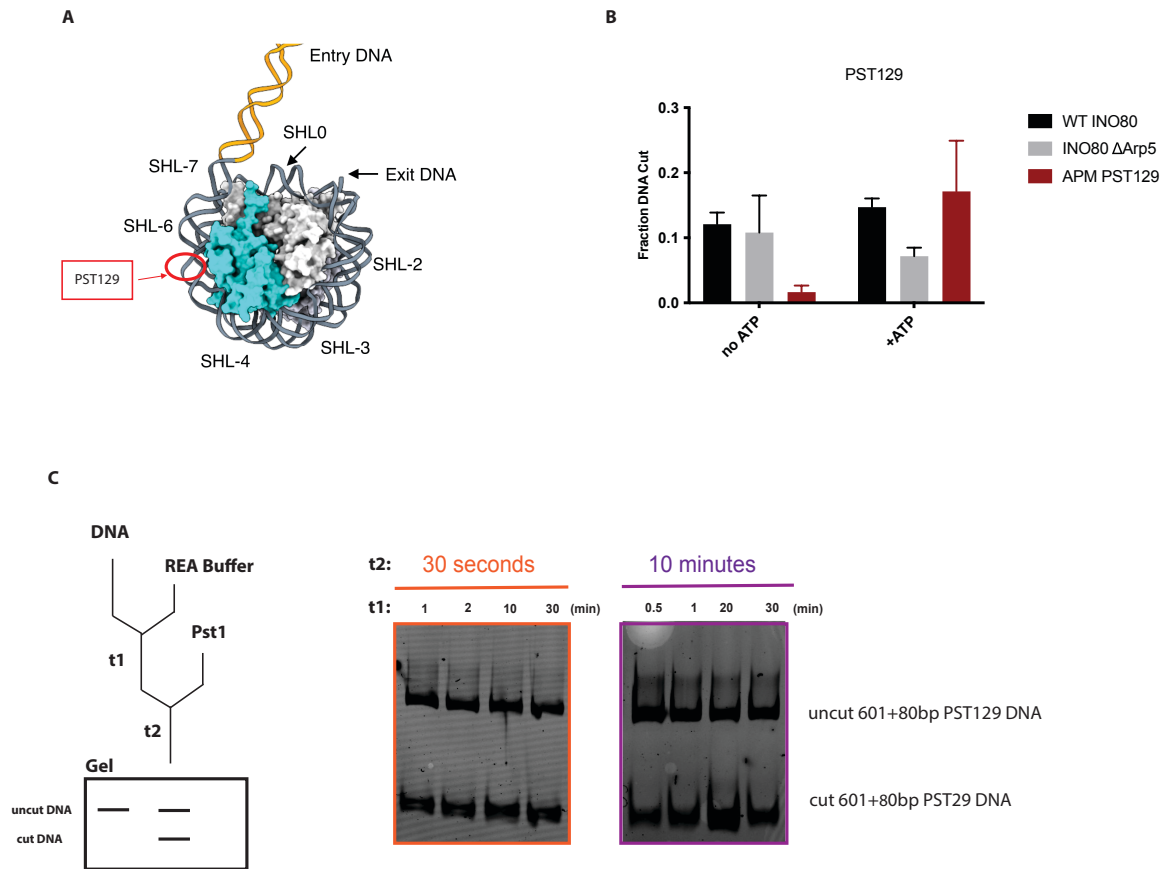
Figure 4.2:

Figure 4.2. Pst18 accessible nucleosome intermediate

A) Example native gel showing the fraction of DNA cut by PstI at PstI site for 601 +40 DNA and 601+80 DNA. The Restriction Enzyme Accessibility (REA) assays were done with saturating amounts of ATP, 15nM nucleosomes, and 30 or 60nM Ino80. Uncut and cut DNA products were separated on a 10% acrylamide and 1X TBE native gel. B) REA rate constants were measured for 30nM WT INO80, 60nM INO80(ΔNhp10), 60nM INO80(ΔArp5), 60nM INO80(ΔArp8), and 60nM INO80(ΔIes2) with 15nM of nucleosomes with 80bps of flanking DNA. C) REA rate constant measured for 30nM WT INO80 and 60nM INO80(ΔArp8) with 15nM nucleosomes with

40bps of flanking DNA and saturating amounts of ATP. D) REA rate constants measured with or without prebinding WT INO80 with nucleosomes. Reaction was started with the addition of saturating amounts of ATP. E) Rate constant of Pst1 cutting of naked Pst18 DNA in REA buffer compared to the commercial NEB buffer. The green bar is the rate constant for WT INO80 remodeling nucleosomes with 80bps of flanking DNA, via native gel sliding assay.
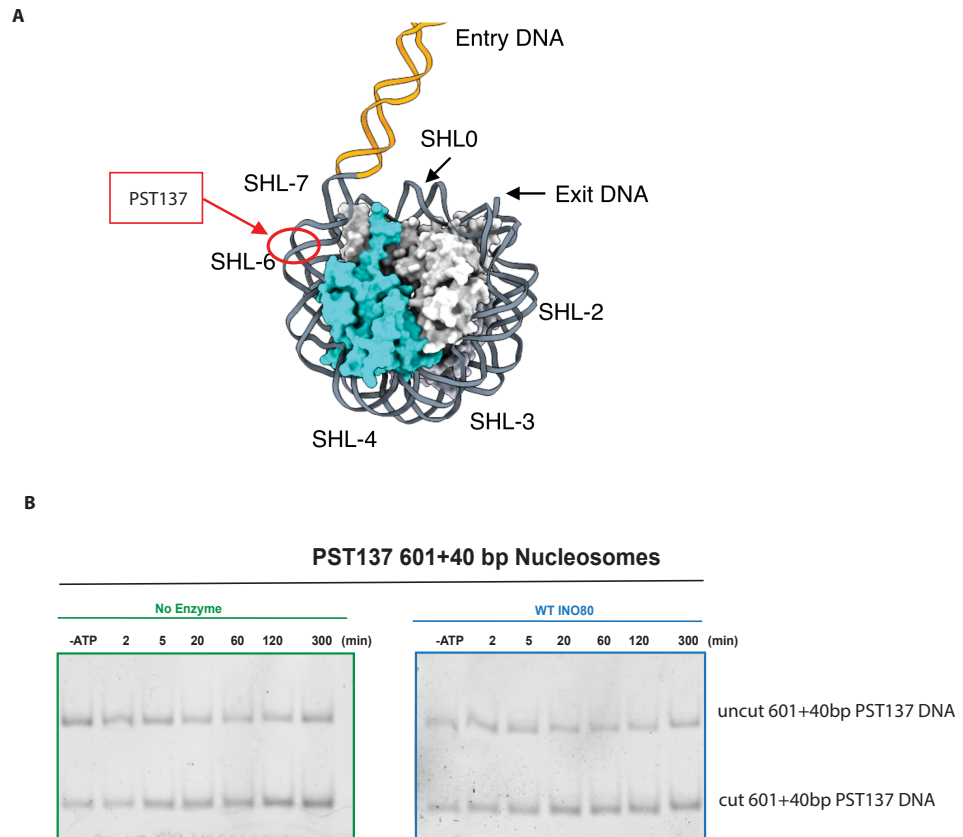
Figure 4.3

A

Entry DNA

SHL0

SHL-7

Exit DNA

SHL-6

SHL-2

PST129

SHL-4

SHL-3

B

PST129

Fraction DNA Cut

no ATP   +ATP

■ WT INO80
■ INO80 ΔArp5
■ APM PST129

C

DNA

REA Buffer

Pst1

t1

t2

Gel

uncut DNA

cut DNA

t2: 30 seconds   10 minutes

t1: 1 2 10 30 (min)   0.5 1 20 30 (min)

uncut 601+80bp PST129 DNA

cut 601+80bp PST29 DNA

Figure 4.3. Pst129 accessible nucleosome intermediate
(A)Shows the placement of the Pst1 cut site, 129 bp away from the DNA exit site (~SHL-5). The observed REA rate constants measured for 60nM WT INO80 or 90nM INO80(Δ*arp5*) with 15nM of WT nucleosomes with 40bp of flanking DNA, in black and grey bars respectively. (B) Observed REA rate constant for 60nM WT INO80 with 15nM acidic patch mutant (APM) nucleosomes with 40bps of flanking DNA (bar in red). Graph on the left are the observed rates without ATP and on the right, assays were performed in the presence of saturating ATP. (C) On the left is a schematic of the experimental design used to test the cutting of 15nM Pst129 DNA by Pst1. On the right, is a native gel of the DNA. Not shown here, but the DNA was not cut prior to starting the reaction. Uncut and cut DNA products were separated on a 10% acrylamide and 1X TBE native gel.

Figure 4.4

A

Entry DNA

SHL0

SHL-7

Exit DNA

PST137

SHL-6

SHL-2

SHL-3

SHL-4

B

PST137 601+40 bp Nucleosomes

No Enzyme

-ATP 2   5   20   60   120   300 (min)

WT INO80

-ATP 2   5   20   60   120   300 (min)

uncut 601+40bp PST137 DNA

cut 601+40bp PST137 DNA

Figure 4.4. Pst137 accessible nucleosome intermediate.
A) Shows the placement of the Pst1 cut, 137 bp away from the DNA exit site (SHL-6).
B) Native gel results of REA conducted with 15nM of PST137 nucleosomes with 40bp of flanking DNA. The native gel boxed in green shows a time course of Pst1 cutting the PST137 nucleosome with no INO80 added. The native gel boxed in blue shows a time course of Pst1 cutting when 60nM of WT INO80 was added at the start of the reaction. Uncut and cut DNA products were separated on a 10% acrylamide and 1X TBE native gel.

Publishing Agreement

It is the policy of the University to encourage open access and broad distribution of all theses, dissertations, and manuscripts. The Graduate Division will facilitate the distribution of UCSF theses, dissertations, and manuscripts to the UCSF Library for open access and distribution. UCSF will make such theses, dissertations, and manuscripts accessible to the public and will take reasonable steps to preserve these works in perpetuity.

I hereby grant the non-exclusive, perpetual right to The Regents of the University of California to reproduce, publicly display, distribute, preserve, and publish copies of my thesis, dissertation, or manuscript in any form or media, now existing or later derived, including access online for teaching, research, and public service purposes.

DocuSigned by:

E29698C523404CC...

Author Signature

11/19/2022

Date

138